Université d'Ottawa · University of Ottawa

PLASTIC INTERACTION RELATIONS FOR HOLLOW STRUCTURAL STEEL SECTIONS

by

Istemi Faruk Ozkan

Thesis submitted to the Faculty of Graduate and Post Doctoral Studies in partial fulfillment of the requirements for the Master of Applied Science Degree in Civil Engineering under the auspices of the Ottawa-Carleton Institute for Civil Engineering

April 2002

Department of Civil Engineering, University of Ottawa

Ottawa, Canada, 2002

Abstract

The first part of this study reports an experimental program consisting of six full-scale tests on pipe sections under load combinations of shearing forces, bending moments, and twisting moments. The experimental results agree very well with the predicted failure loads based on recently developed interaction relations. The experimental program establishes the validity of the analytical techniques used to derive the interaction relations for pipe sections. The verified methodology is extended to derive interaction relations for square hollow structural sections under combinations of normal forces, twisting moments, biaxial bending moments, and biaxial shearing forces. Careful consideration is given to the applicability limits of the developed interaction relations. A stress resultant transformation scheme is devised in order to reduce the number of interaction relations from 20 cases to only three fundamental cases.

To my family

Aileme

Acknowledgements

My special thanks go to my supervisor, Dr. Magdi Mohareb for his support, advice, and patience, without his directions this thesis could not have been done.

The study presented herein was sponsored by the Steel Structures Education Foundation (SSEF) and the National Science and Engineering Research Council (NSERC) of Canada. Their financial support is greatly acknowledged.

The Structures Laboratory Technician and fellow graduate student Mr. Muslim Majid, is greatly acknowledged for his additional assistance in the experimental part of this study. The assistance of the machine shop supporting staff is also appreciated.

I would like to thank to my fellow graduate students, office mates, and friends: Dr. Jocelyn Paquette, Mr. Ayman Dabbas, Mr. John Bougadis, Mr. Farhood Nowzartash, Mr. Patrick Brisson, and Mr. Ozgur Candir. Special thanks are extended to Miss. Erin Debra Freeman for her tireless encouragement and support.

My deepest thanks go to my family for their moral support during all phases of this project. The patience and sacrifice of my mother, father, and brother throughout my studies can never be forgotten.

Table of Contents

CHAPTER 3

Plastic Interaction Relations Square Hollow Structural Sections

CHAPTER 4

Summary and Recommendations for Future Research

List of Tables

Chapter 2

Appendix A

Appendix B

List of Figures

Chapter 1

Chapter 2

Chapter 3

Appendix A

Appendix B

CHAPTER 1

INTRODUCTION

1.1 Background to the Problem

In steel construction, hollow structural steel sections are the preferred choice for load combinations including torsion because of their high torsional resistance and stiffness when compared to open sections. Aesthetics is another reason for selecting circular, square, and rectangular hollow structural sections over their open section counterparts. Tubular sections are also commonly used in offshore structures and power transmission lines. Another major application of tubular steel sections is in the pipeline industry where several thousands of kilometres are contemplated in Canada over the next few years in order to transport oil and gas to the United States.

In these applications, pipe sections may be subjected to load combinations including biaxial bending moments, biaxial shear forces, axial force, internal external pressure, and twisting moments. The general interaction equations for pipe sections under these load combinations were recently developed (Mohareb 2002a and 2002b). The study presented herein focuses on two aspects. These are:

a) Assessing the validity of the interaction equations for pipe sections under load combinations including bending moments, twisting moments, and shearing forces.

b) Extending the lower bound methodology to derive plastic interaction equations for square hollow structural sections under biaxial bending, biaxial shear, axial force and twisting moments.

1.1.1 Theoretical Background

1.1.1.1 Lower Bound Methodology

The lower bound theorem of plasticity states: "By assuming statically admissible stress fields, a lower bound interaction relation is obtained" (Hodge 1981 and Bruneau et al. 1998). Stress fields are statically admissible when they do not violate the yield condition anywhere on the cross-section. Approximate stress fields will always yield lower bound interaction relations while an exact solution can be reached only when the assumed stress fields are exact. The main steps involved in a lower bound solution are:

- Assume stress fields. In order to maximize the lower bound solution, the yield condition has to be met everywhere on the cross-section.

- Obtain the internal stress resultants acting on the cross-section by integrating the stresses and their moments over the cross-section. This leads to expressions of the stress resultant in terms of various geometric parameters of the problem.

- Eliminate the geometric parameters between the stresses in resultant expressions in order to obtain an interaction relation

Under this type of formulation, when an exact solution is sought under internal forces inducing more than one stress component, the challenge is to find the exact expressions for the stresses. This problem can be resolved in some problems through the calculus of variation (Hodge 1981), or through Lagrange multipliers (Santhhadaporn and Chen 1970).

1.1.1.2 Upper Bound Methodology

Upper bound interaction relations are obtained by assuming kinematically admissible strain increments and equating the dissipation in internal strain energy per unit length of

the beam considered to the change in the external work done by the external stress resultants through the associated generalized strain increments. Strain increments are kinematically admissible when they are derivable from assumed displacements. Alternatively, they have to meet strain compatibility relations. When approximate strain increments are assumed, the solution yields upper bound interaction relations. Exact solutions are obtained only when exact strain increments are assumed. The main steps involved in the upper bound solution.

- Assume kinematically admissible strain increments

- At a given cross-section, equate the dissipation in internal strain energy per unit length of member due to assumed kinematically admissible strain increments to the change in external work done by the external stress resultants through associated generalized incremental strains.

- Obtain expressions for stress resultants in terms of intermediate parameters through partial differentiation of the internal strain energy expressions with respect to the corresponding strain increments.

- Eliminate the intermediate parameters between the stress resultant expressions in order to obtain an interaction relation.

1.2 Application to Pipe Sections

A pipe section (Fig. 1.1) subject to axial force A, shearing force components V_x and V_y along two orthogonal axes x and y in the plane of the cross-section, bending moments components M_x and M_y, twisting moment T, and internal (and/or external) pressure p is considered. An interaction relations in the form of $f(A, V_x, V_y, M_x, M_y, T, p) = 0$ is sought such that the condition $f < 0$ is met for any physically possible combination of

internal forces. $f = 0$ corresponds to a fully plastic state of the cross-section. and the condition $f > 0$ is unattainable under the assumptions of the formulation.

The lower bound theorem of plasticity was used to obtain the interaction relations (Mohareb. 2001. Mohareb 2002a). The same solution was obtained by using an upper bound methodology (Mohareb. 2002b). As both of the methods yielded the same interaction equations. these relations must be exact within the limitations of the formulation according to the uniqueness theorem. The assumptions and limitations made in both solutions are summarized in the following.

1.2.1 Main Assumptions

- **Stress Components:** Only the longitudinal stresses. hoop stresses. and circumferential stresses are considered. Other components of the stress tensor are considered negligible. Therefore. the formulation cannot capture effects such as local buckling.

- **Strain formulation:** The formulation is based on small strains. i.e.. no distinction is made between the engineering strains and the finite strains. Also. no distinction is made between the true stress based on the un-deformed cross-section and that based on the deformed cross-section.

- **Cross-sectional distortion:** The pipe cross section is assumed to remain circular under the externally applied loads

- **Idealized stress vs. strain relationship:** A bilinear elastic-perfectly plastic stress versus strain approximation is adopted. The first line passes through the origin and has the same slope as tension coupon tests. The second line has zero slope and passes through the yield point. The additional capacity of the pipe section due to strain hardening was neglected. leading to a lower bound approximation of the section plastic resistance.

- **Yield Condition:** Pipe steel was assumed to yield in accordance with the maximum distortional energy density criterion. Based on the yield condition and the perfectly plastic assumption implied in the previous assumption, it is possible to infer the incompressibility of the material.

- **Local Buckling:** It is assumed that the pipe section attains its fully plastic resistance prior experiencing a strength reduction due to local buckling. Therefore, the formulation is valid for compact sections.

- **Circumferential Shear Stress Distribution:** The formulation is limited to thin tubular sections. Therefore, the circumferential shear stress magnitude was considered as constant through the thickness of the pipe.

1.2.2 Experimental Verification

Upon full-scale tests, Mohareb and Murray (1999) experimentally verified the general interaction equations for load combinations limited to axial force, bending, and internal pressure for steel pipes.

The focus of the first part of this study is to extend the experimental verification of the interaction equations to pipe sections under shear, bending, and twist.

1.3 Application to Square Hollow Structural Sections

In the second part of this study, the lower bound methodology as outlined in Section 1.1.1.1 is used to derive general interaction relations for stocky square hollow structural sections (Classes 1 and 2 in CAN/CSA 2001 or compact sections in LRFD 1999), which are capable of developing their fully plastic capacity prior local buckling. Previous studies developed interaction relations for square hollow structural sections under biaxial bending moments, twisting moments, and axial forces (e.g., Morris and Fenves 1969;

Chen and Atsuta 1972). However, none of them included the contribution of shear forces. This analytical study attempts to fill this void by deriving general interaction relations for square hollow structural sections under general load combinations including biaxial bending, twist, axial force in addition to biaxial shearing forces.

1.4 Outline of the Thesis

The main sections of this thesis are Chapters 2 and Chapter 3. They are written as two separate research papers with a separate list of references and nomenclature at the end of each paper.

Chapter 2 presents an experimental investigation on the validation of plastic interaction equations for steel pipe sections under load combinations including twist, bending and shear.

Chapter 3 presents an analytical derivation of plastic interaction equations for square hollow structural sections including the effect of biaxial shear forces, biaxial bending moments, axial force, and torsion.

Chapter 4 presents a summary of research findings, and gives recommendations for future research.

Appendix A presents the experimental data obtained during the experimental program presented in Chapter 2

Appendix B presents analytical derivations and verifications related to the analytical work presented in Chapter 3.

References for Chapter 1

AISC. (1999). *Load and resistance factor design specification for structural steel buildings*. American Institute of Steel Construction, Chicago.

Bruneau, M., Uang, C., and Whittaker, A. (1998). "Ductile design of steel structures." McGraw-Hill, NY.

CAN/CSA S16 (2001). "Limit States Design of Steel Structures", Canadian Standards Association, Rexdale, Ont.

Santathadaporn, S. and Chen, W. F. (1970). "Interaction curves for sections under combined biaxial bending and axial force." Bulletin no. 178, Welding Research Council, Bulletin No:1.

Chen, W. and Atsuta, T. (1972). "Interaction equations for biaxially loaded sections." *J. Struct. Engrg.*, ASCE, Vol. 98 (ST5), 1035-1051.

Hodge, Ph. G. (1981). *Plastic analysis of structures*. Krieger, Malabar, Fla.

Mohareb, M. (2002a). "Plastic interaction relations for pipe sections.", *J. Eng. Mech.*, ASCE, Jan. Vol.128(1), 112-120.

Mohareb, M. (2002b). "Plastic resistance of pipe sections-an upper bound solution.", accepted for publication by *J. Struct. Eng.*, ASCE.

Mohareb, M. (2001). "Exact yield hyper surface for thin pipes.", *Int. J. of Pressure Vessels and Piping*, 78(7), 507-514.

Mohareb, M. and Murray, D. W. (1999). "Mobilization of fully plastic moment capacity for pressurized pipes subjected to axial loading" *ASME J. Offshore Mech. Arct. Eng.*, 121 (4), 237-241.

Morris, G. and Fenves, S. (1969). "Approximate yield surface equations", *J. Eng. Mech Division*, ASCE, Vol. 95 (EM4), 937-954.

List of Symbols for Chapter 1

A internal axial force

M_x internal bending moment with respect to x-axis

M_y internal bending moment with respect to y-axis

p pressure (positive for net internal pressure)

T internal twisting moment

V_x internal shearing force in the direction of x-axis

V_y internal shearing force in the direction of y-axis

$f(A, V_x, V_y, M_x, M_y, T, p)$ interaction relation in terms of stress resultants A, V_x, V_y, M_x, M_y, T, and p

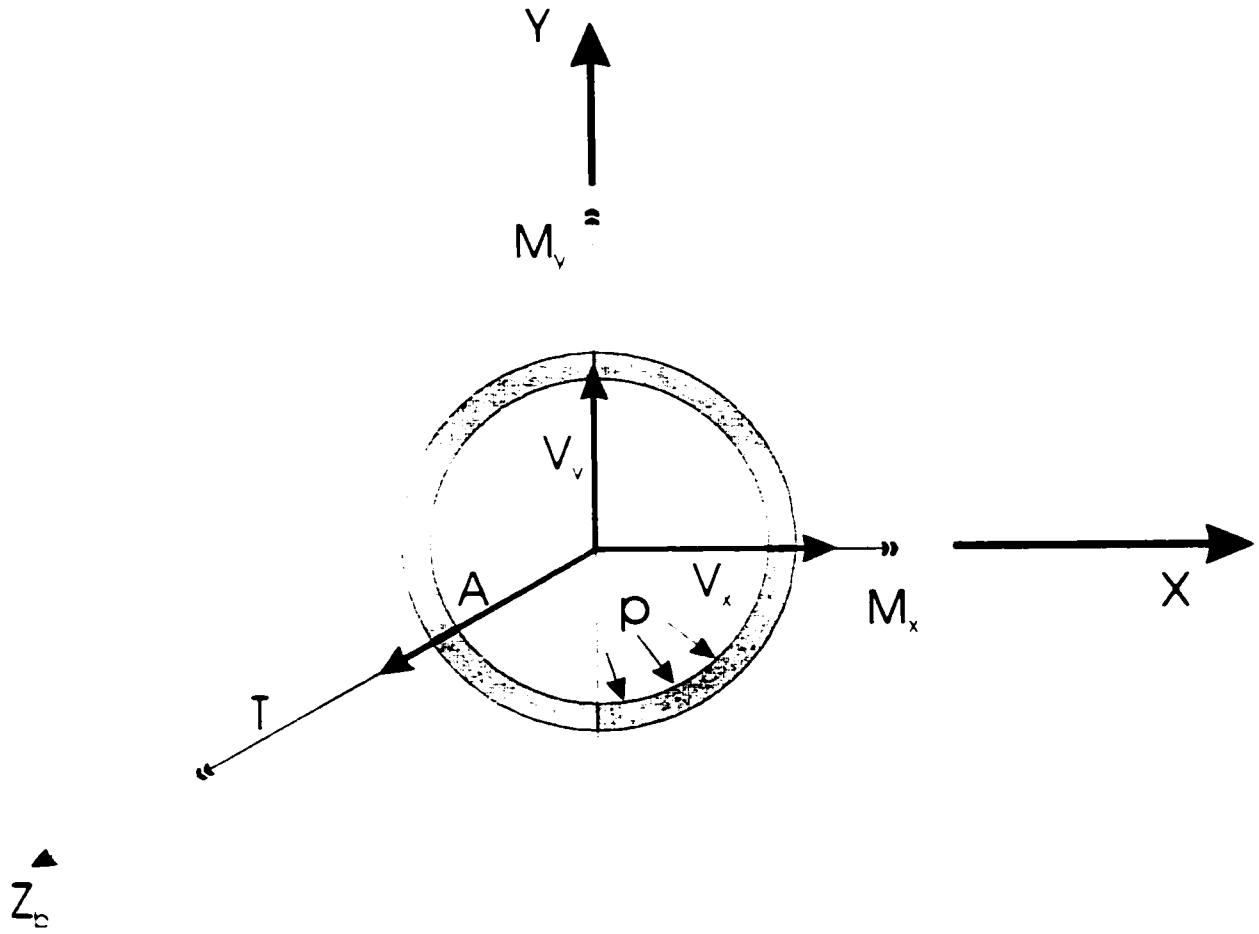

Figure 1.1 Internal Forces Acting on Pipe Cross-section

CHAPTER 2

TESTING OF STEEL PIPES UNDER BENDING TWIST AND SHEAR

2.1 Introduction

Recent analytical developments resulted into interaction relations for pipes subjected to biaxial bending, biaxial shear, torsion, axial force, and internal/external pressure. This chapter reports an experimental program consisting of six full-scale tests in order to assess the validity of the analytically derived interaction relations under various loading combinations including shearing forces, bending moments, and twisting moments. This program is believed to be an important step in adopting the general interaction relations in limit state design codes in a number of applications including steel pipelines, offshore structures, and structural steel codes as they offer a more practical and less expensive option than non-linear finite element analyses.

2.2 Literature Review

A summary of early experimental and analytical work (Gerald and Becker 1957) provides a number of interaction relations for pipes under various combinations of internal forces. These are limited to pipes that undergo local buckling prior attaining their plastic resistance. Lower bound plastic interaction relations for hollow structural sections including thin walled tubular sections were established under combinations of biaxial bending moments, twisting moment and axial force by Fenves and Morris (1969). Pillai and Ellis (1971) conducted an experimental study on pipe sections subject to combined axial force and biaxial bending moments and proposed a simplified interaction relation. Chen and Atsuta (1972) formulated lower and upper bound interaction relations for tubular sections under biaxial bending moments and axial forces. The exactness of their

solution was demonstrated through the agreement between the two bounds. Their solution also agreed with that developed by Fenves and Morris (1969) when the torque term is omitted. Bouwkamp and Stephen (1973) conducted a series of tests including the combined effect of internal pressure, axial force and bending moments on 48in diameter pipes. Sherman (1976) experimentally investigated the flexural behavior of the tube sections beyond ultimate moment capacity. Yamaki (1976) conducted tests on fiberglass pipes to investigate the post-buckling behavior of pipe sections under pure torsion. Prion and Birkemoe (1988) conducted a series of tests on large fabricated tubes subjected to combinations of axial load and bending. Obaia et al. (1991) analytically and experimentally investigated the inelastic shear behavior of large diameter pipes subjected to transverse loads. They proposed an interaction equation for the shear capacity based on regression analysis of their test results. Mohareb et al. (1994) and Mohareb and Murray (1999) developed interaction expressions including internal pressure, axial force and bending moments. Their analytical results agreed well with experimental results. Upon full-scale experimental verification, the interaction relations were adopted in limit state design of submarine pipelines by DNV (1996). Haunch and Bai (1998) modified the solution of Mohareb et al (1994) by incorporating the effect of corrosion into the formulation. Mohareb (2002a) developed a lower bound general plastic interaction relation for pipe sections under normal force, torsion, biaxial bending moments, biaxial shear forces and internal or external pressure by assuming statically admissible stress fields. Using Lagrange multipliers (Mohareb 2001), the interaction expressions obtained were shown to maximize the lower bound solution. An upper bound solution was developed by Mohareb (2002b) by deriving kinematically admissible strain fields. The solution obtained coincided with that based on the lower bound formulation, demonstrating the exactness of the solution. It is of interest to note that by omitting the shear and torsion terms from the general expressions, the axial force-bending-internal pressure interaction expressions reported in Mohareb et al. (1994) are recovered. The experiment results in Mohareb and Murray (1999) on bending moment-axial force-internal pressure combinations demonstrate the validity of the interaction relations for pipes with a diameter to thickness ratio in the range of 50 to 60. Experiments on steel pipes under loading combinations including twist and shear are scarce at best. It is the

objective of this investigation to partially fill this void by conducting tests on steel pipes under combinations of torsion, bending moments, and shear forces.

2.3 *Plastic Interaction Equations*

The plastic interaction relations for pipe sections subjected to combinations of normal forces, internal or external pressure, twisting moments, biaxial bending moments, and biaxial shearing forces (Mohareb 2002a) are

$$M_{ry}^2 + M_{rz}^2 = \left(1 - \frac{3}{4} p_r^2 - \tau_r^2\right) \cos^2 \left\{ \frac{\frac{\pi}{2}\left(A_r - \frac{1}{2} p_r\right)}{\sqrt{1 - \frac{3}{4} p_r^2 - \tau_r^2}} \right\} \tag{2.1}$$

$$\frac{V_{ry}^2 + V_{rz}^2}{\tau_r^2} = \cos^2\left(\frac{\pi}{2} \frac{T_r}{\tau_r}\right) \tag{2.2}$$

In Eqs. 2.1 and 2.2, M_{ry} is the ratio of internal bending moment M_y to the plastic moment resistance $M_p = 4r^2 t F_y$, M_{rz} is the ratio of internal bending moment M_z to the plastic moment resistance M_p, p_r is the ratio of the pressure p (positive for a net internal pressure) to the yield internal pressure $p_y = F_y t/(r - t)$, A_r (positive when in tension) is the ratio of the internal axial force A to the axial resistance $A_y = 2\pi r t F_y$, V_{ry} is the ratio of internal shear force V_y to the plastic shear resistance $V_p = 4rt(F_y/\sqrt{3})$, V_{rz} is the ratio of internal shear force V_z to the plastic shear resistance V_p, and T_r is the ratio of internal twisting moment T to the plastic twisting moment $T_p = 2\pi r^2 t F_y/\sqrt{3}$. The terms r, t, and F_y are the radius, wall thickness, and yield strength of the pipe, respectively. The shear ratio τ_r is a dimensionless parameter that intrinsically relates the twist and shear force ratios (Eq. 2.2) to the moment, axial force, and internal pressure ratios (Eq. 2.1). Equations 2.1 and 2.2 relate the seven loading parameters, M_{ry}, M_{rz}, V_{ry}, V_{rz}, T_r, p_r, and A_r

when the section reaches its fully plastic state and can be used to judge whether a given internal force combination is attainable only when the following applicability limits are met.

$$0 \le V_n^2 + V_m^2 \le \tau^2 \quad 0 \le T_r \le \tau \quad \text{and} \quad V_n^2 + V_m^2 \le \cos^2\left(\frac{\pi}{2} T_r\right) \qquad \text{(2.3a, b, c)}$$

$$-2\sqrt{\frac{1-\tau_r^2}{3}} \le p_r \le 2\sqrt{\frac{1-\tau_r^2}{3}} \qquad (2.4)$$

$$\frac{1}{2} p_r - \sqrt{1 - \frac{3}{4} p_r^2 - \tau_r^2} \le A_r \le \frac{1}{2} p_r + \sqrt{1 - \frac{3}{4} p_r^2 - \tau_r^2} \qquad (2.5)$$

The limits in Eqs.2.3 through 2.5 are based on geometric constraints (Mohareb 2002a). In the absence of shear forces and twisting moments, and under uniaxial moments ($M_m = 0$), the interaction relations take the form

$$M_n^2 = \left(1 - \frac{3}{4} p_r^2\right) \cos^2\left\{\frac{\frac{\pi}{2}\left(A_r - \frac{1}{2} p_r\right)}{\sqrt{1 - \frac{3}{4} p_r^2}}\right\} \qquad (2.6)$$

which matches the interaction relation in Mohareb et al. (1994) and Mohareb and Murray (1999). Thus, the full-scale tests they conducted on 12in and 20in diameter pipes (outside diameter to thickness ratios of 51 and 64, respectively) under bending, axial force, and internal pressure validate the general interaction relations (Eqs. 2.1 and 2.2) for load combinations including axial force, bending, and twist.

The focus of this experimental investigation is to extend the experimental database to include pipes under twisting moments, shearing force, and bending moments. In the

absence of axial force A_r, and internal pressure p_r, and in the case of uniaxial shear, and bending, V_x=0, $M_n = 0$. Eqs. 2.1 and 2.2 lead to

$$V_n = \sqrt{1 - M_x^2} \cos \frac{\pi T_r}{2\sqrt{1 - M_x^2}} \tag{2.7}$$

The scope of this part of the thesis is to experimentally assess the validity of Eq. 2.7 under various M_x, V_n, and T_r ratios.

2.3.1 Interaction Surface

The surface plot in Fig. 2.1 depicts the interaction relation between T_r, M_x, and V_n based on Eq. 2.7 in the positive octant of the (T_r, M_x, V_n) space. A given internal force combination corresponds to a point in the (T_r, M_x, V_n) space. An attainable stress resultant combination has to lie inside the yield surface while a point on the surface indicates a fully plastic state of the cross section. The peak shear force resistance corresponds to zero bending moment and twisting moments, in which case the magnitude of the shear force ratio is unity, (i.e. shearing force resistance is equal to fully plastic shear capacity). As the magnitude of either T_r or M_x is increased, the corresponding shear force ratio V_n decreases. The twisting moment ratio has a maximum value of unity when both M_x and V_n are equal to zero. Also, the bending moment ratio has a maximum value of unity when both T_r and V_n vanish.

2.4 Experiment Design

2.4.1 Selection of Pipes

Local buckling behavior of pipes is largely influenced by diameter-to-thickness ratio, D/t, (Batterman 1965, Redy 1979, Gellin 1980, and Gresnigt 1986). The D/t ratio of the specimens was selected to prevent local buckling from occurring prior attaining the fully

plastic resistance under pure flexure (Class 2 in CAN/CSA 2001 or compact sections in LFRD 1999). All pipes tested had a nominal outside diameter of 406mm and a thickness of 9.5mm (i.e., nominal diameter to thickness ratio $D/t = 42.7$). The measured outside diameter of the tubes averaged 406.4mm. The height of the specimens and the eccentricity at which the force is applied were changed between tests in order to vary the applied bending moment to shear force ratio, M_f/V_f, and twisting moment to shear force ratio, T/V_f (Fig. 2.2). Table 2.1 summarizes the actual dimensions of the specimens tested. Three different heights of the specimens are shown in Fig. 2.3. Each of the six tests is designated by a descriptor of the form VxxTyyMzz, where V, T, and M are the descriptors for the shear, torsion, and bending moment, respectively. The numbers xx, yy, and zz, are the respective percentages of the fully plastic resistance in shear, twist, and bending at full plastification of the cross-section as determined by Eq. 2.7. For example dimensions a and b of Specimen V15T86M31 are selected such that the specimen is expected to reach the fully plastic state under a shear force $V_f = 15\%V_p$, a twisting moment $T = 86\%T_p$, and a bending moment $M_f = 31\%M_p$, as predicted by Eq. 2.7. All specimens were cut from the same piece of pipe. The specified minimum yield strength (SMYS) was 350Mpa (350W steel).

2.4.2 Loading Combinations

Given the dimensions a and b, the shear force, twisting moments and bending moments that would fully plastify the section were predicted from Eq. 2.7. These are summarized in Table 2.1 for all six specimens tested. All predicted values were based on the measured cross-sectional dimensions and yield strength as determined by extension-under load method from tension tests.

2.5 *Description of the Experiments*

2.5.1 Ancillary tests

The stress vs. engineering strain relationship of the pipe material was determined by testing two longitudinal tension coupons with dimensions according to ASTM (1989) specifications. The location from which the tension coupons are cut and their dimensions are given in Figs. 2.4a and 2.4b, respectively. The tension tests were carried out using displacement control under a slow rate of loading to capture the static values of stresses. The load versus deformation response was recorded throughout the range of deformation and until rupture occurred. An extensometer of 50mm gage length was mounted on the central portion of the tension coupon to measure longitudinal strains. Two longitudinal (one on each side of the coupon) and two transverse strain gages were mounted on the central portion of the tension coupon. As the specimens were cut from the curved pipe surface, they had a slight curvature. In the absence of curved grips, the tests were performed with straight grips, which introduced slight eccentricity between the line of application of the tensile force and the center of gravity of the coupon cross-section. For small strain values, averaging the strain readings on both sides of the coupon eliminated the error due to eccentricity. After yield, only the extensometer readings gave reliable readings, and the strain gage readings were discarded.

As is illustrated in Fig. 2.5, the stress vs. strain curve of pipe steel exhibited gradual yielding (as opposed to a distinct yield plateau) and gradually entered into strain hardening range. The data used to obtain the stress vs. engineering strain curves is tabulated in Tables A.1 and A.2 in Appendix A. In ASTM standards, two methods are proposed to determine the yield strength of steel. These are: a) the offset method corresponding to a defined plastic strain (usually taken as 0.002), and b) extension-under-load method corresponding to a specified total strain (usually taken as 0.005). The two methods resulted an average yield strength prediction of 319 MPa and 330 MPa, respectively. Determination of these yield strength values for each stress vs. engineering

strain curve is illustrated in Figs. 2.6 and 2.7. Other section properties are summarized in Table 2.2.

2.5.2 Experimental setup

The experimental program was carried out at the Structural Engineering Laboratory of University of Ottawa. The test setup is illustrated in Fig. 2.2. The pipe specimen was positioned vertically and welded to a 1219x1219x76.2mm base plate with a SMYS of 300MPa. The thickness of the base plate was judged to prevent potential warping of the specimen in the post buckling state. The plate was restrained from moving horizontally by means of two shear keys installed on compression side of the base plate. The diameter of the shear keys $d_s = 75mm$ was $1mm$ less than the diameter of the holes in the concrete floor in order to ensure near perfect contact between the shear keys and the holes in the concrete floor, thus preventing lateral displacements of the plate during the test. On the tension side of the base plate, potential uplift was prevented by means of two anchor rods with a diameter $d_r = 70mm$. The top of the specimen was welded to a 457x457x50.8mm plate with a SMYS of 300MPa. The top plate was fillet welded all around its perimeter to the bottom of the loading arm. The loading arm (Fig.2.8) consisted of a built up section, fabricated by welding four 22 mm thick 457x2.590 plates (300W material) by means of full penetration welds at the plate corners. Three sets of four holes were flame cut along the length of the loading arm in order to provide three possible attachment locations for the hydraulic jack to vary the eccentricity, b, accordingly. The centerlines of three sets of holes were 914mm apart. A 1.000 kN MTS hydraulic actuator (Fig.2.9) with a maximum stroke of $\pm 250mm$ (a total of 500mm difference between the longest and the shortest positions) was used to provide a horizontal force at an eccentricity, b, from the centerline of the specimen. The actuator was pin connected to the loading arm while bearing on a stiff loading frame (Fig. 2.10) at the other end. The experimental setup is illustrated in Fig. 2.11.

2.5.3 Fabrication Sequence

Each of the six specimens was beveled at both ends at an angle of nearly 35^0 (Fig. 2.12). The pipe was centered on the base plate then welded through a three-pass weld. The loading arm was then positioned horizontally and then welded to the top plate of the specimen, which was centered relative to the specimen centerline.

A rigid loading frame was used to provide a longitudinal support to the actuator. One end of the actuator was bolted to the frame at the desired height and the other end bolted to the loading arm. Prior the application of any loads, the stroke was at its longest position. The jack was electronically controlled to reduce its stroke by specified incremental amounts throughout the test. Under this arrangement, the force provided by the hydraulic jack was tensile throughout the test, thus avoiding potential buckling of the testing frame.

After each test was completed, the specimen was flame cut at the top and bottom ends, and removed. The surface of the base and top plates were ground smooth and the process was repeated for the next specimen. While the loading frame was kept in its position (Fig. 2.2) throughout all six tests, the position of the base plate was changed between tests to accommodate various eccentricities (b).

2.5.4 Load Measurements

The stroke of the actuator was gradually reduced resulting in an application of the external force, P, to the specimen located at a distance b from the pipe centerline (Fig. 2.13). The reactions, V, M, and T, at the bottom section of the specimen are P, Pa, and Pb, respectively. After each stroke decrement, the stroke was kept constant for three to four minutes before a set of electronic measurements was recorded. The pause allowed the readings to stabilize, thus eliminating any artificially high load readings due to material viscous effects. Special care was given to capture the points of initiation of local buckling.

2.5.5 Instrumentation

Eight strain gauges provided longitudinal and transversal readings. Electronic displacement devices including temposonics, linear variable differential transducers (LVDTs), and cable transducers (PT101s) were used to measure the displacements at the locations illustrated in Fig. 2.14a, depending on the spatial constraints.

The strain gauges were located 50mm above the bottom end between the base plate and the bottom of the specimen. Fig. 2.14b shows the locations of the strain gauges along the pipe circumference. Strain readings on the compression side of the specimen were reliable only before local buckling. Because the position of the strain gauges relative to the location of the local buckle strongly influences their readings, the longitudinal compressive strains in the post buckling range of the deformation are judged to be of little value.

From the horizontal displacement readings taken at points 1, 2 and 8, the angle of twist and the lateral displacement at the top of the specimen can be determined. Displacements along the initial direction of the loading arm were measured at point 7. Displacement measurement devices at points 3 through 6 provided readings of the movements of the specimen in the plane including the centerline of the specimen and that of the loading arm. The displacement measuring devices used for each test are listed in Table 2.3

2.6 Experimental Results

2.6.1 Buckling Patterns and Location

All specimens initiated local buckling near the bottom end. Figs. 2.15 and 2.16 show the final buckled configurations of the specimens tested along directions CG and AE in Fig. 2.14b, respectively. Specimens V17T00M98 and V25T00M97, under no twist, exhibited a single outward bulge local buckle on the compression side after the peak point was attained. The buckle resembled to those obtained in Mohareb et al. (1994) under bending.

axial force and internal pressure. The buckle was symmetric about the plane of bending. For specimens V15T86M31 and V24T71M51, local buckling initiated at location G on the neutral axis (at the location where the shear stresses induced by twist and shear were additive). The buckle then progressed to cover the whole height of the specimen. The crest of the buckle seemed to form a line inclined at 45 degrees with the horizontal plane. The remaining specimens V12T68M66, V13T77M51 initiated buckling at the point of maximum compressive stresses and buckling patterns assumed an asymmetric mode as the test progressed. At the end of the test, the buckles were localized over a shorter height of the specimen than specimens V15T86M31 and V24T71M51 but larger than those of specimens V15T86M31 and V24T71M51. The crest line of the buckle was inclined at a milder angle (close to 30 degrees with the horizontal).

2.6.2 Load vs. Deformation

The jack load vs. applied stroke is plotted in Fig. 2.17 for the six specimens tested. All specimens exhibited softening characterized by the negative slope of the curve after a peak value of the load is reached. In all cases, the softening behavior seemed to take place after the onset of local buckling. The buckled configurations of all specimens are illustrated in Fig 2.18. The recorded peak forces were in close agreement with those predicted by Eq. 2.7. The location of the sensors and data collected from the sensors can be seen in Figs. A.1 through A.6, and Tables A.3 through A.25 in Appendix A, respectively.

2.6.3 Comparison between Experimental and Analytical Results

The experiments aimed at assessing the validity of the interaction equations developed in Mohareb (2002a) and Mohareb (2002b). Under an applied load P, the reactive stress resultants at the bottom section of the pipe are Pa, Pb, and P, respectively. By substituting into Eq. 2.7, a value of P is obtained. This magnitude is referred to as P_{a1} for F_y=330MPa (the yield strength obtained from extension-under-load method) P_{a2} for

F_y=319MPa (the yield strength obtained from offset method) and. Table 2.4 summarizes the value of P_{u1} and P_{u2} for the six tests. The experimentally obtained jack forces P_e are provided for comparison. The ratio (P_{u1}/P_e) varied between 90% and 97%. with an average value of 94% and a standard of deviation of 2.5%. The ratio (P_{u2}/P_e) varied between 86% and 94% and a standard of deviation of 2.8% indicating a very close agreement between analytical predictions and experimental results.

2.7 Design Example

A pipe has an average diameter of 318mm and a thickness of 6.4mm. The specified minimum yield strength of the pipe steel is 359MPa. It is required to determine whether the pipe can withstand the following combination of internal forces. based on yielding considerations. Twisting moments T=60kNm. bending moments M_y=120kNm and M_z=50kNm. compressive axial force A=200kN. shearing forces V_y=36kN and V_z=48kN. and internal pressure p=10MPa.

The diameter to thickness ratio for the pipe is 51 compared to limiting values of D/t of 65.7 and 51.4 for pure bending and pure compression. respectively. based on classifications limits given in CAN/CSA S16-2001. This value suggests that the fully plastic capacity of the pipe under axial force and bending moments is likely to be attained prior the occurrence of localized strains. Similar limiting values for shear and twist are not available. Nevertheless. it will be assumed that shear and torsion will not result into local buckling prior the fully plastic resistance of the section is mobilized. The limiting resistances for twisting moments. bending moments. axial forces. shearing forces. and internal pressure are T_p=208.4 kNm. M_p=229.8 kNm. A_y=4547.7 kN. V_p=835.8 kN. and p_y=14.7MPa. respectively. The corresponding resistance ratios are $T_r = 0.288$. $M_{ry} = 0.522$. $M_{rz} = 0.218$. $A_r = -0.044$. $V_{ry} = 0.043$. $V_{rz} = 0.057$. and $p_r = 0.682$. Checking whether the given shear-twist combination lies within the domain defined with Eqs. 2.3a. b. c reveals that the twisting moment-shearing force combination is attainable. The corresponding shear stress ratio τ_r is determined from Eq. 2.2 as 0.330. Based on

this value, the pressure limit check given in Eq. 2.4 is performed. Bounds for p_r are found as $-1.088 \le p_r \le 1.088$. This condition is met for the computed value of $p_r = 0.682$. Next, the axial force limit check as per Eq. 2.5 is performed, leading to the condition $-0.393 \le A_r \le 1.076$. The calculated value $(A_r = -0.044)$ lies within the acceptable range. The final step is to calculate the maximum resultant moment ratio from Eq. 2.1. The equation predicts a maximum resultant moment ratio $M_r = \sqrt{M_{ry}^2 + M_{rz}^2}$ of 0.499, which is less than the applied resultant moment ratio of $M_r = \sqrt{M_{ry}^2 + M_{rz}^2} = 0.566$. Therefore, the section is judged inadequate and a thicker pipe section should be considered. The procedure can be easily modified to incorporate the resistance factors commonly used in limit state design codes by dividing the ratios T_r, M_{ry}, M_{rz}, A_r, V_{ry}, V_{rz}, and p_r by the appropriate resistance factor ($\phi = 0.9$ in CAN CSA-S16-2001) and repeating the procedure on the amplified force ratios.

2.8 *Conclusions and Recommendations:*

The project investigated the plastic capacity and post-buckling behavior of the compact pipe sections under the action of shear force, bending moments, and torsion. The principal conclusions of the work are as following.

1. All specimens exhibited significant deformations in the plastic range of deformation. The onset of local buckling was detected immediately prior the attainment of their peak load.

2. The pipe post buckling behavior is characterized by softening of the resistance curve as a single wrinkle develops and amplifies.

3. The local buckling configuration is highly dependant on the bending, torsion, and shear ratios. For the short specimens (V15T86M31 and V24T71M51) with lower bending moments and higher torsion and shear, wrinkling appeared as a

diagonal buckle. For the medium and tall specimens V12T68M66 and V13T77M51 with lower shear force and higher bending moment and torsion, a wrinkle initiated at the maximum compression fiber and progressed into an un-symmetric mode. For specimens with no torsion but with high bending moments and relatively low shear, V17T00M98, and V25T00M97, an outward bulging local buckle symmetric about the plane of bending was observed.

4. For all tests, the interaction equations in Mohareb (2002a) predicted a lower capacity than those recorded in the tests. The average ratio between the experimental results and the analytical predictions is 94% based on the yield strength determined by extension-under-load method and 91% based on offset method. Strain hardening effects, which were not taken into consideration in formulations, are responsible for this under estimation. This experimental validation is believed to be an important step in adopting Eqs. 2.1 and 2.2 into design codes.

5. Based on the experimental program presented in this section and the one reported in Mohareb and Murray (1999), it can be concluded that for steel pipes with yield strength close to 350 MPa and with diameter to thickness ratios of 41 and less, the interaction relations developed in Mohareb (2002a) and Mohareb (2002b) yield very good predictions and are recommended for pipeline design.

6. The conservative predictions of the analytically derived interaction relations suggest it is possible to extend the applicability of the interaction relations to thinner pipes with D/t in excess of 41. However, experimental evidence is needed prior making conclusive design recommendations in this regard.

7. Current design codes include the conditions under which a tubular section can develop its fully plastic capacity prior undergoing local buckling under the effect of pure bending moments or pure axial compressive forces are given as a function of the D/t ratio and yield strength of the pipe. Under more complex

loading conditions including twist, shear, and internal pressure, similar limiting conditions are not known. A comprehensive finite element analysis and corroborative experimental study is needed in order to define these limiting conditions.

References for Chapter 2

ASTM (1989). *American standard test methods for tension testing of metallic materials [Metric]*', designation E 8M-89. USA.

AISC. (1999). *Load and resistance factor design specification for structural steel buildings*. American Institute of Steel Construction. Chicago.

Bai. Y., and Hauch. S., (1998). "Analytical Collapse Capacity of Corroded Pipes". Proc. of the 8th *Inter. Offshore and Polar Eng. Conf.*, Vol. II. Montreal. pp.182-188

Batterman. S.C. (1965). "Plastic buckling of axially compressed cylindrical shells." AIAA J., 3(2). 316-325.

Boresi. A. and Sidebottom. O. (1985). *Advanced mechanics of materials*. 4th Ed., Wiley. New York.

Bouwkamp. J. G., and Stephen. R. M. (1973). "Large diameter pipe under combined loading." *Transp. Engrg. J.*, ASCE. 99(3). 521-536.

CAN CSA-S16.1 (1974). [Canadian Standards Association. CSA (1974)] Canadian Standards Association. Rexdale. Ont.

CAN CSA S16 (2001). "Limit States Design of Steel Structures". Canadian Standards Association. Rexdale. Ont.

Chen. W. and Atsuta. T. (1972). "Interaction equations for biaxially loaded sections." *J. Struct. Engrg.*, ASCE. Vol. 98 (ST5). 1035-1051.

Det Norske Veritas. (1996). "Rules for Submarine Pipelines." Oslo. Norway.

Galambos. T. (1998) *Guide to stability design criteria for metal structures*. 5th edition. John Wiley & Sons. Inc.. New York. USA.

Gerald. G. and Becker. H.. (1957). "Handbook of Structural Stability. Part III-Buckling of Curved Plates and Shell". *National Advisory Committee for Aeronautics. Tech. Note* No. 3783.

Gellin. S. (1980). "The plastic buckling of long cylindrical shells under pure bending." *Int. J. Solids and Struct.*. 16. 397-407.

Gresnigt. A. M. (1986). "Plastic design of buried steel pipelines in settlement areas." *Heron*. 31(4).

Hodge. Ph. G. (1981). *Plastic analysis of structures*. Krieger. Malabar. Fla.

Mohareb. M. (2002a). "Plastic interaction relations for pipe sections.". *J. Eng. Mech.*. ASCE. Jan. Vol.128(1). 112-120.

Mohareb. M. (2002b). "Plastic resistance of pipe sections-an upper bound solution.". accepted for publication by *J. Struct. Eng.*. ASCE.

Mohareb.. M. (2001). "Exact yield hyper-surface for thin pipes.". *Int. J. of Pressure Vessels and Piping*.78(7). 507-514.

Mohareb. M. and Murray. D. W. (1999). "Mobilization of fully plastic moment capacity for pressurized pipes subjected to axial loading" *ASME J. Offshore Mech. Arct. Eng.*. 121 (4). 237-241.

Mohareb. M.. Elwi. A.. Kulak. G. L.. and Murray. D. W. (1994). "Deformational behavior of line pipe." *Struct. Eng. Rep. No. 202*. Dept. of Civ. Engrg.. University of Alberta. Edmonton. Alberta. Canada.

Morris, G. and Fenves, S. (1969). "Approximate yield surface equations". *J. Eng. Mech Division*, ASCE, Vol. 95 (EM4): 937-954.

Obaia, K. H., Elwi, A., Kulak, G. L. (1991). "Inelastic transverse shear capacity of large fabricated steel tubes." *Struct. Eng. Rep. No. 170*, Dept. of Civ. Engrg., University of Alberta, Edmonton, Alberta, Canada.

Pillai, S. U., and Ellis, J. S. (1971). "Hollow tubular beam-columns in biaxial bending." *J. Struct. Eng.*, ASCE, 97(ST5), 1399-1406.

Prion, H. and Birkemoe, P. (1988). "Experimental behaviour of unstiffened fabricated tubular steel beam columns." University of Toronto, Department of Civil Eng. Pub. No. 88-03, Toronto, Ont., Canada.

Reddy, B. D. (1979). "An experimental study of the circular cylinders in pure bending." *Int. J. Solids and Struct.*, 15(9), 669-683.

Sherman, D. R. (1976). "Tests of Circular Steel Tubes in Bending". *J. of Struct. Division*, ASCE, Vol.102, No. ST11, pp.2181-2195.

Timoshenko S. and Goodier J. (1987). *Theory of Elasticity*, 3rd Ed., McGraw-Hill, New-York.

von Karman, T. and Chien (1946). "Torsion with variable twist" *Journal of Aeronautical Sciences*, vol. 13, No.10, (1946), 503-510.

Yamaki, H. (1976). "Experiments on the postbuckling of the circular cylinder shell under Torsion." *Proc. IUTAM. Symp. Buckl. of Struct.*, Springer-Verlag, Heidelberg, pp. 312-330.

List of Symbols for Chapter 2

a	distance from the centerline of the loading arm to the critical section of the specimen (the bending arm)
A	internal axial force
A_r	ratio of the internal axial force (A) to the axial resistance (A_y)
A_y	axial resistance
b	distance from the centerline of the MTS Jack to the centerline of the specimen (eccentricity of the load applied)
d_a	diameter of the anchor rods
d_k	diameter of the shear keys
D	mean diameter of the pipe section
F_y	yield strength of the specimen material
$LVDT$	Linear variable differential transducer
M	bending moment at the critical section of the specimen due to the applied jack load
M_p	plastic moment resistance of the pipe section
M_r	resultant bending moment ratio $\left(\sqrt{M_{rx}^2 + M_{ry}^2}\right)$
M_{rx}	ratio of the internal bending moment (M_x) to plastic bending moment resistance (M_p)
M_{ry}	ratio of the internal bending moment (M_y) to plastic bending moment resistance (M_p)
M_x	internal bending moment with respect to x-axis
M_y	internal bending moment with respect to y-axis
p	pressure (positive for net internal pressure)
p_r	ratio of the pressure (p) to the yield internal pressure (p_y)
p_y	yield internal pressure
P	load applied by the MTS Jack
P_{a1}	analytically calculated jack load for F_y=330MPa (the yield strength obtained from extension-under-load method)

P_{u2}	analytically calculated jack load for F_y=319MPa (the yield strength obtained from offset method)
P_e	jack force recorded during experiments
PT101	cable transducer (deflection measurement sensor)
r	mean radius of the pipe section
SMYS	specified minimum yield strength
T	internal twisting moment
T_p	plastic twisting moment resistance of the pipe section
T_r	ratio of internal twisting moment (T) to plastic twisting moment resistance (T_p)
Temposonic	cable transducer (deflection measurement sensor)
V	shearing force at the critical section of the specimen due to the applied jack load
V_p	plastic shear resistance of the pipe section
V_r	resultant shear force ratio $\left(\sqrt{V_{rx}^2 + V_{ry}^2}\right)$
V_x	internal shearing force in the direction of x-axis
V_y	internal shearing force in the direction of y-axis
V_{rx}	ratio of the internal shearing force (V_x) to plastic shear resistance (V_p)
V_{ry}	ratio of the internal shearing force (V_y) to plastic shear resistance (V_p)
z_r	dimensionless parameter that intrinsically relates the twist and shear force ratios

Table 2.1 Pipe Geometry and Predicted Stress Resultants at Fully Plastic State

Test Descriptor	Specimen Height (mm)	Average Thickness (t) (mm)	Average Diameter-thickness Ratio D/t	Bending Moment Arm (a) (mm)	Eccentricity (b) (mm)	Predicted Stress Resultants*		
						Shear (kN)	Torsion (kNm)	Moment (kNm)
V15T86M31	422	9.23	44.0	727	1829	204	374	148
V12T68M66	1641	9.25	43.9	1946	1829	162	297	316
V17T00M98	1641	9.24	44.0	1946	0	243	0	474
V25T00M97	1032	9.23	44.0	1337	0	349	0	466
V13T77M51	1032	9.25	43.9	1337	1829	185	338	247
V24T71M51	422	9.26	43.9	727	914	337	308	245

*In the prediction of the stress resultants, the yield strength, F_y=330MPa, is used as determined by extension under load method from tension coupon tests.

Table 2.2 Material Properties

MATERIAL PROPERTIES	TENSION COUPON TEST-1	TENSION COUPON TEST-2	AVERAGED VALUES
Modulus of Elasticity (MPa)	189,090	187,255	188,172
Yield Strength determined by offset method (MPa) (Specified offset value=0.002)	325	313	319
Yield Strength determined by Extension-under-load method (MPa) (Specified extension under load value=0.005)	338	322	330
Poisson's Ratio	0.26	Not obtained	

Table 2.3 Deflection Measurement Devices

TEST DESCRIPTOR	Location of the Deflection Measuring Devices in Fig. 2.14a							
	1	2	3	4	5	6	7	8
V15T86M31	LVDT 1	LVDT 2	PT101-A	LVDT 4	PT101-B		LVDT 3	
V12T68M66	Temposonic 3	Temposonic 1	LVDT 2	PT101-B	PT101-A		Temposonic 2	
V17T00M98			LVDT 2	PT101-B	LVDT 4	PT101-A	Temposonic 2	Temposonic 1
V25T00M97			LVDT 2	PT101-B	LVDT 1	PT101-A	Temposonic 2	Temposonic 1
V13T77M51	Temposonic 1	Temposonic 2	LVDT 2	PT101-B	PT101-A		Temposonic 3	
V24T71M51	Temposonic 1	Temposonic 2	LVDT 2	PT101-A	LVDT 4			

Table 2.4 Comparison Between Experimental and Analytical Results

Test Descriptor	P_{a1}[1] (kN)	P_{a2}[2] (kN)	P_e[3] (kN)	P_{a1}/P_e	P_{a2}/P_e
V15T86M31	204	197	210	0.97	0.94
V12T68M66	162	157	171	0.95	0.92
V17T00M98	243	235	253	0.96	0.93
V25T00M97	349	337	370	0.94	0.91
V13T77M51	185	178	198	0.93	0.90
V24T71M51	337	326	377	0.90	0.86
			Average	0.94	0.91
			Standard deviation	2.5%	2.8%

[1] The actuator load calculated analytically by using the yield strength value obtained from extension-under-load method

[2] The actuator load calculated analytically by using the yield strength value obtained from offset method

[3] Actuator load recorded during experiments

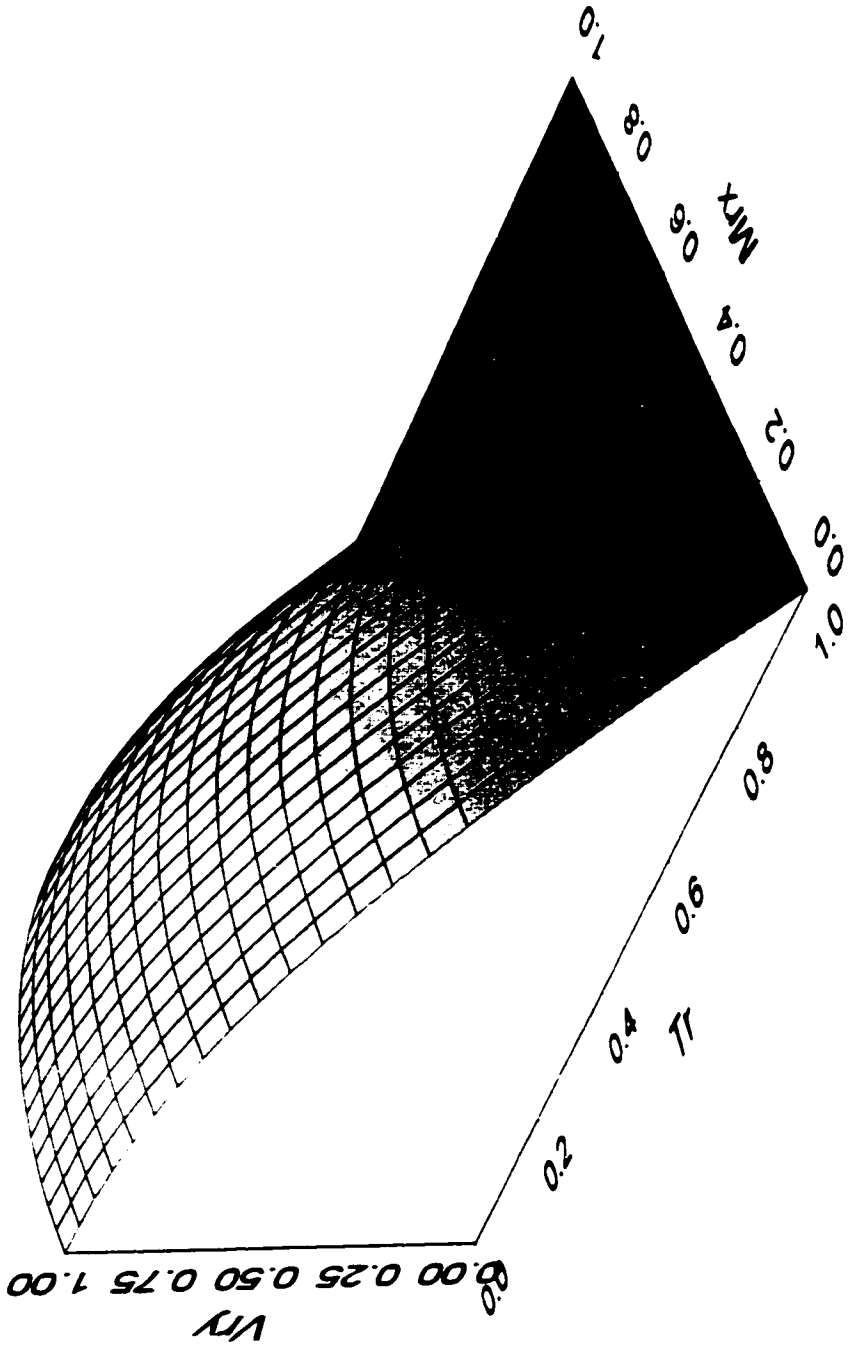

Figure 2.1 Shear-Twist-Bending Interaction Surface

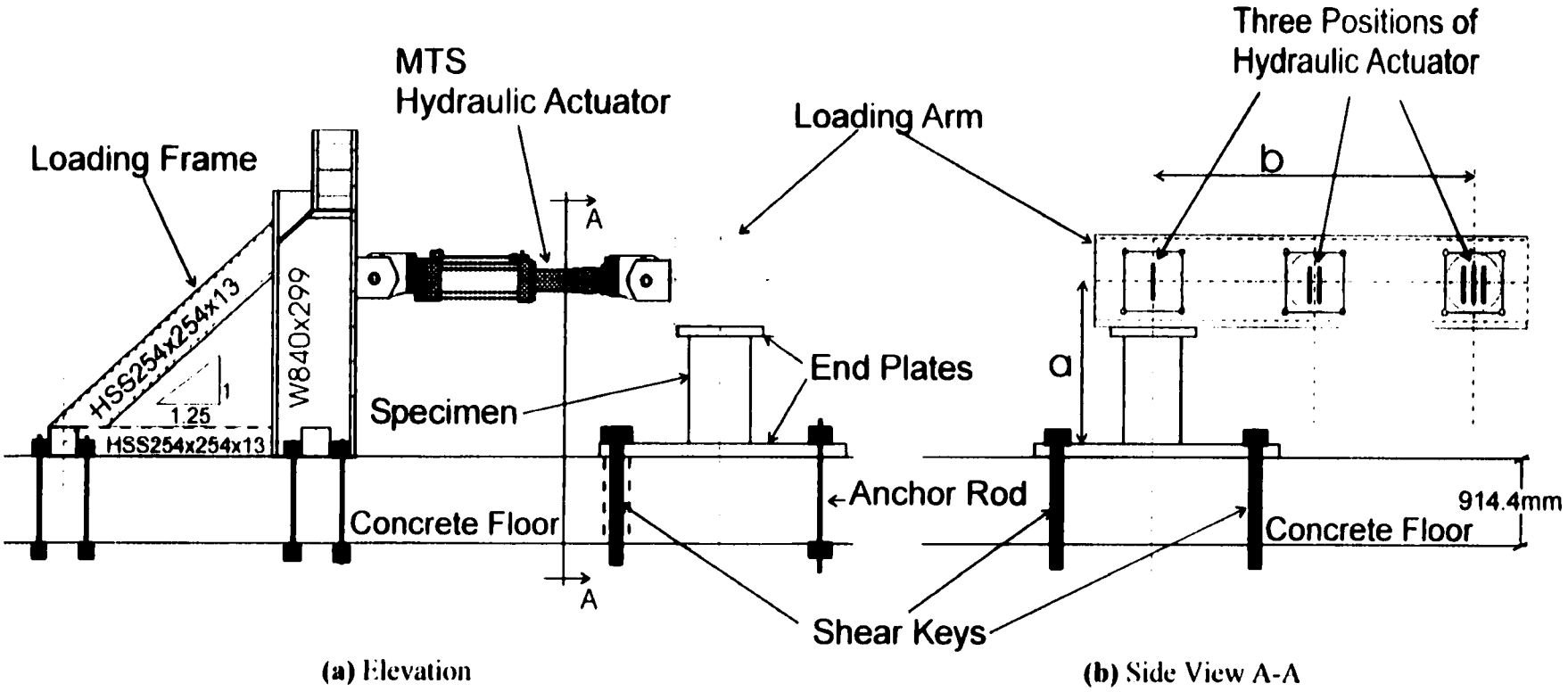

(a) Elevation (b) Side View A-A

Figure 2.2 Test Setup

Figure 2.3 Different Heights of the Specimens

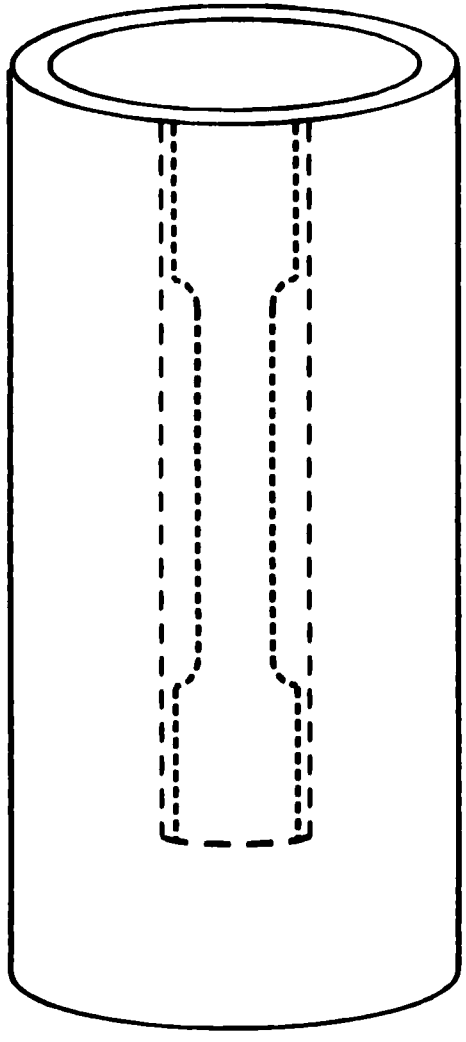

(a) Location from Which Longitudinal Tension Test Specimens are Cut

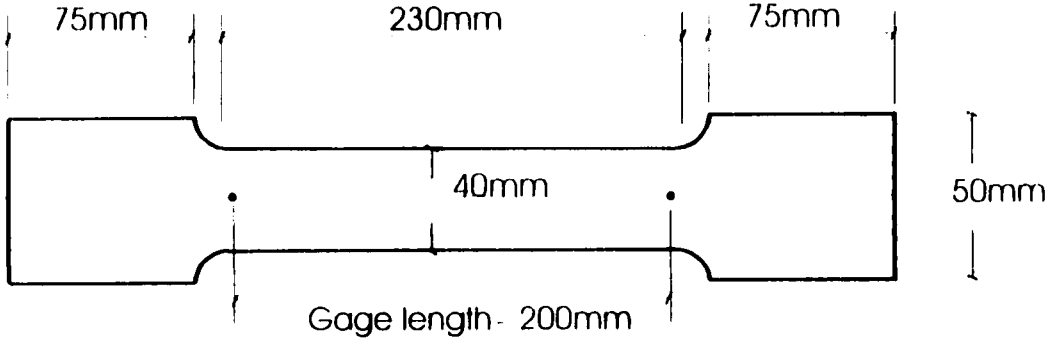

(b) Tension Coupon Test Specimen

Figure 2.4 Tension Coupon Test Specimen Location and Dimensions

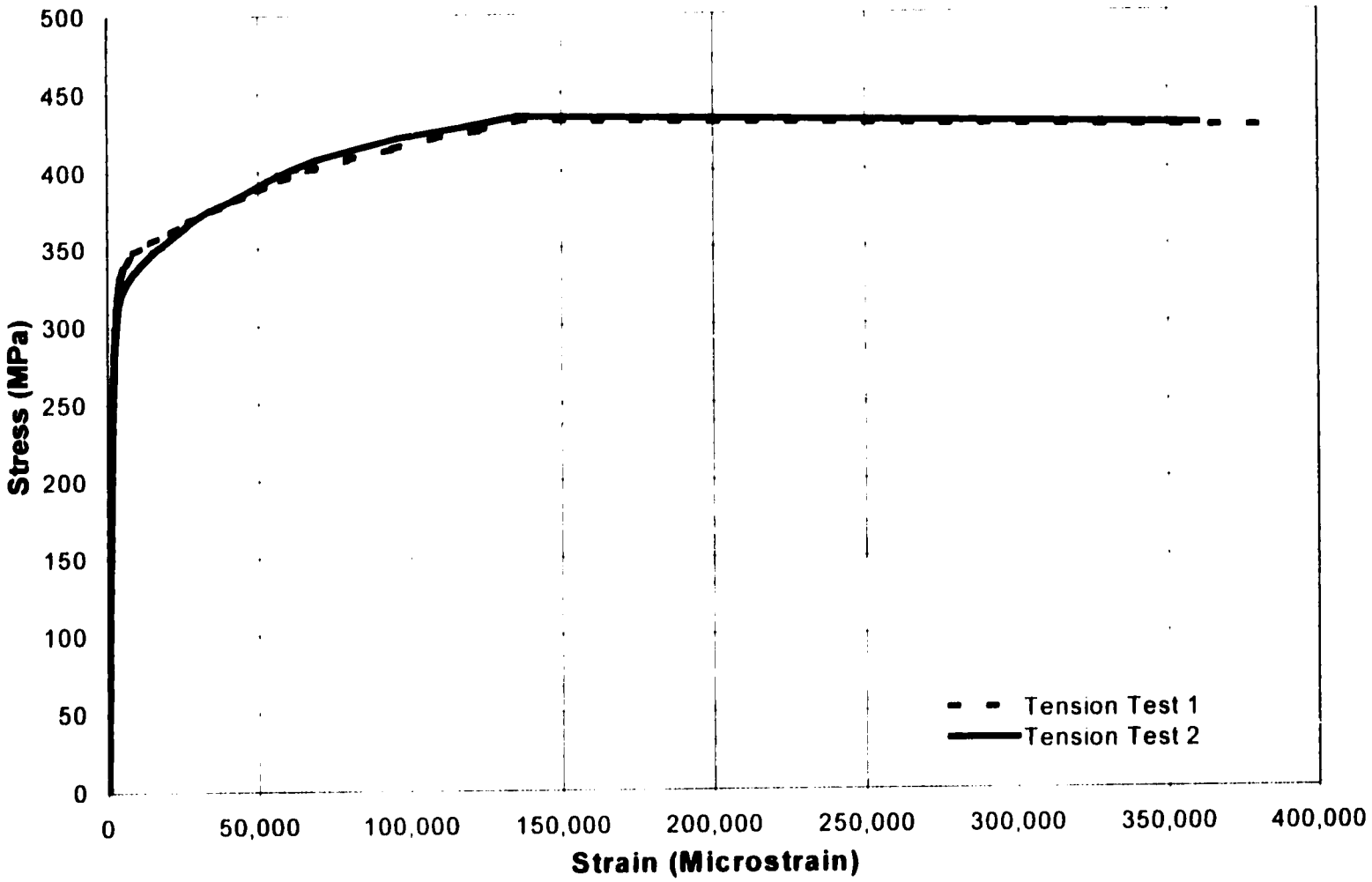

Figure 2.5 Stress vs. Engineering Strain Curves of the Tension Coupon Tests

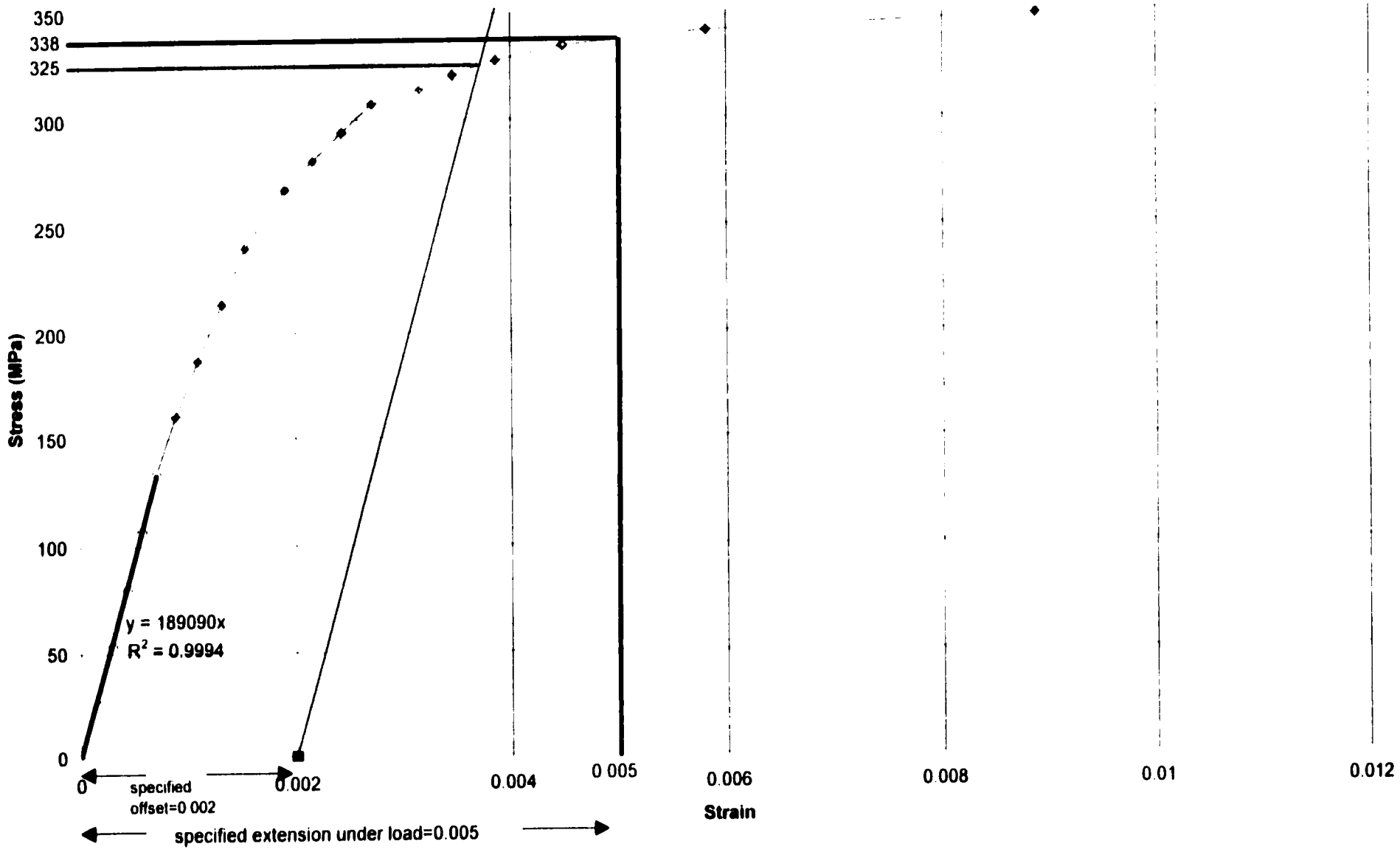

Figure 2.6 Estimating the Yield Strength (Tension Coupon Test 1)

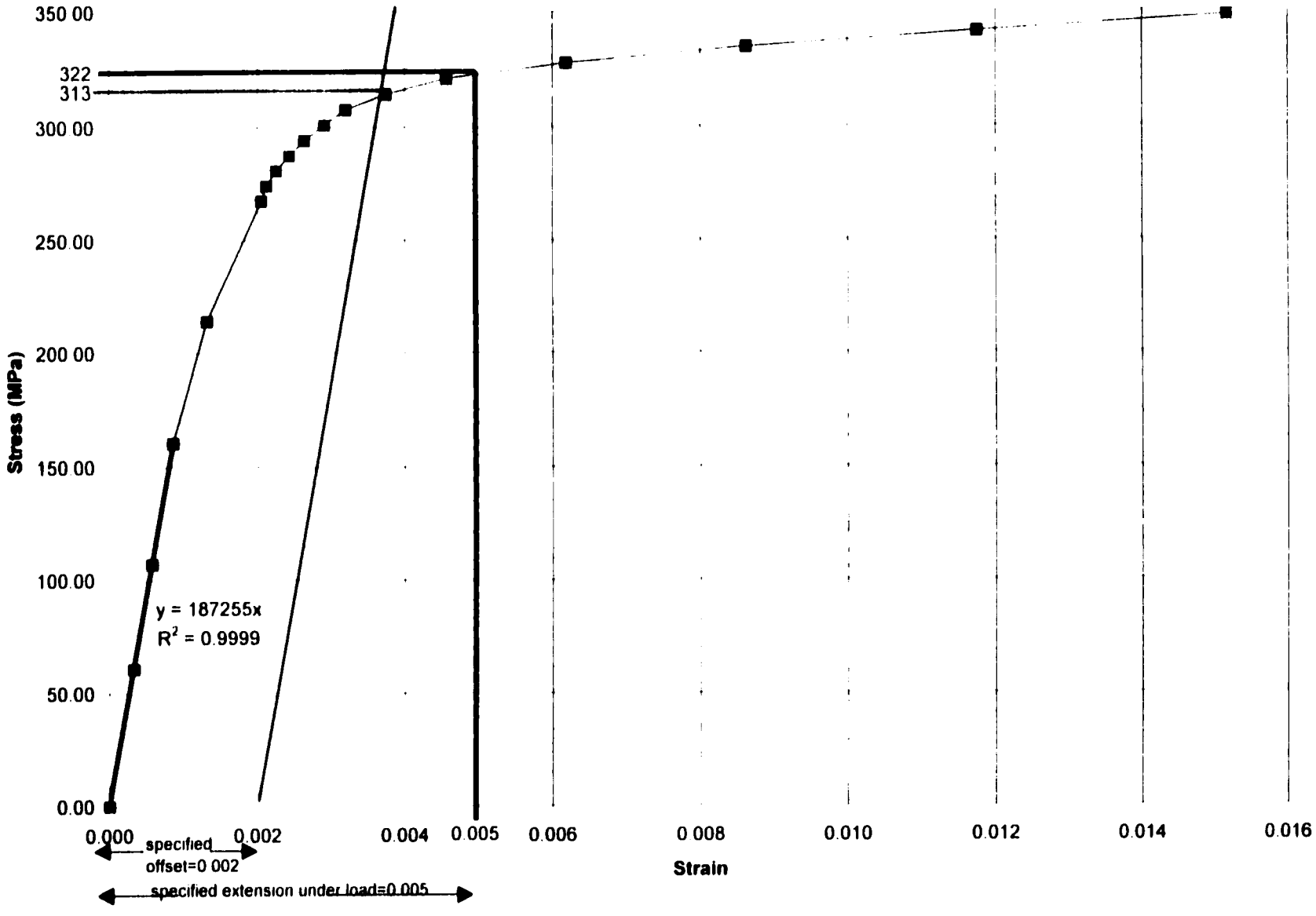

Figure 2.7 Estimating the Yield Strength (Tension Coupon Test 2)

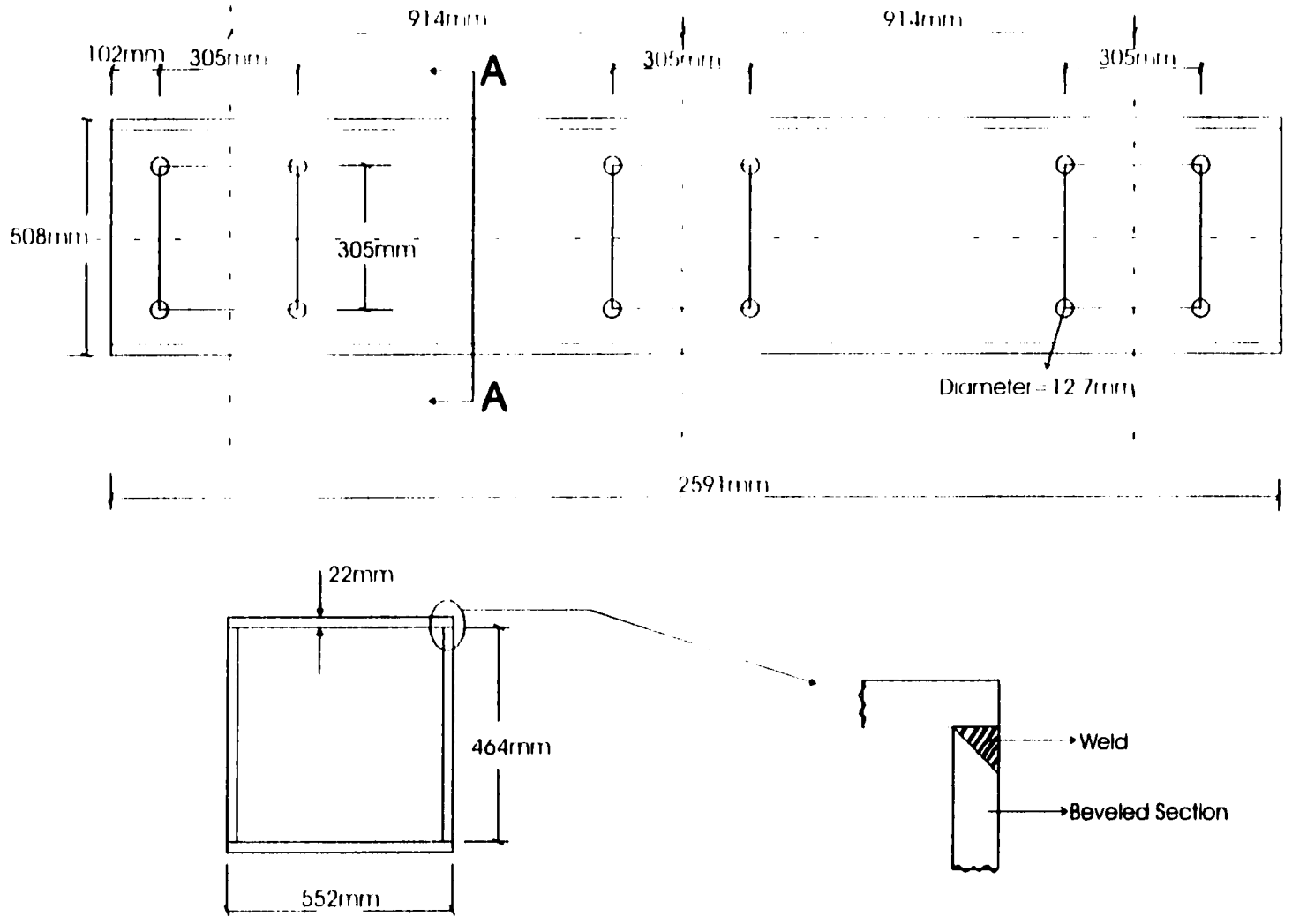

Figure 2.8 Loading Arm

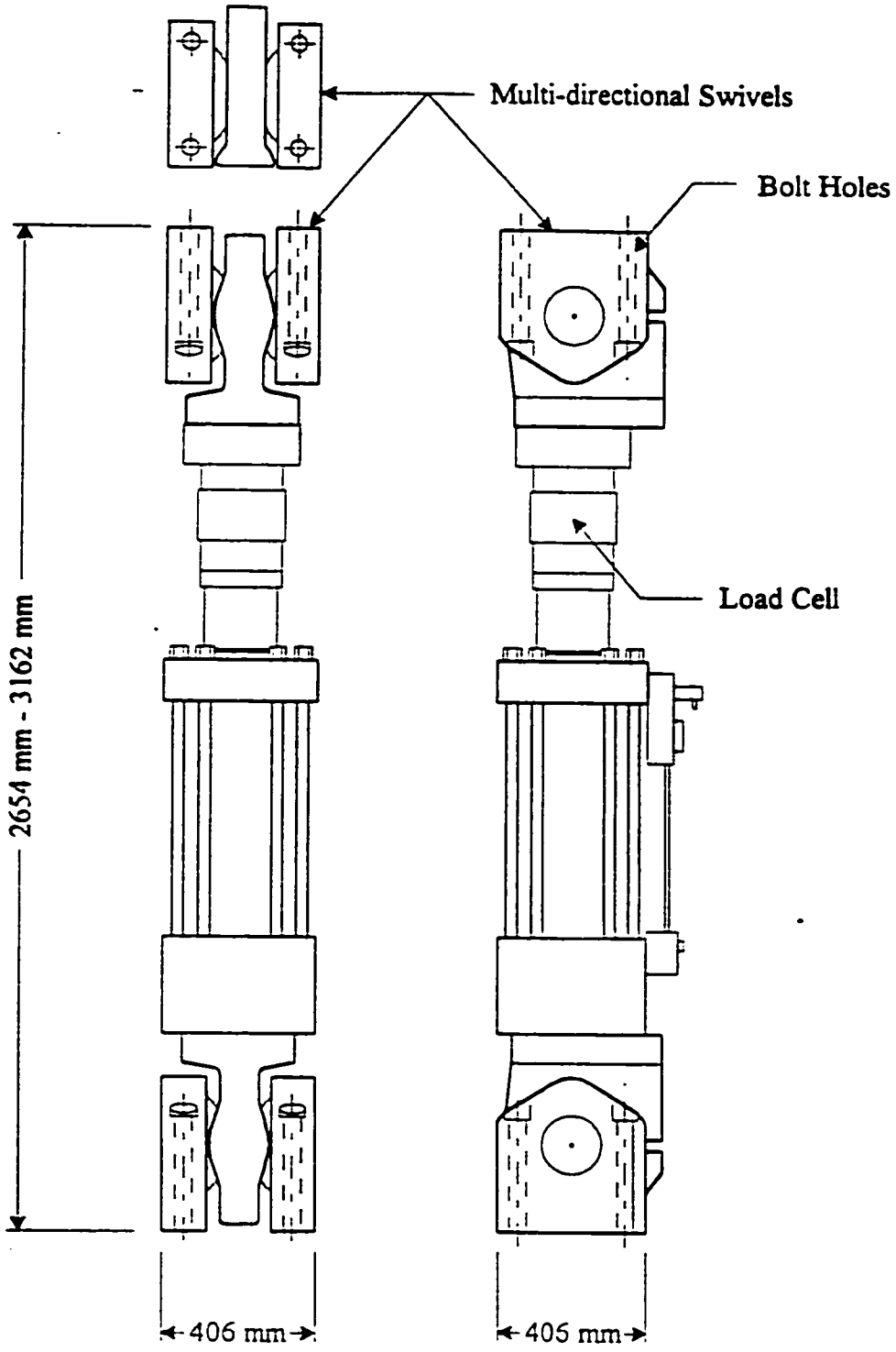

Figure 2.9 Details of the MTS Actuator

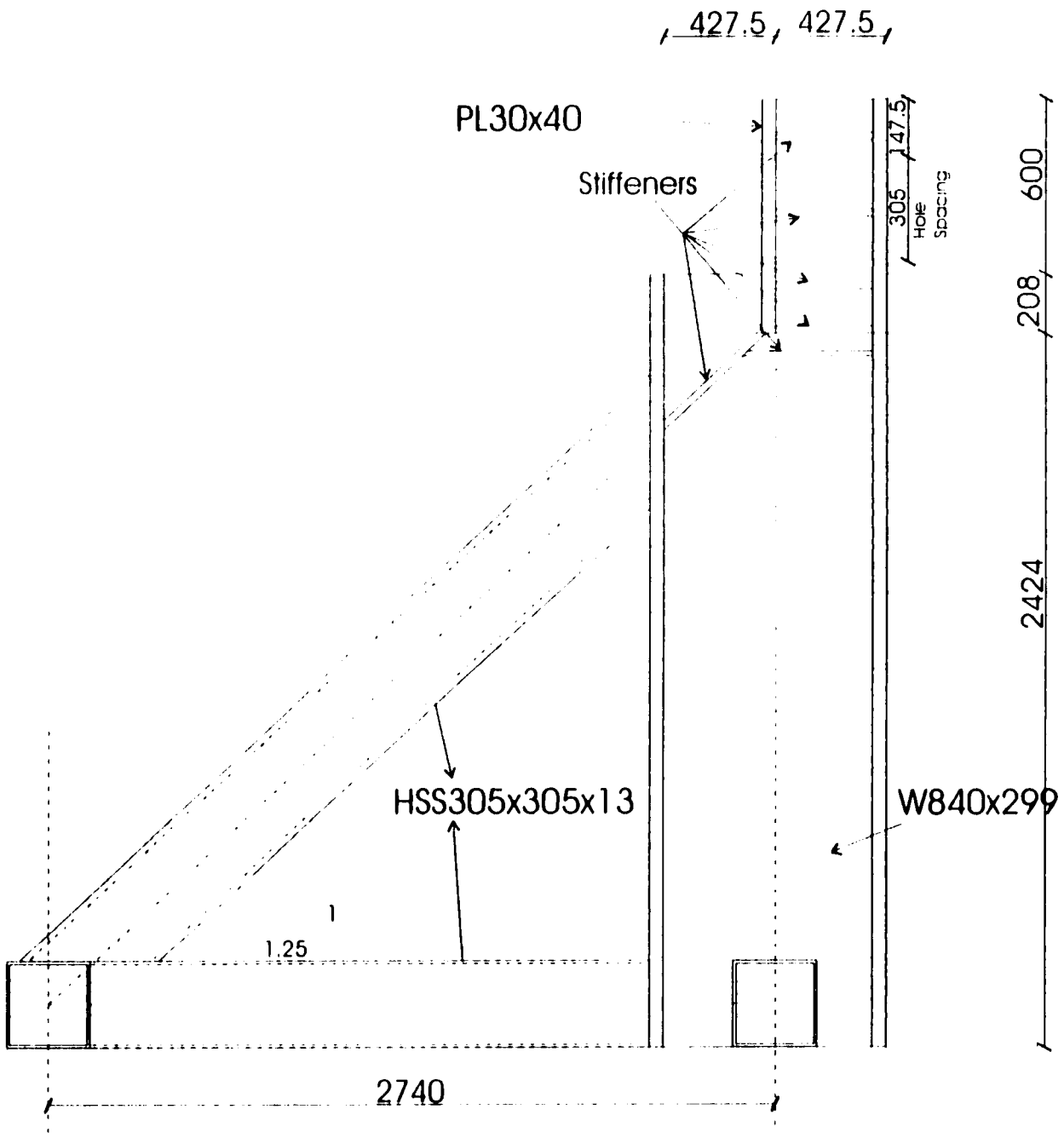

Figure 2.10 Loading Frame

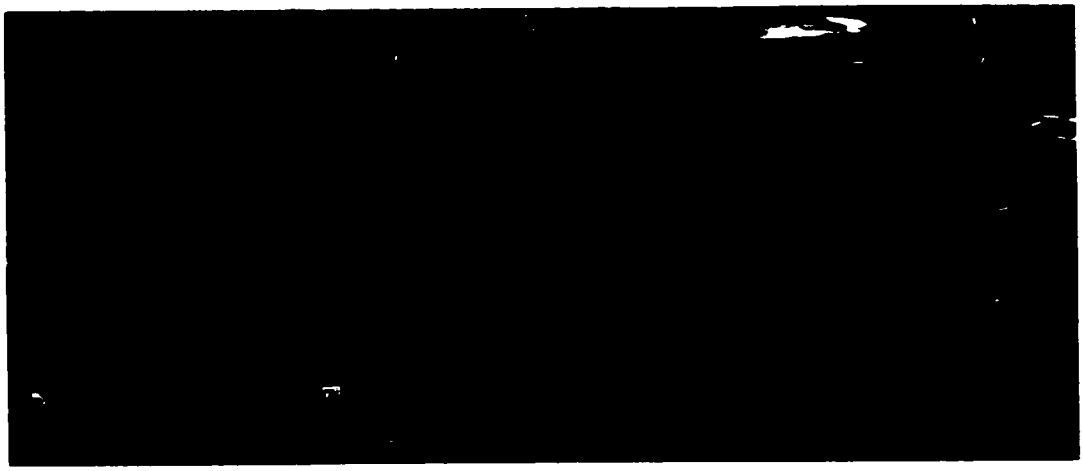

(a) Specimen V15T86M31 (before the sensors attached)

(b) Specimen V15T86M31 (after the sensors attached)

Figure 2.11 Experimental Setup

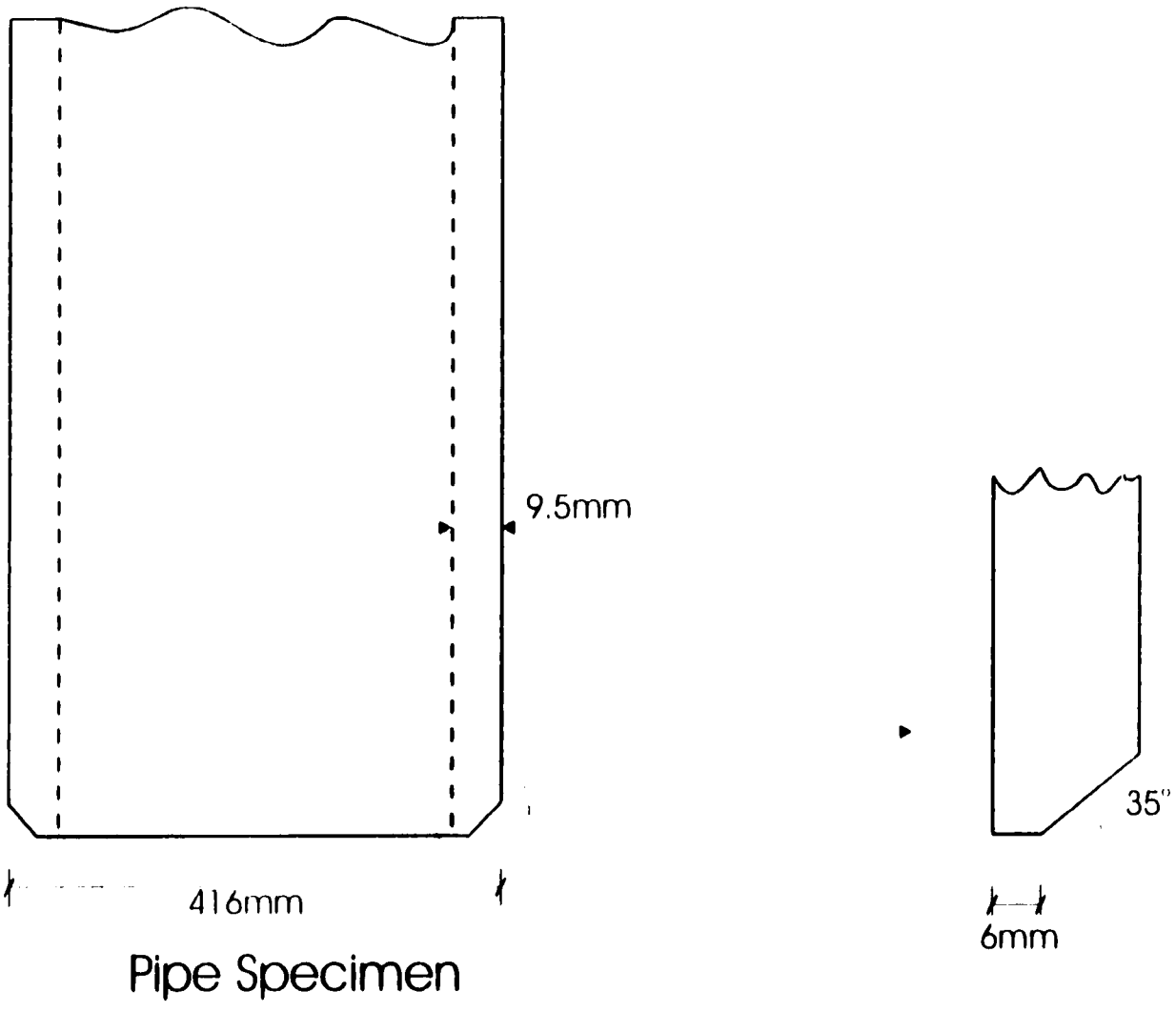

Figure 2.12 End Beveling

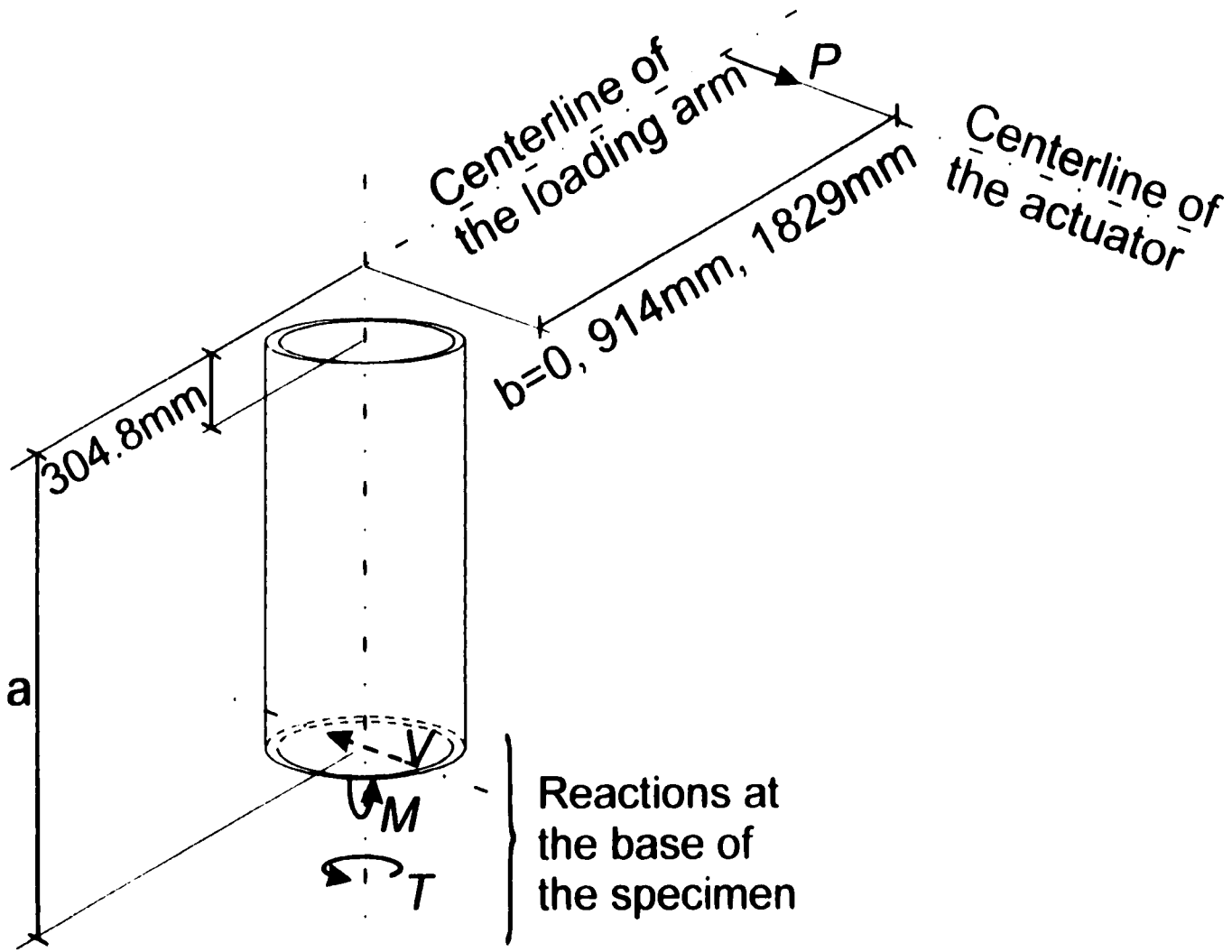

Figure 2.13 Free-body Diagram of the Tests

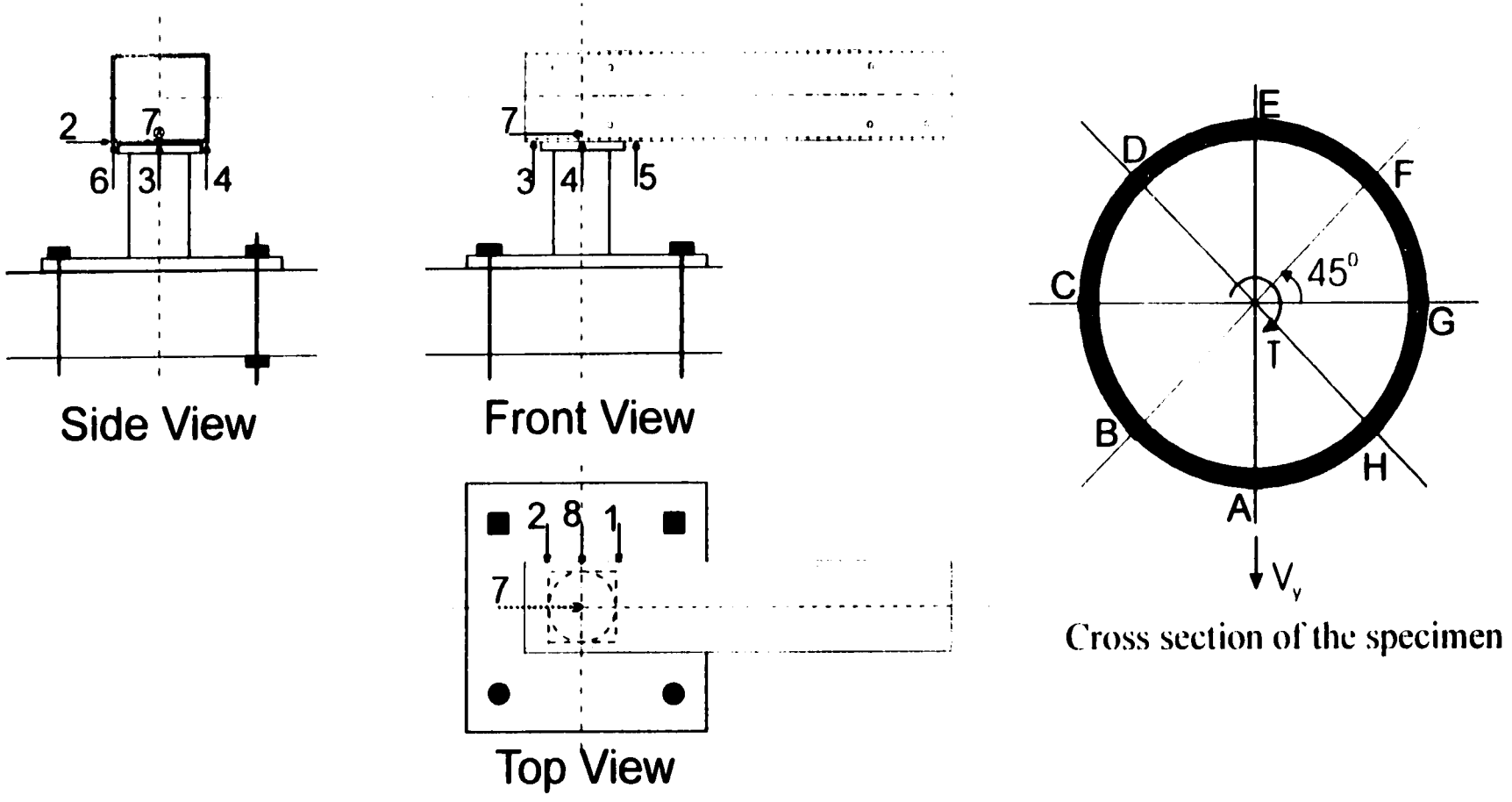

(a) Deflection Measurement Devices

(b) Strain Gages

Figure 2.14 Deflection and Strain Measurement Devices

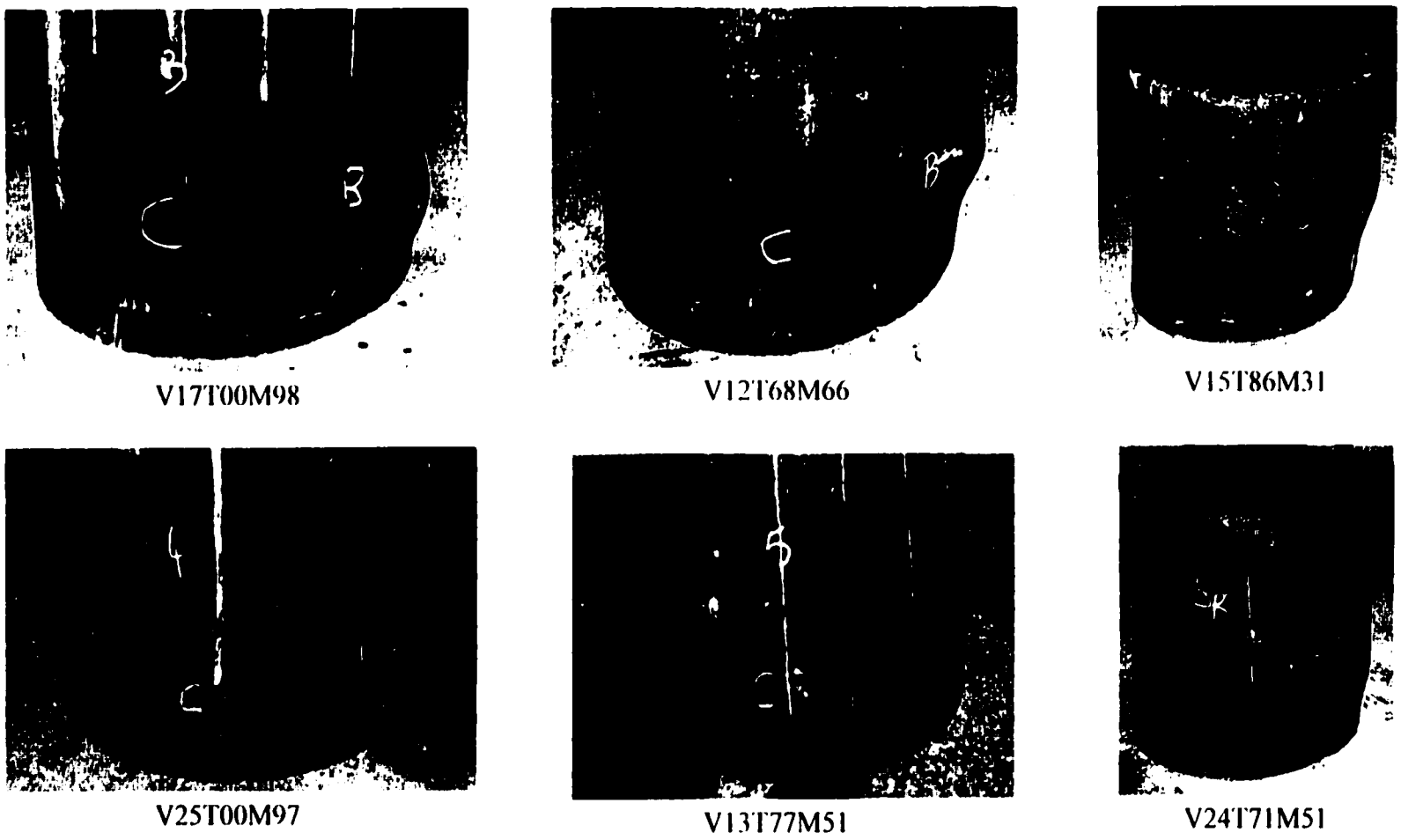

Figure 2.15 Buckled Configurations (Side View Looking along CG)

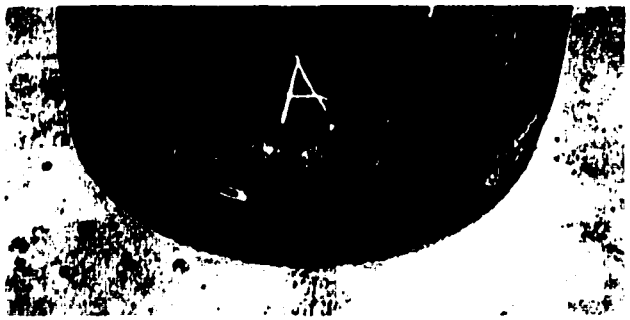

V17T00M98

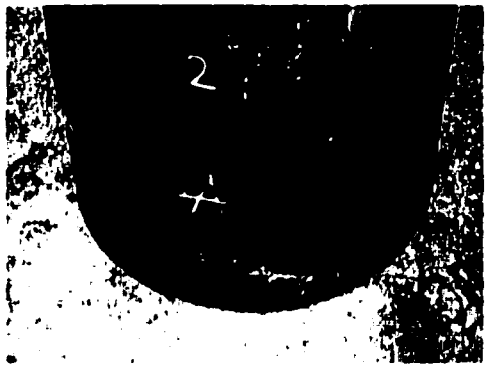

V12T68M66

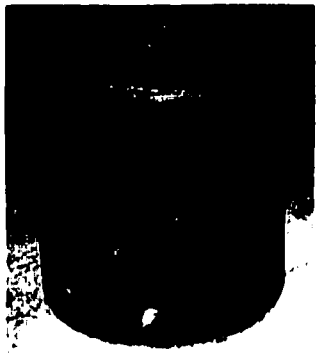

V15T86M31

V25T00M97

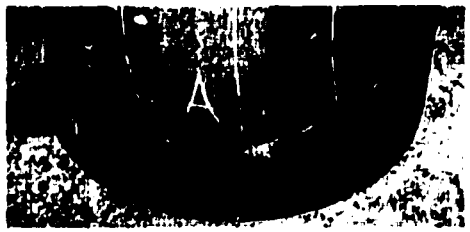

V13T77M51

V24T71M51

Figure 2.16 Buckled Configurations (Front View Along AE)

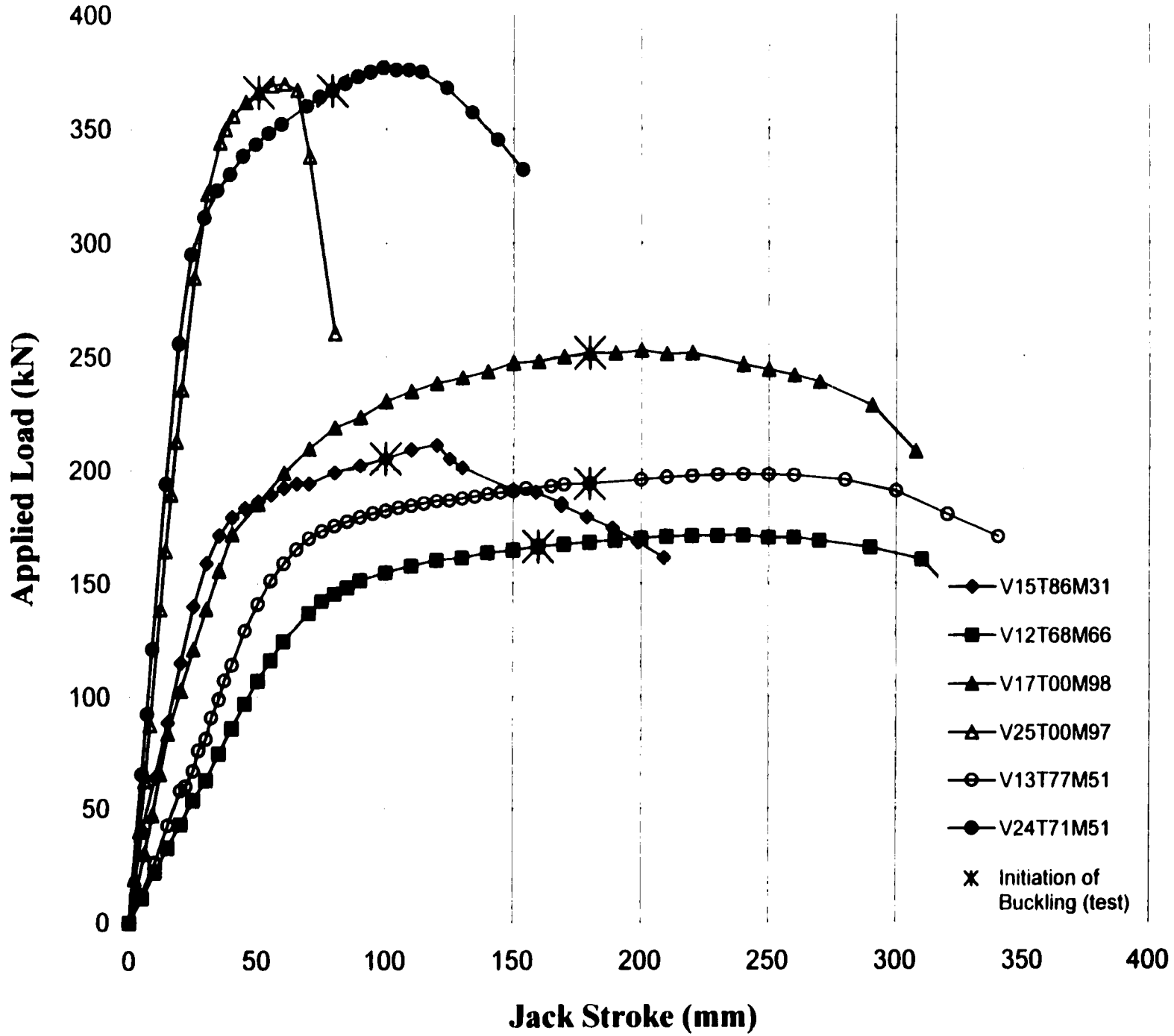

Figure 2.17 Applied Load vs. Jack Stoke

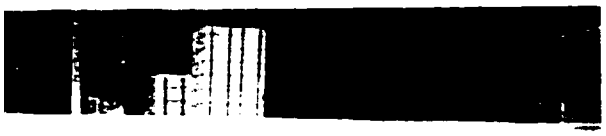

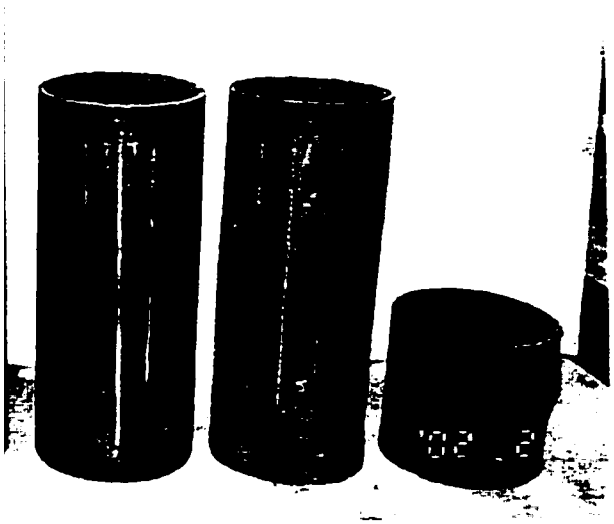

View AE

iew GC

Shapes of the Specimens

CHAPTER 3

PLASTIC INTERACTION RELATIONS FOR SQUARE HOLLOW STRUCTURAL SECTIONS

3.1 Introduction

In this Chapter, general interaction relations and their applicability limits for hollow structural square sections subject to combinations of normal force, twisting moment, biaxial bending moments, and biaxial shearing forces are developed.

In current steel structures codes such as AISC LRFD (1999) and CAN/CSA S16 (2001), general plastic interaction relations including the effect of torsion and shear is unavailable. The objective of this chapter is to partially fill this void.

3.2 Literature Review

General principles for the analytical developments of lower bound and upper bound plastic interaction relations are presented in Chen and Atsuta (1972) and Hodge (1981). Early work by Gaydon and Nutall (1957) resulted in upper bound interaction relations for hollow rectangular sections subject to combined twisting and uniaxial bending moments. Morris and Fenves (1969) established lower bound plastic interaction relations for thin walled hollow structural rectangular sections under combinations of biaxial bending, torsion, and axial forces. Chen and Atsuta (1972) formulated lower and upper bound interaction relations for box sections under biaxial bending and axial forces. The agreement between the two bounds demonstrated the exactness of their solution (within the limitations of the formulation). Their solution was also found to agree with those developed by Morris and Fenves (1969) when the torque term is omitted. Pillai and Ellis (1971) conducted an experimental study on hollow structural sections subject to

combined axial forces and uniaxial bending moments and proposed a simplified interaction relation based on their work. Interaction relations for square hollow structural beam columns subjected to bi-axial moments and axial forces were proposed by Pillai (1974) and later verified by an experimental investigation conducted by Pillai and Kurian (1977) on ten full-scale tests. Pillai's interaction relations were adopted in the CAN/CSA-S16.1-1974 [Canadian Standards Association. CSA (1974)] and subsequent versions for the strength design of compact sections (Classes 1 and 2). The effect of residual stresses on the plastic resistance of welded box sections was investigated by Zhou and Chen (1986). None of the solutions enumerated incorporate the effect of shear, a feature that is added in this chapter.

3.3 Statement of the Problem

Interaction relations for hollow structural square sections subjected to the combined action of the axial force, twisting moment, biaxial bending moments, and biaxial shearing forces are sought. It is assumed that the fully plastic resistance of the cross-section (commonly referenced as the cross-sectional capacity limit state in the design codes) will be attained. Other possible modes of failure including tensile strain localization, overall buckling, local buckling and the effect of residual stresses are beyond the scope of this study. The formulation is based on the lower bound theorem of plasticity.

A hollow structural square section having a side length a along the mid-surface, constant thickness t, and steel yield F_y is subjected to shearing force components V_x and V_y, axial force V_z, bending moment components M_x, M_y and twisting moment M_z acting along the principal centroidal axes x, y and z of the cross section (Fig. 3.1). It is required to determine whether or not the section can withstand the applied combination of internal forces under the assumption that the fully plastic resistance of the section is reached. In a mathematical form, this requirement signifies a family of interaction relations of the form $f^*(V_x, V_y, V_z, M_x, M_y, M_z, t, a, F_y) = 0$. On account of non-dimensional analysis considerations, it is possible to reduce the number of arguments of

functions f_i^*, i.e. $f_i^{**}(v_x, v_y, v_z, m_x, m_y, m_z, t/a) = 0$ in which the dimensionless terms $v_y = V_y / V_{yp} = \sqrt{3} V_y / (2atF_y)$ and $v_y = V_y / V_{yp} = \sqrt{3} V_y / (2atF_y)$ are the ratios of the applied shear forces to the plastic shear capacity of the section. Ratio $v_z = V_z / V_{zp} = V_z / (4atF_y)$ is that of the applied axial force to the axial yield resistance. Ratios $m_x = M_x / M_{xp} = M_x / (1.5a^2 tF_y)$ and $m_y = M_y / M_{yp} = M_y / (1.5a^2 tF_y)$ are those of the applied bending moments to the plastic bending resistance of the section and $m_z = M_z / M_{zp} = \sqrt{3} M_z / (2a^2 tF_y)$ is the ratio of the applied twisting moment to the plastic twisting resistance. It is noted that the resistances $V_{xp}, V_{yp}, V_{zp}, M_{xp}, M_{yp}$ and M_{zp} are those that would fully plastify the cross-section in the absence of any other stress resultants. The formulation is restricted to thin sections (as discussed in the section on assumptions), i.e., $t/a \approx 0$. This eliminates the dependence of functions f_i^{**} on the dimensionless parameter t/a, i.e., $f_i^{**}(v_x, v_y, v_z, m_x, m_y, m_z) \approx 0$. A yield function f_i^{**} is applicable only when a well defined set of applicability limits $g_i^{**}(v_x, v_y, v_z, m_x, m_y, m_z) \leq 0$ are met. When a yield function f_i^{**} is known to be applicable, the condition $f_i^{**} \leq 0$ is met for any physically possible combination of stress resultants, the condition $f_i^{**} = 0$ signifies that a fully plastic state is attained under the applied stress resultant combination considered, and the condition $f_i^{**} > 0$ is unattainable under the assumptions of the formulation.

3.4 Assumptions

3.4.1 Idealized Stress vs. Strain Relationship

The stress vs. strain diagram is assumed to be bi-linear elastic-perfectly plastic. The first line passes through the origin and has the same slope as the initial slope of a tension coupon test. The second line has zero slope and passes through the yield point. The

additional capacity of the section due to strain hardening is neglected, leading to a lower bound approximation of the section plastic resistance.

No distinction is made between true stress vs. logarithmic strain and the engineering stress vs. engineering strain as the formulation is limited to small strains. This assumption was adopted in Mohareb and Murray (1999) and Mohareb (2001) in developing plastic interaction relations for pipe sections and yielded predictions in very good agreement with experimental results.

3.4.2 Yield Criterion

The section material is assumed to yield in accordance with the maximum distortional energy density yield criterion. Hence, a given point on the section will yield when the following condition is met (Boresi and Sidebottom 1985)

$$0.5\left[(\sigma_{nn}-\sigma_{ss})^2+(\sigma_{ss}-\sigma_{zz})^2+(\sigma_{nn}-\sigma_{zz})^2+6\left(\tau_{sn}^2+\tau_{sz}^2+\tau_{nz}^2\right)\right]=F_y^2 \qquad (3.1)$$

In Eq. 3.1, σ_{nn}, σ_{ss}, σ_{zz}, τ_{sn}, τ_{sz}, and τ_{nz} are the stress tensor components at the point considered. The tangential direction is denoted by s, the normal to the section perimeter is n and longitudinal direction is denoted by z (Fig. 3.2). The normal vectors to sides 1, 2, 3 and 4 are denoted as $\vec{\mathbf{n}}_1$, $\vec{\mathbf{n}}_2$, $\vec{\mathbf{n}}_3$, and $\vec{\mathbf{n}}_4$, respectively.

3.4.3 Width to Thickness Ratio

The formulation is applicable to cases where the section is capable of attaining its fully plastic resistance before undergoing local buckling. For simple loading combinations including axial force and bending moments, sections capable of attaining their fully plastic resistance prior local buckling are termed compact sections in AISC LRFD (1999) and Class 1 or 2 in CAN/CSA S16.1 (2001). Limiting values of the width to thickness ratio, a/t, for those hollow structural sections are given in these codes as

$(a/t)_{lim} \le 525/\sqrt{F_y}$ in which the yield strength F_y is expressed in Mega-Pascal (Mpa) units. For more general loading combinations including shear and twist, the limiting conditions at which a hollow structural section would buckle locally before attaining its fully plastic resistance necessitate a comprehensive study and are outside the scope of this paper.

3.4.4 Thin Wall Assumption

The formulation is restricted to sections with thin walls. Therefore, the gradient of the stress fields across the thickness of the section are negligible, the dependence of the stress fields on the normal coordinate n is thus eliminated, i.e., the stress components σ_{nn}, τ_{nz} and τ_{sn} vanish (or nearly vanish) at the outside and inside perimeters of the thin walled section. The normal stress σ_{ss} can be assumed to vanish in the absence of any external or internal pressure. It follows that $\sigma_{nn} \approx \tau_{nz} \approx \tau_{sn} \approx \partial\sigma_{zz}/\partial n \approx \partial\tau_{zs}/\partial n \approx \partial\sigma_{sn}/\partial n \approx \partial\tau_{nz}/\partial n \approx \partial\tau_{sn}/\partial n \approx 0$. Based on these simplifications, the yield condition, Eq. 3.1, for a given section $z = z_0$ takes the simpler form.

$$\sigma(s)^2 + 3\tau(s)^2 = F_y^2 \tag{3.2}$$

In Eq. 3.2, the indices s and z are omitted, and symbols $\sigma_{zz} = \sigma(s)$ and $\tau_{zs} = \tau(s)$ are introduced.

3.4.5 Residual Stresses

The effect of residual stresses in hot rolled sections and stress-relieved sections is assumed small enough to be neglected. For welded sections, Zhou and Chen (1986) have shown that the presence of residual stress increases the plastic resistance of sections subject to uniaxial bending and axial forces. On the other hand, residual stresses were

found to reduce the plastic resistance of welded box sections subjected to biaxial bending and axial force combinations. Similar observations are expected for the more general solution presented in this chapter.

3.4.6 Plastic Neutral Axis

Santathadaporn and Chen (1970) have shown that the curve delineating compressive and tensile stress regions (plastic neutral axis) for a wide flange section subject to biaxial bending and axial force has to assume the equation of a straight line. This requirement is a necessary requirement in maximizing stress resultants based on a lower bound formulation (i.e., in order to yield an exact solution). The proof can be extended to other sections and the result is adopted in the solution for cases I and II in this chapter. For Case III, the requirement is violated in strict sense. However, it is shown that the error introduced is small.

3.4.7 Idealized Section

For a very stocky hollow structural section (width to thickness ratio is small), there exist a large number of possible positions of the plastic neutral axis (PNA) relative to the inside and outside perimeters of the section. Fig. 3.3 shows the five fundamental cases that need to be considered. It is noted that the number of PNA positions would exceed 40. However, these cases can be handled through proper transformation (Refer to the section on Transformation Law for Interaction Relations). Each of the possible PNA locations would correspond to a distinct interaction equation and a set of applicability limits. Since most of the hollow square structural sections used in North America typically have high width-to-thickness ratios $(a\ t \geq 10)$, the area of each side can be assumed to be concentrated along the side centreline with zero thickness (Fig. 3.4b) while introducing a slight approximation. This approximation reduces the number of fundamental cases to be considered from five (Fig. 3.3) to three (Fig. 3.5), while ensuring the consistency between the interaction equations at the borderline of different cases (e.g., the interaction relations for Case I where $\alpha = 0$ (Fig. 3.5a) is identical to that obtained for Case II where

$\beta = 1.0$ (Fig. 3.5b)). Figure 3.6 summarizes all possible stress patterns for an idealized (thin) section. In the derivations the focus would be on developing the fundamental cases I-1, II-1, and III-1. A transformation scheme will be developed to reduce the interaction relations from the fundamental case.

3.4.8 Cross-Section Warping

Based on an elastic analysis, von Karman and Chien (1946) have shown that square hollow structural sections of constant thickness do not warp under twisting moments. It will be assumed that this result remains valid in the plastic range of deformation, i.e., no warping stresses are assumed to take place due to torsion.

3.5 Derivations

3.5.1 Methodology

According to the lower bound theorem of plasticity, by assuming a stress field that meets the yield condition anywhere on the section, a lower bound interaction relation is obtained. The solution yields the exact interaction relation only when the exact stress field is assumed. As a step towards assuming an exact stress distribution, consideration is given to the 3D equilibrium conditions.

3.5.1.1 Equilibrium Conditions

The 3D equilibrium conditions for an infinitesimal element of the section under no body forces (Timoshenko and Goodier 1987) are:

$$\frac{\partial \sigma_{zz}}{\partial z} + \frac{\partial \tau_{zs}}{\partial s} + \frac{\partial \tau_{zn}}{\partial n} = 0 \tag{3.3}$$

$$\frac{\partial \tau_{sz}}{\partial z} + \frac{\partial \sigma_{ss}}{\partial s} + \frac{\partial \tau_{sn}}{\partial n} = 0 \tag{3.4}$$

$$\frac{\partial \tau_{zn}}{\partial z} + \frac{\partial \tau_{sn}}{\partial s} + \frac{\partial \sigma_{nn}}{\partial n} = 0 \tag{3.5}$$

As discussed in the section on assumptions, the variation of stresses across the wall thickness can be neglected. This assumption eliminates the dependence of all stress tensor components on the radial coordinate n, i.e. $\sigma_{zz} = \sigma_{zz}(s,z)$, $\tau_{sz} = \tau_{sz}(s,z)$, $\sigma_{ss} = \sigma_{ss}(s,z)$, $\tau_{ns} = \tau_{ns}(s,z)$ and $\tau_{nz} = \tau_{nz}(s,z)$. In addition, in the absence of any traction acting on the outside or inside surfaces of the section, stress components σ_{nn}, τ_{ns}, and τ_{nz} assume zero values at $n = \pm t/2$. Because of the independence of σ_{nn}, τ_{ns} and τ_{nz} on coordinate n, it can be concluded that $\sigma_{nn}(s,z) = \tau_{ns}(s,z) = \tau_{nz}(s,z) = 0$. These simplifications are used in solving the equilibrium equations (Eqs. 3.3 through 3.5) for the stress fields, yielding.

$$\tau_{zs} = \tau_{zs}(s) \tag{3.6}$$

$$\sigma_{zz}(s,z) = -z\tau_{zs}'(s) + f(s) \tag{3.7}$$

in which the prime denotes differentiation with respect to coordinate s. By differentiating the yield condition in Eq. 3.2 with respect to the coordinate s, the following expression is obtained.

$$\sigma_{zz}\frac{d\sigma_{zz}}{ds} + 3\tau_{zs}\frac{d\tau_{zs}}{ds} = 0 \tag{3.8}$$

From Eq. 3.7, by substituting into Eq. 3.8, the relation

$$\tau'(s)\tau''(s)z^2 - [f(s)\tau''(s) + f'(s)\tau'(s)]z + f(s)f'(s) + 3\tau(s)\tau'(s) = 0 \tag{3.9}$$

is recovered. In order to satisfy Eq. 3.9 for an arbitrary value of the coordinate z, the conditions $\tau'(s)\tau''(s) = 0$ and $f(s)\tau''(s) + f'(s)\tau'(s) = 0$ must be satisfied. It can be

shown that the two conditions are met only when the condition $\tau'(s)=0$ is realized. For the first condition to be met, either $\tau'(s)=0$ (case 1) or $\tau''(s)=0$ (case 2).

Under case 1, the condition $\tau'(s)=0$ will realize the second condition identically. By substituting into Eq. 3.8, the condition $\sigma(s)\sigma'(s)=0$ is recovered. For a section with non-zero moments and/or axial forces, the solution $\sigma(s)=0$ is rejected, therefore $\sigma'(s)=0$. As a result, both the normal stress $\sigma(s)$ and the shear stress $\tau(s)$ are piecewise constant functions.

Under case 2, the condition $\tau''(s)=0$ is met. For the condition $f(s)\tau''(s)-f'(s)\tau'(s)=0$ to hold, the term $f'(s)\tau'(s)$ must vanish. Therefore, either $\tau'(s)$ vanishes leading to the solution under case 1, or $f'(s)=0$. By differentiating Eq. 3.7 with respect to coordinate s, the relationship $\sigma'_{zz}(s,z)=-z\tau_{zs}''(s)+f'(s)=0$ is obtained, which indicates that the normal stress is a function of coordinate z, i.e., $\sigma_{zz}(s,z)=\sigma_{zz}(z)$. By substituting the condition $\sigma'_{zz}(s,z)=0$ into Eq. 3.8, the condition $\tau(s)\tau'(s)=0$ is reached. For non-zero shearing forces and twisting moments, the condition $\tau(s)=0$ is rejected, and therefore $\tau'(s)=0$, leading to the same solution as in case 1.

In summary, both the tangential shear and the normal stresses have to assume constant piecewise distributions over the cross-section in order to satisfy the equilibrium conditions.

3.5.1.2 Section Corners as Points of Shear Stress Discontinuity

By applying the 3D equilibrium conditions for an element at the corner of the section (Fig. 3.7), it can be demonstrated (Appendix B.1) that the tangential shear stresses acting on two faces connected to the corner $s=s_c=ia$, ($i=1,2,3$ and 4), are in general unequal, i.e., $\tau(s_c)_- \neq \tau(s_c)_+$.

In the derivation of plastic interaction relations of pipe sections in (Mohareb 2001), it has been mathematically demonstrated that, at the plastic limit, the section consists of no more than two contiguous blocks: the first block is subject to a tangential shear of constant magnitude and the other block is subject to an equal and opposite tangential shear stress. By extending this result to the square hollow structural section, it can be inferred that the only points of possible discontinuity for the tangential shear stress are those located at the corners of the section. Therefore, it will be assumed that the shear stress is given by $\tau(s) = \tau_i$, $(i-1)a < s < ia$, in which corner i takes the values 1,2,3, and 4.

A section under pure torsion will be subject to a constant tangential stress $\tau_{mz}(s) = \tau_{mz} = M_z/(2a^2t) = m_z F_y/\sqrt{3}$. Under a shearing force V_x, an elastic analysis predicts a nearly constant tangential shear stress distribution along the sides parallel to the force, i.e., $\tau_{vx}(s) \approx \tau_{vx} = V_x/(2at) = v_x F_y/\sqrt{3}$. Similarly, under a shearing force V_y, the stresses along the sides parallel to the y-axis are $\tau_{vy}(s) \approx \tau_{vy} = V_y/(2at) = v_y F_y/\sqrt{3}$. The shear stress distribution is assumed to remain constant along the sides parallel to the forces throughout the plastic range of deformation, in agreement with established plastic design procedure (LRFD 1999 and CAN/CSA 2001). The tangential shear stresses due to the combined effect of shear and torsion are obtained by summing their respective contributions with the proper signs. By taking the shear stresses as positive in the positive x and y directions (Fig. 3.8), the resultant shear stresses on the four sides are obtained as $\tau_1 = \tau_{vx} - \tau_{mz}$, $\tau_2 = \tau_{vy} - \tau_{mz}$, $\tau_3 = \tau_{vx} + \tau_{mz}$ and $\tau_4 = \tau_{vy} + \tau_{mz}$, in which subscripts 1 through 4 denote the four sides of the section.

3.5.1.3 Normal Stresses

The yield condition in Eq.3.2 is solved for the normal stress as $\sigma_i = \pm\sqrt{1-\tau_{ir}^2}$ in which the normalized shear stresses $\tau_{ir} = \sqrt{3}\tau_i/F_y$, normalized normal stresses $\sigma_i = \Omega_i/F_y$, and Ω_i is the normal stress that would yield side i in the presence of a shear stress τ_i. The

stresses causing compression (along the negative z direction) are negative and those causing tension (along the positive z direction) are positive (Fig 3.9).

There is a one to one correspondence between any set of applied normalized forces m_z, v_x, and v_y and the normal stress ratios σ_1, σ_2, and σ_3. This allows the expression of the yield functions f_i^{**} and their limits of applicability g_{ii}^{**} to be expressed in the alternative form $f_i(\sigma_1, \sigma_2, \sigma_3, \sigma_4, m_x, m_y, v_z) = f_i(\{\mathbf{x}\}) = 0$ and $g_{ii}(\sigma_1, \sigma_2, \sigma_3, \sigma_4, m_x, m_y, v_z) = g_{ii}(\{\mathbf{x}\}) \le 0$, respectively in which vector $\{\mathbf{x}\} = \{\sigma_1, \sigma_2, \sigma_3, \sigma_4, m_x, m_y, v_z\}$. This alternative form results into simpler expressions and will be adopted in the following formulations. The normal stress ratio σ_4 is not an independent quantity and is related to other three stress ratios $\sigma_1, \sigma_2, \sigma_3$ and the applied stress resultant ratios m_z, v_x, v_y through the relation $\sigma_4 = \pm\sqrt{4 - (4m_z^2 + 2v_x^2 + 2v_y^2 + \sigma_1^2 + \sigma_2^2 + \sigma_3^2)}$. In the following formulations, it is found convenient to retain normal stress ratio σ_4.

3.5.1.4 Sign Convention for Stress Resultants

The axial force V_z is positive when in tension (acting along the positive z direction). Shear forces V_x, and V_y are positive when acting along the positive directions of along the x, and y axes respectively. Moments M_x, M_y, and M_z are positive when they induce positive rotations about the x, y, and z axes respectively following the right hand rule sign convention.

3.5.1.5 Shear and Torsion Applicability Limits

For the normal stresses in Eq. 3.2 to assume real values, the conditions

$$g_{i1}(\{\mathbf{x}_i\}) = v_z + |m_x| - 1.0 \le 0 \tag{3.10}$$

$$g_{i2}(\{\mathbf{x}_i\}) = |v_z| + |m_x| - 1.0 \le 0 \tag{3.11}$$

have to be met. A stress resultant combination not meeting any of the above two requirements is unattainable under the limitations of the formulation. Equations.3.10 and 3.11 constitute the first applicability limits for any admissible combination of stress resultants and need to be checked prior the application of any of the interaction relations to follow.

3.5.2 Normal Stresses – Fundamental Cases

Depending on the magnitude and sign of the applied stress resultants there can be twenty different patterns of stress distribution for the idealized section (Fig. 3.6). In the following sections, interaction relations and applicability limits are derived only for three fundamental cases (I-1, II-1, and III-1). The remaining seventeen cases can be derived through permutation of the ratios $\sigma_1, \sigma_2, \sigma_3, \sigma_4, m_x, m_y$, and v_z with the appropriate signs and are handled subsequently through transformations of axes.

3.5.2.1 Case I–1 – Interaction Relation

The axial force V_z and bending moments M_x and M_y are obtained by integrating the longitudinal stresses and their respective moments about the section centroid. In a dimensionless form, these are expressed as:

$$v_z = \frac{V_z}{4atF} = \frac{1}{4atF}\int_A \sigma\, dA = \frac{1}{4}(\sigma_1 - 2\alpha\sigma_1 - \sigma_2 - 2\gamma\sigma_3 + \sigma_3 + \sigma_4) \tag{3.12}$$

$$m_x = \frac{M_x}{M_{xp}} = \frac{1}{1.5a^2tF_y}\int_A \sigma\, y dA = -\frac{1}{3}(2\alpha\sigma_1 - 2\alpha^2\sigma_1 + \sigma_2 - 2\gamma^2\sigma_3 + 2\gamma\sigma_3 + \sigma_4) \tag{3.13}$$

$$m_{\cdot} = \frac{M_{\cdot}}{M_{\cdot p}} = \frac{1}{1.5a^2 tF_{\cdot}} \int_{A} \sigma x dA = \frac{1}{3}(\sigma_{\cdot} - 2\alpha\sigma_{\cdot} - \sigma_{\cdot} + 2\gamma\sigma_{\cdot}) \tag{3.14}$$

Variables α and γ (Fig. 3.5a) are dimensionless coordinates identifying the locations αa (along side 1) and γa (along side 3), where the neutral axis intersects the cross-section. From Fig. 3.5a, the conditions $0 \le \alpha \le 1$ and $0 \le \gamma \le 1$ have to be met for Case I-1 to be applicable. By solving Eq. 3.14 for α and substituting into Eq. 3.13, two possible values for the coordinate α are obtained as $\alpha_{1,2} = (B \pm \sqrt{A})/C$ in which constants $B = \sigma_{\cdot}(\sigma_{\cdot} - \sigma_{\cdot} - 3m_{\cdot})$, $C = 2\sigma_{\cdot}(\sigma_{\cdot} + \sigma_{\cdot})$, and

$$A = \sigma_{\cdot}\sigma_{\cdot}\left[(\sigma_{\cdot} + \sigma_{\cdot})^2 + 2(\sigma_{\cdot} + \sigma_{\cdot})(\sigma_{\cdot} + \sigma_{\cdot} + 3m_{\cdot}) - 9m_{\cdot}^2\right] \tag{3.15}$$

have been introduced. The corresponding values for γ are obtained by substituting into Eq. 3.13 yielding $\gamma_{1,2} = (E \pm \sqrt{A})/F$, in which constants $E = (\sigma_{\cdot} + \sigma_{\cdot} + 3m_{\cdot})\sigma_{\cdot}$ and $F = 2\sigma_{\cdot}(\sigma_{\cdot} + \sigma_{\cdot})$ have been defined. By eliminating α and γ between Eqs. 3.12 through 3.14, the interaction relation for Case I-1 is recovered

$$\begin{aligned} f_{\cdot}(\mathbf{x}) = {} & \left[(\sigma_{\cdot} - \sigma_{\cdot})(\sigma_{\cdot} + \sigma_{\cdot}) + 4\sigma_{\cdot}(\sigma_{\cdot} + \sigma_{\cdot}) - 3m_{\cdot}(\sigma_{\cdot} - \sigma_{\cdot})\right]^2 \\ & - 4\sigma_{\cdot}\sigma_{\cdot}\left[(\sigma_{\cdot} + \sigma_{\cdot})^2 + 2(\sigma_{\cdot} + \sigma_{\cdot})(\sigma_{\cdot} + \sigma_{\cdot}) + 6m_{\cdot}(\sigma_{\cdot} + \sigma_{\cdot}) - 9m_{\cdot}^2\right] = 0 \end{aligned} \tag{3.16}$$

3.5.2.2 Case I–1 – Limits of Applicability

In addition to the applicability limits in Eqs.3.7 and 3.8, coordinates α and γ have to assume real values, i.e., $A \ge 0$, or

$$g_{\cdot}(\mathbf{x}) = 9m_{\cdot}^2 - (\sigma_{\cdot} + \sigma_{\cdot})(\sigma_{\cdot} + \sigma_{\cdot} + 2\sigma_{\cdot} + 2\sigma_{\cdot} + 6m_{\cdot}) \le 0 \tag{3.17}$$

Also, coordinates $\alpha_{1,2}$ and $\gamma_{1,2}$ have to remain within the bounds $0 \le \alpha_{1,2} \le 1$ and $0 \le \gamma_{1,2} \le 1$. Noting that $C > 0$ and $F > 0$, the bounds for $\alpha_{1,2}$ and $\gamma_{1,2}$ can be shown to lead to the following conditions.

$$g_{14}(\{\mathbf{x}\}) = -\sigma_1(\sigma_1 + \sigma_3 + 3m_1) - \sqrt{A} \le 0 \tag{3.18}$$

$$g_{15}(\{\mathbf{x}\}) = \sigma_1(-\sigma_1 - \sigma_3 + 3m_1) + \sqrt{A} \le 0 \tag{3.19}$$

$$g_{16}(\{\mathbf{x}\}) = \sigma_3(-\sigma_1 - \sigma_3 + 3m_1) - \sqrt{A} \le 0 \tag{3.20}$$

$$g_{17}(\{\mathbf{x}\}) = -\sigma_3(\sigma_1 + \sigma_3 + 3m_1) + \sqrt{A} \le 0 \tag{3.21}$$

$$g_{18}(\{\mathbf{x}\}) = -\sigma_1(\sigma_1 + \sigma_3 - 3m_1) - \sqrt{A} \le 0 \tag{3.22}$$

$$g_{19}(\{\mathbf{x}\}) = \sigma_1(-\sigma_1 - \sigma_3 - 3m_1) + \sqrt{A} \le 0 \tag{3.23}$$

$$g_{20}(\{\mathbf{x}\}) = \sigma_3(-\sigma_1 - \sigma_3 - 3m_1) - \sqrt{A} \le 0 \tag{3.24}$$

$$g_{21}(\{\mathbf{x}\}) = -\sigma_3(\sigma_1 + \sigma_3 - 3m_1) + \sqrt{A} \le 0 \tag{3.25}$$

For the interaction relation in Eq. 3.16 to be applicable, either the applicability limits in Eqs. 3.18 through 3.21 or those in Eqs. 3.22 through 3.25 should be met. The derivations related to these applicability limits of Case I-1 are given in Appendix B.2

3.5.2.3 Case II-1 – Interaction Relation

A similar treatment on the stress distribution in Fig. 3.5b leads to the axial force and bending moment ratios $v_2 = 0.25[(1-2\gamma)\sigma_2 + (1-2\beta)\sigma_3 + \sigma_1 + \sigma_4]$,

$m_x = -[(2\gamma - 1)\sigma_2 + 2(1-\beta)\beta\sigma_3 + \sigma_4]/3$. and

$m_y = -[2\sigma_2\gamma(\gamma - 1) - \sigma_3(2\beta - 1) - \sigma_1]/3$. Variables β and γ are dimensionless coordinates identifying the locations βa (along side 2) and γa (along side 3) where the neutral axis intersects the cross-section. By solving the expression for the axial force ratio for β and by substituting into the expression for m_x, coordinate γ can be obtained as $\gamma = \pm\sqrt{G}/2\sigma_3$ in which $G = 2\sigma_3(3m_x - 4v_2 + \sigma_1 + \sigma_3 + 2\sigma_4)$. The negative sign of γ is discarded in order to meet the geometric constraint $0 \le \gamma \le 1$ (Fig. 3.5b). By back-substitution into equation for axial force, and solving for coordinate β, the expression $\beta = [(\sigma_1 + \sigma_2 + \sigma_3 + \sigma_4 - 4v_2) - \sqrt{G}]/2\sigma_2$ is recovered. The interaction equation for Case II-1 is obtained by eliminating γ and β from the expressions for v_2, m_x, and m_y, leading to

$$f_2(\{\mathbf{x}\}) = 2\sigma_2(4v_2 + 3m_y - 2\sigma_1 - \sigma_2 - \sigma_4) + \left[4v_2 - \sigma_1 - \sigma_2 - \sigma_3 - \sigma_4 + \sqrt{2\sigma_3(3m_x - 4v_2 + \sigma_1 + \sigma_3 + 2\sigma_4)}\right]^2 = 0 \quad (3.26)$$

3.5.2.4 Case II-1 – Limits of applicability

Coordinates β and γ can only assume real values i.e., $G \ge 0$, or

$$g_{23}(\{\mathbf{x}\}) = (4v_2 - \sigma_1 - \sigma_3 - 2\sigma_4) - 3m_x \le 0 \quad (3.27)$$

In addition, the bounds $0 \le \beta \le 1$, and $0 \le \gamma \le 1$ have to be met. Noting that the conditions $\sigma_2 > 0$ and $\sigma_3 > 0$ always hold true and the condition $0 \le \gamma$ is identically satisfied for any combination of real stresses, the following applicability limits are reached.

$$g_{24}(\{\mathbf{x}\}) = \sqrt{2\sigma_3(3m_x - 4v_2 + \sigma_1 + \sigma_3 + 2\sigma_4)} - (\sigma_1 + \sigma_2 + \sigma_3 + \sigma_4 - 4v_2) \le 0 \quad (3.28)$$

$$g_{25}(\{\mathbf{x}\}) = (\sigma_1 - \sigma_2 + \sigma_3 + \sigma_4 - 4v_2) - \sqrt{2\sigma_3(3m_x - 4v_2 + \sigma_1 + \sigma_3 + 2\sigma_4)} \le 0 \qquad (3.29)$$

$$g_{26}(\{\mathbf{x}\}) = \sqrt{2\sigma_3(3m_x - 4v_2 + \sigma_1 + \sigma_3 + 2\sigma_4)} - 2\sigma_{3r} \le 0 \qquad (3.30)$$

The conditions $g_{2i}(\{\mathbf{x}\}) \le 0, i = 1....6$ need to be satisfied for interaction relation in Eq. 3.27 to be applicable. The derivations related to the applicability limits for Case II-1 (Eqs. 3.28 through 3.30) are given in Appendix B.3.

3.5.2.5 Case III-1 – Interaction Relation

Cases I and II are unable to represent physically attainable load combinations such as those corresponding to the neutral axis positions 3, 4, 5 in Fig. 3.3. While it is possible to derive interaction relations for each of these cases separately, the resulting relations are cumbersome, and they result in slight discontinuities with the interaction relations derived in Cases I and II. In order to consolidate the interaction relations based on these cases into a single interaction expression, it is assumed that the curve delineating the compressive and tensile longitudinal stresses crosses the same side at two points (e.g., along side 2 in Fig 3.5b). While in principle, this approximation violates the straightness requirement of neutral axis (Santathadaporn and Chen 1970), it is shown (Appendix B.4), the assumption yields an excellent approximate solution erring on the conservative side when compared to more accurate solutions based on thick wall section representation as the error does not exceed 1%. Further, the proposed approximation ensures the continuity of the yield surfaces given in Cases I and II while meeting the Drucker convexity requirement (Hodge 1981) $(\partial f_3 / \partial \{\mathbf{y}\})^T d\{\mathbf{y}\} > 0$ in which $\{\mathbf{y}\} = \{v_1, v_1, v_2, m_x, m_1, m_2\}^T$ for the yield surface. The normalized axial force and bending moments corresponding to Case III-1 are found as $v_2 = (2\beta_1 - 2\beta_2 + 1)\sigma_2 + \sigma_1 + \sigma_3 + \sigma_4/4$, $m_x = (2\beta_1 - 2\beta_2 + 1)\sigma_2 - \sigma_4/3$, and $m_1 = 2(\beta_1^2 - \beta_1 - \beta_2^2 + \beta_2)\sigma_2 + \sigma_1 - \sigma_3/3$. The coordinates, β_1 and β_2, are eliminated from the axial force and biaxial bending moment expressions yielding

$$f_3(\{\mathbf{x}\}) = 4v_z - (3m_x + 2\sigma_4 + \sigma_1 + \sigma_3) = 0 \tag{3.31}$$

It is of interest to note the independence of the interaction relation on the magnitude of the normalized moment m_y. A similar observation is reported in Morris and Fenves (1969).

3.5.2.6 Case III-1 – Limits of Applicability

From Fig. 3.5c, coordinates β_1 and β_2 have to meet the conditions $0 \le \beta_2 \le 1$ and $0 \le \beta_1 \le \beta_2$. These geometric constraints lead to the following applicability limits.

$$g_{31}(\{\mathbf{x}\}) = \sigma_4 - \sigma_2 + 3m_y \le 0 \tag{3.32}$$

$$g_{32}(\{\mathbf{x}\}) = (6m_y - \sigma_2 - 2\sigma_1 + 2\sigma_3)\sigma_2 + (6m_x + \sigma_4)\sigma_4 + 9m_x^2 \le 0 \tag{3.33}$$

$$g_{33}(\{\mathbf{x}\}) = (\sigma_4 - 3\sigma_2)(\sigma_2 - \sigma_4) + 2\sigma_2(\sigma_1 - \sigma_3) - 3m_x(2\sigma_4 + 3m_x) + 6\sigma_2(2m_x - m_y) \le 0 \tag{3.34}$$

The conditions ($g_{3i}(\{\mathbf{x}\}) \le 0, i = 1....5$) need to be satisfied for the interaction relation in Eq. 3.31 to be applicable. The derivations related to the applicability limits of Case III-1 (Eqs. 3.32 through 3.34) are given in Appendix B.5.

3.6 *Transformation Law for Interaction Relations*

For a given combination of internal forces V_x, V_y, V_z, M_x, M_y, and M_z, when the conditions $g_{1j}(\{\mathbf{x}\}) \le 0, j = 1....7$ are met, the yield condition $f_1(\{\mathbf{x}\}) = 0$ is known to be applicable (Case I-1). In Fig. 3.10, two sets of coordinates are adopted, a fixed coordinate system XYZ along which the applied shear forces V_x, V_y and twisting moment M_z are assumed to act, and another rotating coordinate system xyz along which the bending

moments M_x, M_y, and the normal force V_z are acting. For Case I-1 in Fig. 3.10a, both coordinate systems coincide. It is required to determine the yield condition for the case where V_x, V_y, and M_z remain acting along the fixed axes XYZ while the bending moments M_x, M_y, and the normal force V_z undergo a 90 degree clockwise rotation about the z axis along with the rotating coordinate system xyz (Case I-2 in Fig. 3.10b). In this case, by renumbering sides 1 through 4 so that $\langle \sigma_1, \sigma_2, \sigma_3, \sigma_4 \rangle = \langle \sigma_4', \sigma_1', \sigma_2', \sigma_3' \rangle$, the yield condition and the applicability limits for Case I-2 can be expressed as $f_1(\{\mathbf{x}_2\}) = 0$ and $g_{1,j}(\{\mathbf{x}_2\}) \le 0, j = 3....7$ in which $\{\mathbf{x}_2\} = \langle \sigma_1', \sigma_2', \sigma_3', \sigma_4', m_x, m_y, v_z \rangle^T$. It is of interest to revert back to the fixed coordinate system notation to the original side numbering scheme. From Fig. 3.10, the required relationship takes the form

$$\{\mathbf{x}_2\}_{7,1} = \langle \sigma_2, \sigma_3, \sigma_4, \sigma_1, -m_y, m_x, v_z \rangle^T = [\mathbf{T}_2]_{7,7} \{\mathbf{x}\}_{7,1} \tag{3.35}$$

in which matrix $[\mathbf{T}_2]_{7,7}$ is a transformation matrix to be applied to the argument vector $\{\mathbf{x}\}_{7,1}$ for sub-case 2. In a partitioned format, matrix $[\mathbf{T}_2]_{7,7}$ can be expressed as

$$[\mathbf{T}_2]_{7,7} = \begin{bmatrix} [\mathbf{t}_1]_{4,4} & [\mathbf{0}]_{4,3} \\ [\mathbf{0}]_{3,4} & [\mathbf{t}_2]_{3,3} \end{bmatrix}, [\mathbf{t}_1]_{4,4} = \begin{bmatrix} 0 & 1 & 0 & 0 \\ 0 & 0 & 1 & 0 \\ 0 & 0 & 0 & 1 \\ 1 & 0 & 0 & 0 \end{bmatrix}, [\mathbf{t}_2]_{3,3} = \begin{bmatrix} 0 & -1 & 0 \\ 1 & 0 & 0 \\ 0 & 0 & 1 \end{bmatrix} \tag{3.36}$$

When the applied moments M_x, M_y undergo a second 90^0 rotation (180^0 clockwise from the original orientation), the relations $f_1(\{\mathbf{x}_3\}) = 0$ and $g_{1,j}(\{\mathbf{x}_3\}) \le 0, j = 3....7$ (subscript 3 here denotes the sub-case number) hold true. The transformation law in Eq.3.31 needs to be applied twice to the argument vector $\{\mathbf{x}\}$ to revert to the fixed coordinate system of, i.e., $\{\mathbf{x}_3\}_{7,1} = [\mathbf{T}_2]_{7,7} \{\mathbf{x}_2\}_{7,1} = [\mathbf{T}_2]_{7,7} ([\mathbf{T}_2]_{7,7} \{\mathbf{x}\}_{7,1}) = [\mathbf{T}_3]_{7,7} \{\mathbf{x}\}_{7,1}$, in which matrix $[\mathbf{T}_3]$ is the transformation matrix corresponding to sub-case 3. The algorithm can be extended to any number of rotations leading to a general expression of the

transformation matrix $[\mathbf{T}_n]$ corresponding to any sub-case number n. The transformation law thus derived is quite general and is applicable for the first four cases (n=1to 4) of Cases I, II, and III.

For sub-cases n=5 to 8 of Cases II and III, the stress distributions (Fig. 3.6) are opposite in sign to those for case sub-cases n=1 to 4, respectively. Therefore, the interaction relations are identical to those for sub-cases n=1 to 4 with the exception that the bending moment and the axial force terms will have opposite signs. Therefore, a multiplier $(-1)^{\text{int}\left(\frac{n-1}{4}\right)}$ is applied to matrix $[\mathbf{t}_2]$ to make the transformation law equally valid for sub-cases 5 through 8, as well. The general transformation law for any sub-case n becomes

$$[\mathbf{T}_n]_{6\times 6} = \begin{bmatrix} [\mathbf{t}_1]_{4\times 4}^{n-1} & [\mathbf{0}]_{4\times 2} \\ [\mathbf{0}]_{2\times 4} & (-1)^{\text{int}\left(\frac{n-1}{4}\right)}[\mathbf{t}_2]_{2\times 2}^{n-1} \end{bmatrix}, n = 1...8 \tag{3.37}$$

In summary, using the general transformation law in Eq.3.37, the yield condition and its associated limits of applicability for any fundamental case (i=I to III) and sub-case (n=1 to 8) can be expressed as $f_i([\mathbf{T}_n]\{\mathbf{x}\}) = 0$, $g_{ij}(\{\mathbf{x}\}) \le 0, j = 1,2$ and $g_{ij}([\mathbf{T}_n]\{\mathbf{x}\}) \le 0, j \ge 3$, respectively. A summary of interaction equations for all cases and sub-cases is provided in Appendix B.6.

3.7 Results

3.7.1 Comparisons with Other Analytical Solutions

When the shear force terms (v_x and v_y) of the interaction equations established for cases I and III are set equal to zero, the relations reduces to $4v_z^2 + (9/4)m_y^2 + 3\left(m_z^2 - m_x\sqrt{1-m_z^2}\right) - 3 = 0$ and $v_z - (3/4)m_x - \sqrt{1-m_z^2} = 0$, respectively. These formulas are identical to the interaction relations of Morris and Fenves (1969) for a square hollow section.

3.7.2 Interaction Surface

The surface plot in Fig. 3.11a depicts the portion of the yield surface in the m_x, m_y, v_z space lying in the positive octant in the absence of the shear forces and twisting moment. The interaction expression for cases I-2, I-3, II-2, III-2, and III-3 from Fig. 3.6 were generating the surface plot. The bounds between these different cases are illustrated in Fig. 3.11b. The peak axial force ratio corresponds to zero biaxial moments, in which case the magnitude of the axial force ratio is unity, (i.e., the axial force resistance is equal to the fully plastic axial resistance). As the magnitude of either m_x or m_y is increased, the corresponding axial force ratio, v_z, decreases.

3.7.3 Effect of Torsion

Fig. 3.12a depicts the biaxial bending moments-axial force interaction surface for the case where torsion ratio is 0.5 under no shear force ($v_x = v_y = 0$). Again, the peak axial force occurs when $m_x = m_y = 0$. However, the peak magnitudes of m_x, m_y, and v_z reduce to 0.866. By comparison with Fig. 3.12a, it is noted that the presence of the twisting moment reduces the magnitude of the peak axial force ratio, and shrinks the domain of the interaction surface. This is illustrated by the smaller volume enclosed by the interaction surface intersection with the plane $v_z = 0$.

3.7.4 Effect of Shearing Force

Figure 3.12b illustrates the effect of shearing force on the biaxial moment-axial force interaction surface. A shear force of 0.5 in the direction of positive y-axis causes a reduction in peak axial force ratio to 0.933. Again, the presence of shearing force shrinks the domain of applicability of interaction surface. The peak value of m_x is attained when $m_y = v_z = 0$ with a magnitude of 0.955 while a peak magnitude of 0.911 is reached for m_y when $m_x = v_z = 0$.

3.8 Design Example

The pipe support shown in Fig. 3.13 consists of an HSS102x102x4.8 (350W material) 3.5m high column supporting a horizontal cantilever member. A factored vertical force P kN due to the self-weight of the pipe and the fluid it is conveying is applied near the cantilever tip, 1 m from the column centreline. Under thermal loads, a horizontal frictional force 0.3P kN is generated between the pipe shoe (support) and the top of steel of the supporting member, acting normal to the cantilever centreline. It is required to determine the maximum load P that the vertical column can withstand based on the cross-section plastic strength.

The plastic resistances are first determined: $V_{zp} = 4atF_y = 653kN$, $V_{yp} = V_{xp} = 2at(F_y/\sqrt{3}) = 189kN$, $M_{xp} = M_{yp} = 1.5a^2tF_y = 238kNm$, and $M_{zp} = 2a^2t(F_y/\sqrt{3})kNm$. The stress resultants at the critical section at the bottom of the column are then calculated: $V_x = 0$, $V_y = 0.3P$, $V_z = -P$, $M_x = -1.05P$, $M_y = 1.0P$, and $M_z = 0.30P$ (all in kN and meter units). The corresponding non-dimensional ratios are $v_x = 0$.

$v_y = 0.3P/189 = 1.58\times10^{-3}P$, $v_z = P/653 = 1.53\times10^{-3}P$, $m_x = 1.05P/238 = 4.41\times10^{-3}P$, $m_y = 1.0P/238 = 4.20\times10^{-3}P$, $m_z = 0.3P/183 = 1.64\times10^{-3}P$. Expressions for the normal stresses are then found:

$$\sigma_1 = \sqrt{1-(m_z - v_y)^2} = \sqrt{1-(1.64\times10^{-3}P - 1.58\times10^{-3}P)^2} = \sqrt{1-0.06\times10^{-6}P^2}.$$

$$\sigma_2 = \sigma_4 = \sqrt{1-m_z^2} = \sqrt{1-(1.64\times10^{-3}P)^2} = \sqrt{1-2.69\times10^{-6}P^2}$$

$$\sigma_3 = \sqrt{1-(m_z + v_y)^2} = \sqrt{1-(1.64\times10^{-3}P + 1.58\times10^{-3}P)^2} = \sqrt{1-10.4\times10^{-6}P^2}$$

From the expressions for $\sigma_1, \sigma_2, \sigma_3, \sigma_4, m_x, m_y, v_z$, by substituting into each of the twenty interaction equations in Appendix B.6, Tables B.6.1, B.6.2, and B.6.3, the

smallest negative root of P is obtained in each case. In this problem, the above procedure was conveniently automated using the solver utility in Microsoft Excel. The smallest of the twenty values of P is the one of interest and will govern the design. In this problem, the value governing the design corresponded to Case II-7, with a value of P=14.9kN. It is possible to introduce the resistance factor $\phi = 0.90$ (as per CAN/CSA S16 2001) into the solution, in which case the predicted factored load would become 13.4kN.

3.9 Conclusions

1. Interaction relations and their applicability limits were developed for square hollow structural sections subject to biaxial bending moments, biaxial shear forces, axial force and torsion. The relations are based on a lower bound solution under the fully plastic condition of the cross-section was assumed. The interaction relations are applicable to cases where local buckling does not occur before the fully plastic resistance of the section is attained.

2. A complete treatment of the problem necessitates the derivation of more than 40 interaction relation and their limits of applicability. Simplifying assumptions were made to reduce this number to 20 cases. The interaction relations for only three fundamental cases were derived. A systematic transformation scheme was devised in order to derive the applicability limits and interaction relations for the remaining 17 cases from fundamental cases. When applying the interaction relations, special care should be taken in ensuring the given internal force ratios fall within the limits of applicability of the derived equations.

3. The interaction relations are potentially applicable to the design of square hollow structural beam columns upon experimental verification.

4. Previously established interaction relations for axial force, biaxial bending moments, and torsion are recovered as special cases of the obtained relations.

References for Chapter 3:

AISC. (1999). *Load and resistance factor design specification for structural steel buildings*. American Institute of Steel Construction. Chicago.

Boresi. A. and Sidebottom. O. (1985). *Advanced mechanics of materials*. 4th Ed.. Wiley. New York.

CAN CSA-S16.1 (1974). [Canadian Standards Association. CSA (1974)] Canadian Standards Association. Rexdale. Ont.

CAN/CSA S16 (2001). "Limit States Design of Steel Structures". Canadian Standards Association. Rexdale. Ont.

Chen. W. and Atsuta. T. (1972). "Interaction equations for biaxially loaded sections." *J. Struct. Engrg.*. ASCE. Vol. 98 (ST5). 1035-1051.

Drucker. D. C. (1951). "A more fundamental approach to plastic stress-strain relations." Proc. *1st U. S. National Congress of Applied Mech.*. Chicago. IL. 487-491.

Gaydon. F. and Nuttall. H. (1957). " On the combined bending and twisting of beams of various sections". *J. Mech. and Physics of Solids*. Vol. 6. 17-21.

Hodge. Ph. G. (1981). *Plastic analysis of structures*. Krieger. Malabar. Fla.

Mohareb. M. (2002a). "Plastic interaction relations for pipe sections". *J. Eng. Mech.*. ASCE. Jan. Vol.128(1). 112-120.

Mohareb. M. and Murray. D. W. (1999). "Mobilization of fully plastic moment capacity for pressurized pipes subjected to axial loading" *ASME J. Offshore Mech. Arct. Eng.*. 121 (4). 237-241.

Morris, G. and Fenves, S. (1969). "Approximate yield surface equations". *J. Eng. Mech Division*, ASCE, Vol. 95 (EM4): 937-954.

Pillai, S. U., and Ellis, J. S. (1971). "Hollow tubular beam-columns in biaxial bending." *J. Struct. Eng.*, ASCE, 97(ST5), 1399-1406.

Pillai, S. U. (1974). "Beam-columns of hollow structural sections." *Can. J. Civ. Eng.* 1(2), 194-198.

Pillai, S. U., Kurian V. J. (1977). "Tests on hollow structural section beam columns." *Can. J. Civ. Eng.* 4, 257-262.

Santathadaporn, S., and Chen, W. F. (1970). "Interaction curves for sections under combined biaxial bending and axial force." *Bulletin No. 178, Welding Research Council, Bulletin No:1*.

Timoshenko S. and Goodier J. (1987). *Theory of Elasticity*, 3rd Ed., McGraw-Hill, New-York.

von Karman, T. and Chien (1946). "Torsion with variable twist" *Journal of Aeronautical Sciences*, vol. 13, No.10, (1946), 503-510.

Zhou, S. P. and Chen, W. F. (1986). "Design criteria for box columns under biaxial loading." *J. Struct. Eng.*, ASCE, 111(12), 2643-2658.

List of Symbols for Chapter 3

Latin Characters

a side length along the mid-surface

A parameter used in the equation of coordinates α and γ of Case I-1 to simplify the calculations

B parameter used in the equation of coordinate α of Case I-1 to simplify the calculations

C parameter used in the equation of coordinate α of Case I-1 to simplify the calculations

E parameter used in the equation of coordinate γ of Case I-1 to simplify the calculations

$f_i(\sigma_1, \sigma_2, \sigma_3, \sigma_4, v_2, m_x, m_1)$ normalized general interaction equation for case i as a function of $\sigma_1, \sigma_2, \sigma_3, \sigma_4, v_2, m_x$, and m_1

$f_i^*(V_x, V_1, V_2, M_x, M_1, M_2, t, a, F_1)$ general interaction equation for case i as a function of $V_x, V_1, V_2, M_x, M_1, M_2, t, a$, and F_1

$f_i^{**}(v_x, v_1, v_2, m_x, m_1, m_2)$ normalized general interaction equation for case i as a function of v_x, v_1, v_2, m_x, m_1, and m_2

F parameter used in the equation of coordinate γ of Case I-1 to simplify the calculations

F_1 yield strength of the material of the section

$g_{ii}(\sigma_1, \sigma_2, \sigma_3, \sigma_4, v_2, m_x, m_1)$ i^{th} applicability limit for i^{th} case corresponding to interaction equation $f_i(\sigma_1, \sigma_2, \sigma_3, \sigma_4, v_2, m_x, m_1)$

$g_{ii}^{**}(v_x, v_1, v_2, m_x, m_1, m_2)$ i^{th} applicability limit for i^{th} case corresponding to interaction equation $f_i^{**}(v_x, v_1, v_2, m_x, m_1, m_2)$

G parameter used in the equation of coordinate β of Case II-1 to simplify the calculations

m_x ratio of internal bending moment to plastic bending moment resistance with

respect to x-axis

m_x ratio of internal bending moment to plastic bending moment resistance with respect to x-axis

m_y ratio of internal bending moment to plastic bending moment resistance with respect to y-axis

m_z ratio of internal bending moment to plastic bending moment resistance with respect to z-axis

m_z ratio of internal twisting moment to plastic twisting moment resistance

M_x internal bending moment with respect to x-axis

M_{xp} plastic bending moment resistance with respect to x-axis

M_y internal bending moment with respect to y-axis

M_{yp} plastic bending moment resistance with respect to y-axis

M_z internal twisting moment

M_{zp} plastic twisting moment resistance

PNA plastic neutral axis

v_x ratio of internal shearing force to plastic shearing resistance along x-axis

v_y ratio of internal shearing force to plastic shearing resistance along y-axis

v_z ratio of internal axial force to plastic axial resistance along z-axis

v_z ratio of internal axial force to plastic axial resistance along z-axis

V_x internal shearing force along x-axis

V_{xp} plastic shear resistance along x-axis

V_y internal shearing force along y-axis

V_{yp} plastic shear resistance along y-axis

V_z internal axial force

V_{zp} plastic axial resistance

$\bar{\mathbf{n}}_i$ normal vector to the section perimeter at i^{th} side of the cross-section (i=1....4)

n normal coordinate to the section perimeter at i^{th} side of the cross-section (i=1....4)

s tangential coordinate of the section cross-section

s_c tangential coordinate of the section corner

t wall-thickness of the square hollow section

$[t_1]$ sub-matrix of $[T_n]$ related to the transformation of stress terms $\sigma_1, \sigma_2, \sigma_3, and \sigma_4$

$[t_2]$ sub-matrix of $[T_n]$ related to the transformation of terms v_2, m_3, and m_1

$[T_n]$ transformation matrix for n^{th} sub-case. n =1...4 for Case I. n=1...8 for Case II. and n=1...8 for Case III

x' x-axis under 90° rotation in clockwise direction

$\{\mathbf{x}\}$ vector resultant of the stress resultants. $\{\mathbf{x}\} = \sigma_1, \sigma_2, \sigma_3, \sigma_4, m_1, m_3, v_2$

$\{\mathbf{x}_n\}$ vector for the stress resultants corresponding to i^{th} sub-case. n =1...4 for Case I. n=1...8 for Case II. and n=1...8 for Case III

$\{\mathbf{y}\}$ vector resultant of the stress resultants. $\{\mathbf{y}\} = v_1, v_3, v_4, m_2, m_4, m_5$

y' y-axis under 90° rotation in clockwise direction

z A specified coordinate along z-axis

z' z-axis under 90° rotation in clockwise direction

Greek Characters

α general coordinate identifying the location of plastic neutral axis along side 1

α_1 coordinate identifying the location of plastic neutral axis along side 1 for Case I-1

α_2 coordinate identifying the location of plastic neutral axis along side 1 for Case I-1

β general coordinate identifying the location of plastic neutral axis along side 2

β_1 coordinate identifying the location of plastic neutral axis along side 2 for Case III-1

β_2 coordinate identifying the location of plastic neutral axis along side 2 for Case III-1

γ general coordinate identifying the location of plastic neutral axis along side 3

γ_1 coordinate identifying the location of plastic neutral axis along side 3 for Case I-1

γ_2 coordinate identifying the location of plastic neutral axis along side 3 for Case I-1

σ normalized normal stress that plastifies the i^{th} side of the cross-section

σ_i' normalized normal stress that plastifies the i^{th} side of the cross-section under 90° clockwise rotation

σ_{nn} stress normal to the mid-surface along n-axis

σ_{ss} circumferential normal stress due to internal/external pressure

σ_{zz} stress normal to the cross section along z-axis

$\sigma(s)$ stress normal to the cross section along z-axis as a function of circumferential coordinate

τ_i shear stress corresponding to the i^{th} side of the cross-section

τ normalized shear stress corresponding to the i^{th} side of the cross-section

τ_{zs} shear stress on the cross-section under pure torsion (m_z)

τ_{nz} shear stress acting on face n along z direction

τ_{sn} shear stress acting on the cross section along n direction

τ_s shear stress acting on the cross section along the circumferential direction

τ_{xs} shear stress on the cross-section under pure shear force along x-axis (v_x)

τ_{ys} shear stress on the cross-section under pure shear force along y-axis (v_y)

$\tau(s)$ shear stress acting on the cross section along the circumferential direction ias a function of circumferential coordinate

Ω normal stress that plastifies the i^{th} side of the cross-section

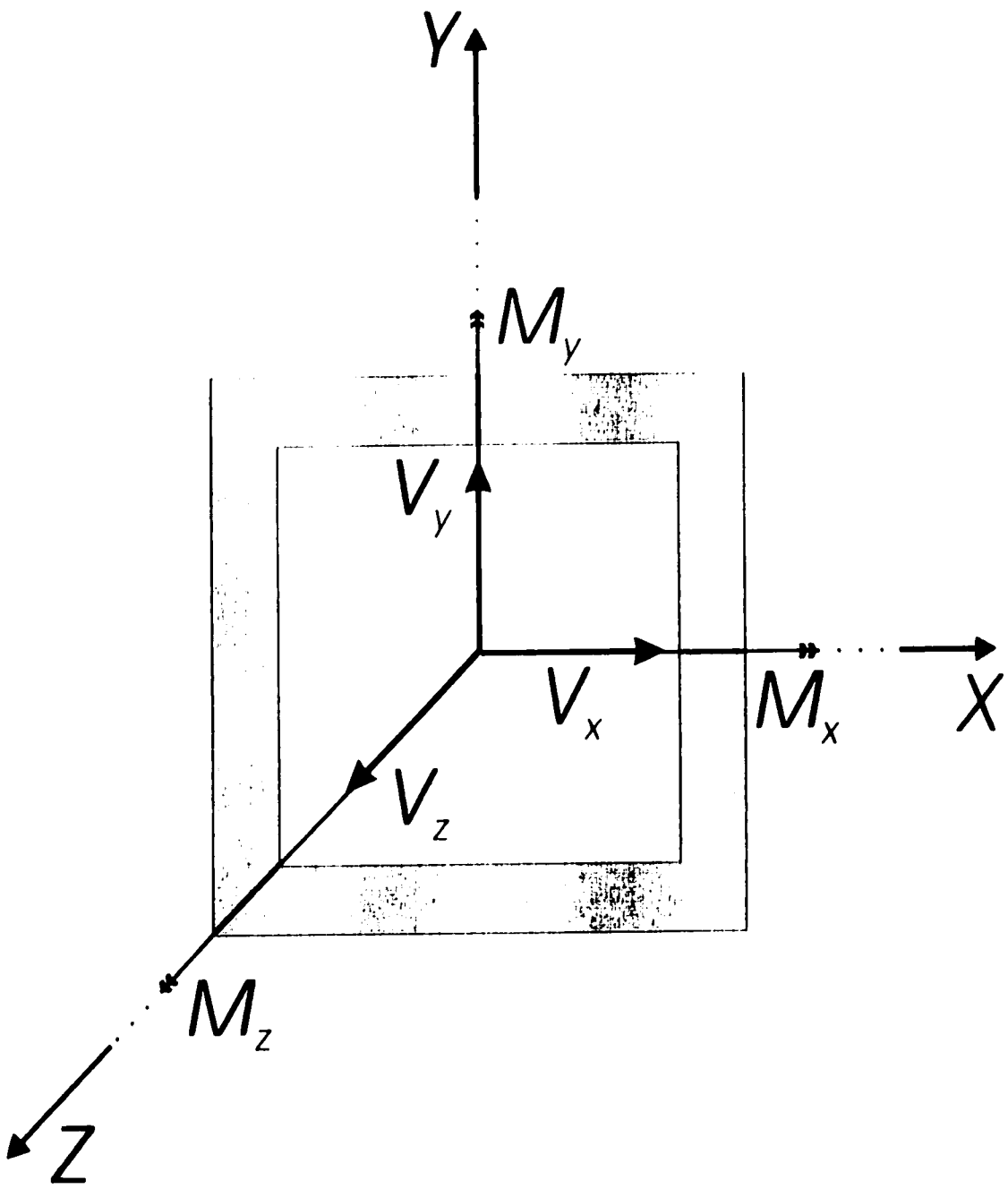

Figure 3.1 Internal Forces Acting on a Square Hollow Section

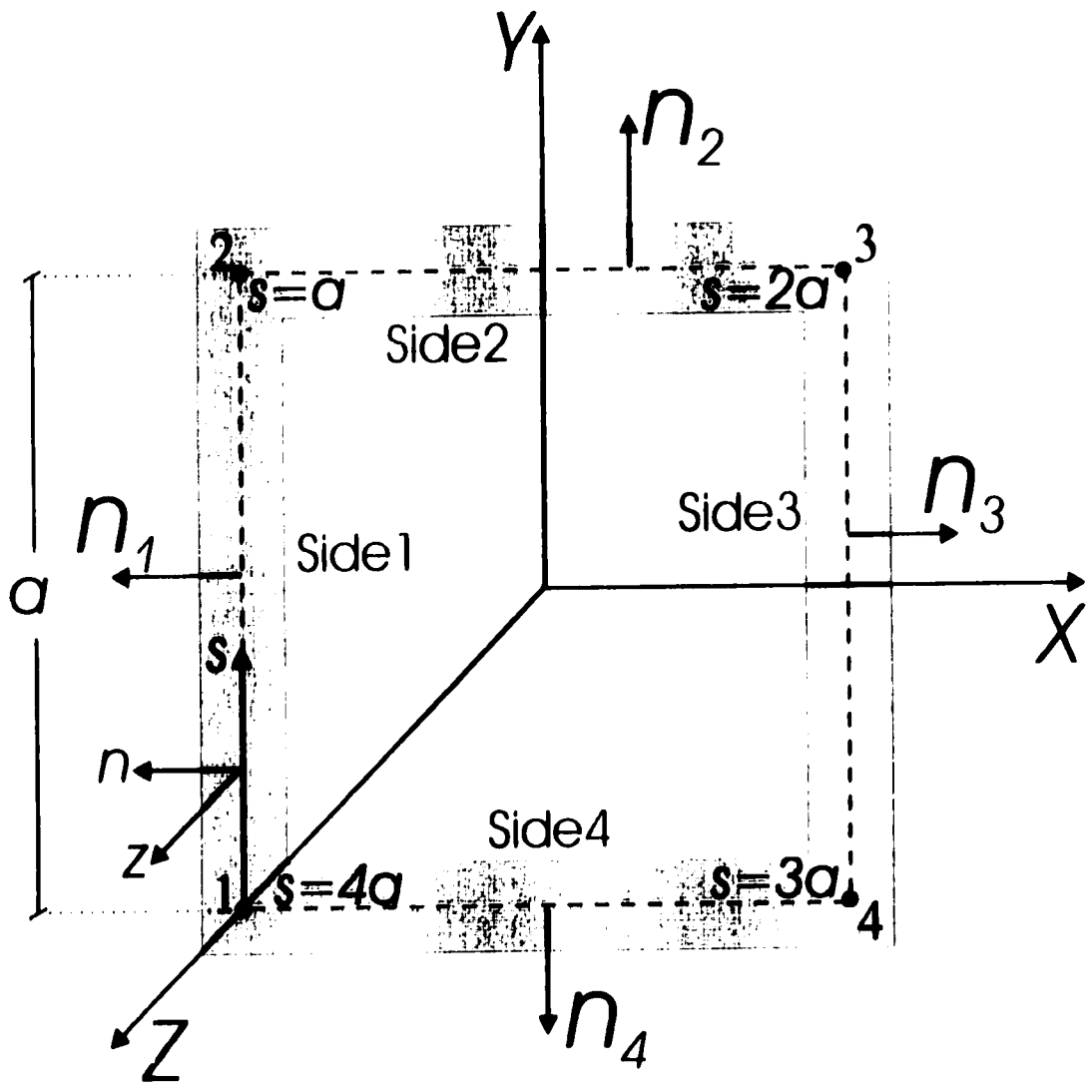

Figure 3.2 Axes Orientation and Coordinates

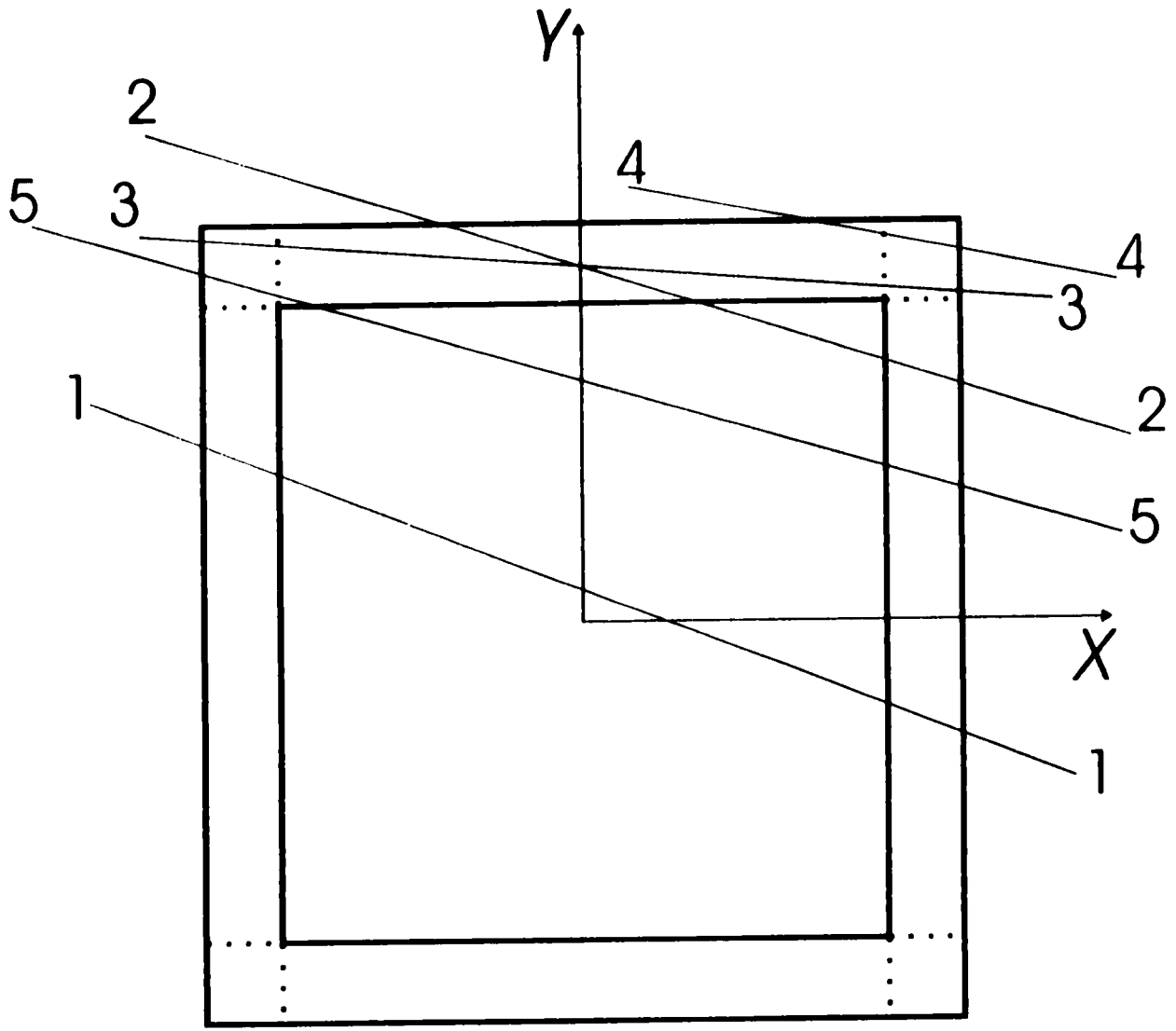

Figure 3.3 Plastic Neutral Axis Locations for a Thick Hollow Structural Section Fundamental Cases

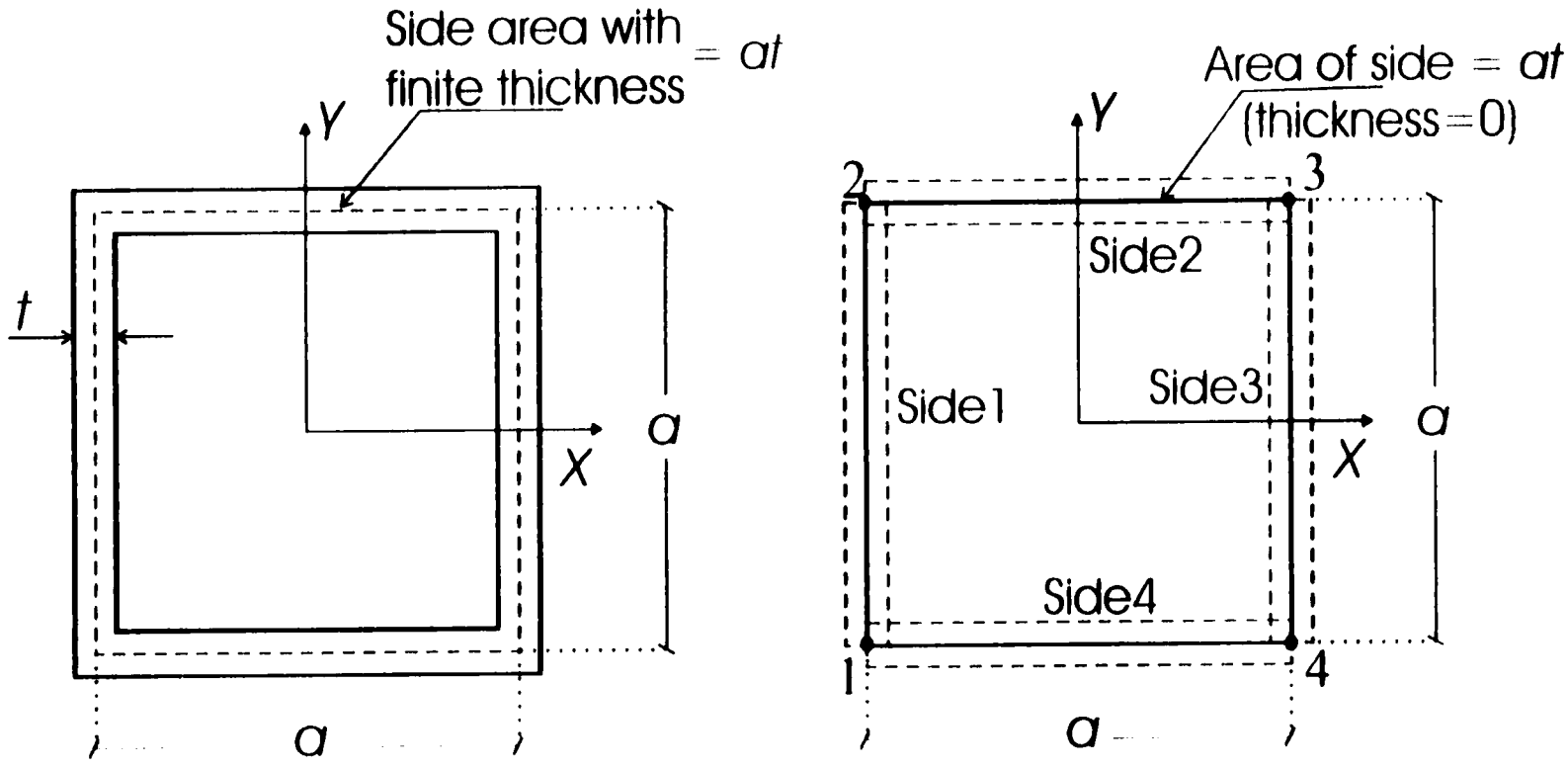

(a) Real Section

(b) Idealized Section

Figure 3.4 Idealization of the Section

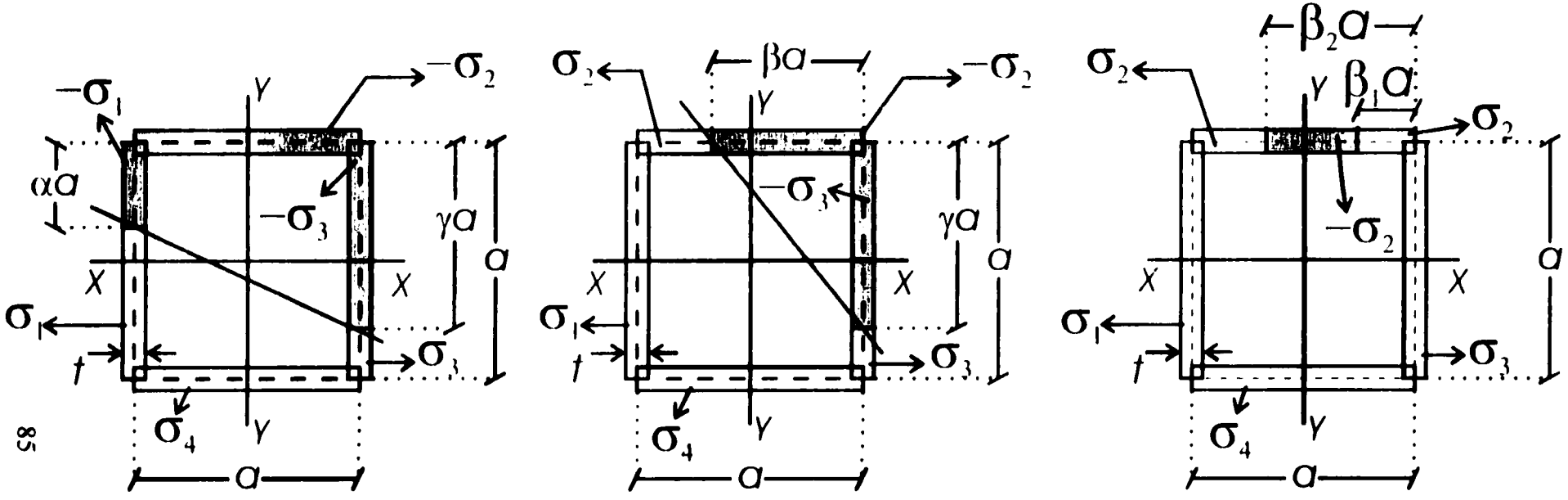

(a) Case I-1 **(b)** Case II-1 **(c)** Case III-1

Figure 3.5 Plastic Neutral Axis Locations for Idealized Hollow Section – Fundamental Cases

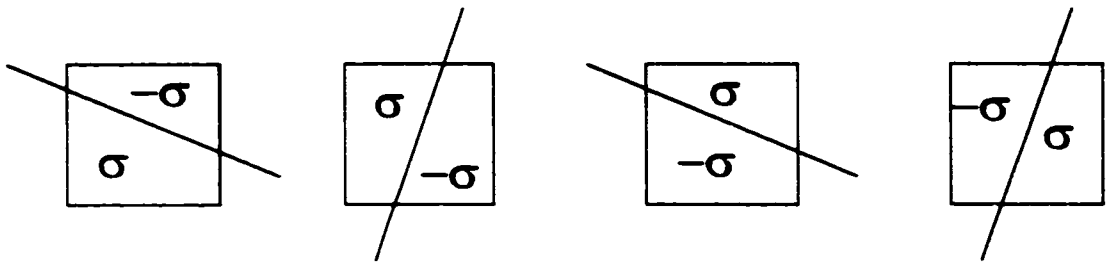

I-1 I-2 I-3 I-4

(a) Case I

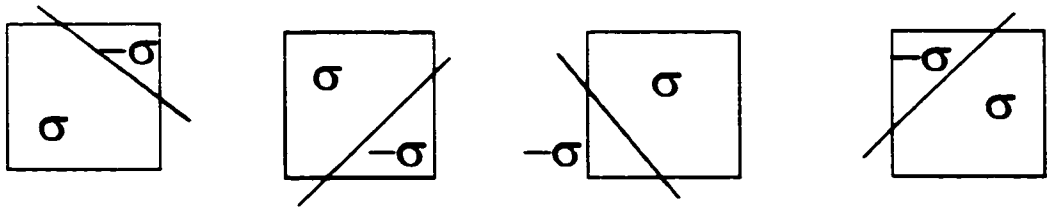

II-1 II-2 II-3 II-4

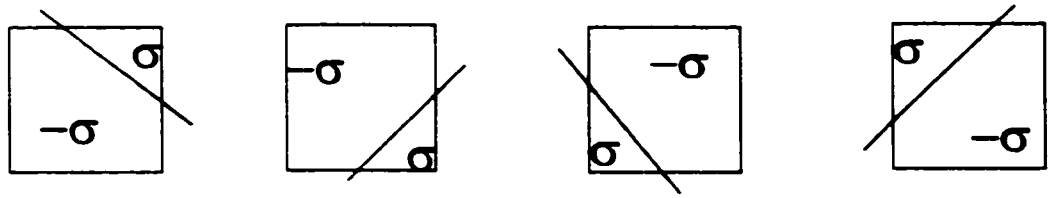

II-5 II-6 II-7 II-8

(b) Case II

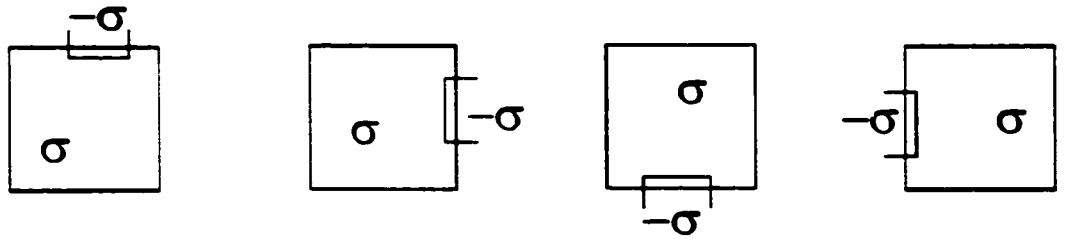

III-1 III-2 III-3 III-4

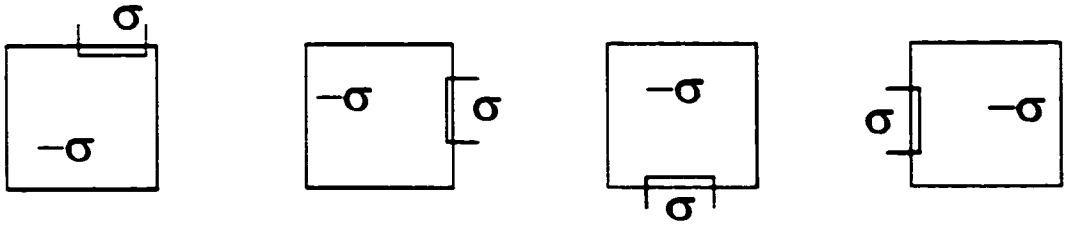

III-5 III-6 III-7 III-8

(c) Case III

Figure 3.6 Summary of Possible Normal Stress Patterns for an Idealized Square Hollow Section

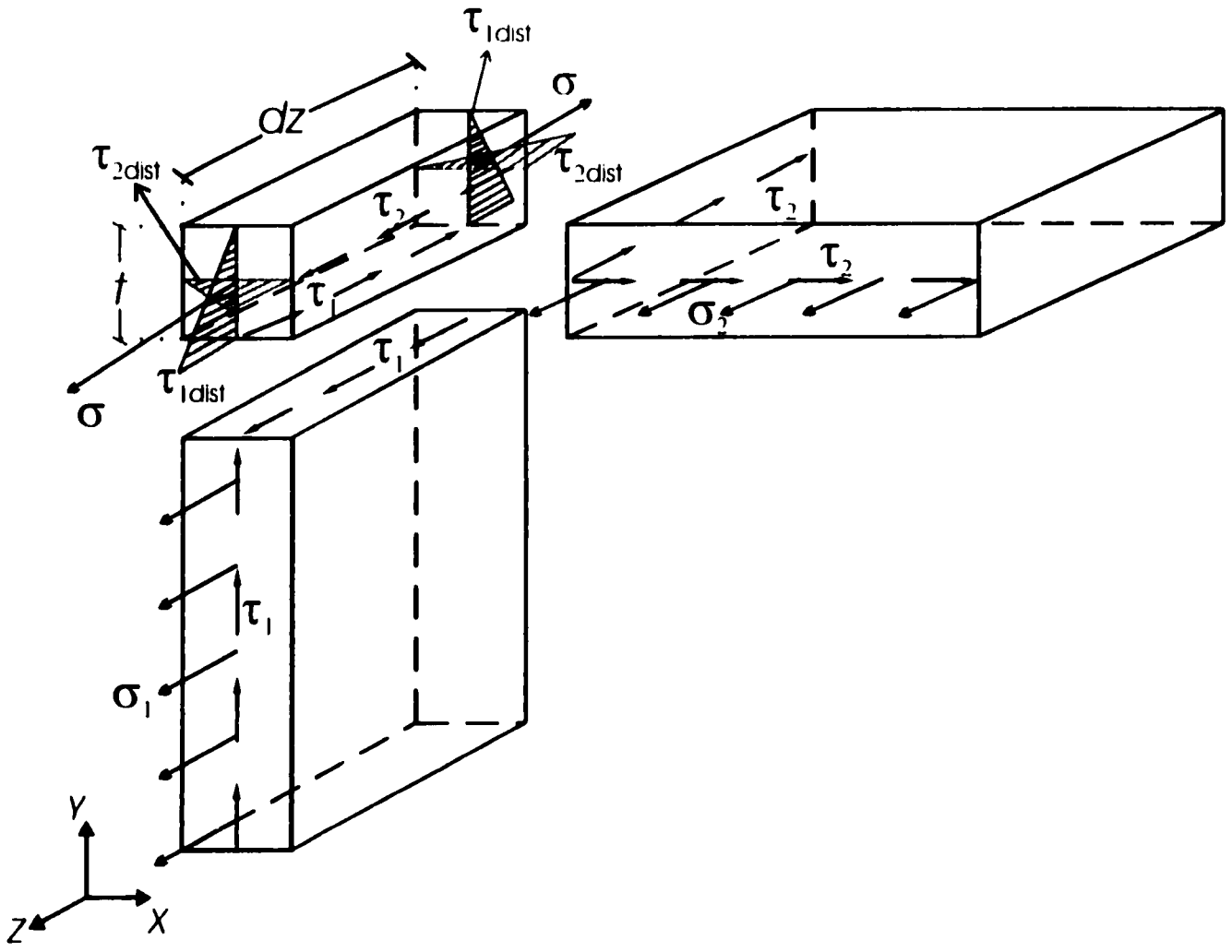

Figure 3.7 Free body Diagram of a Section Corner

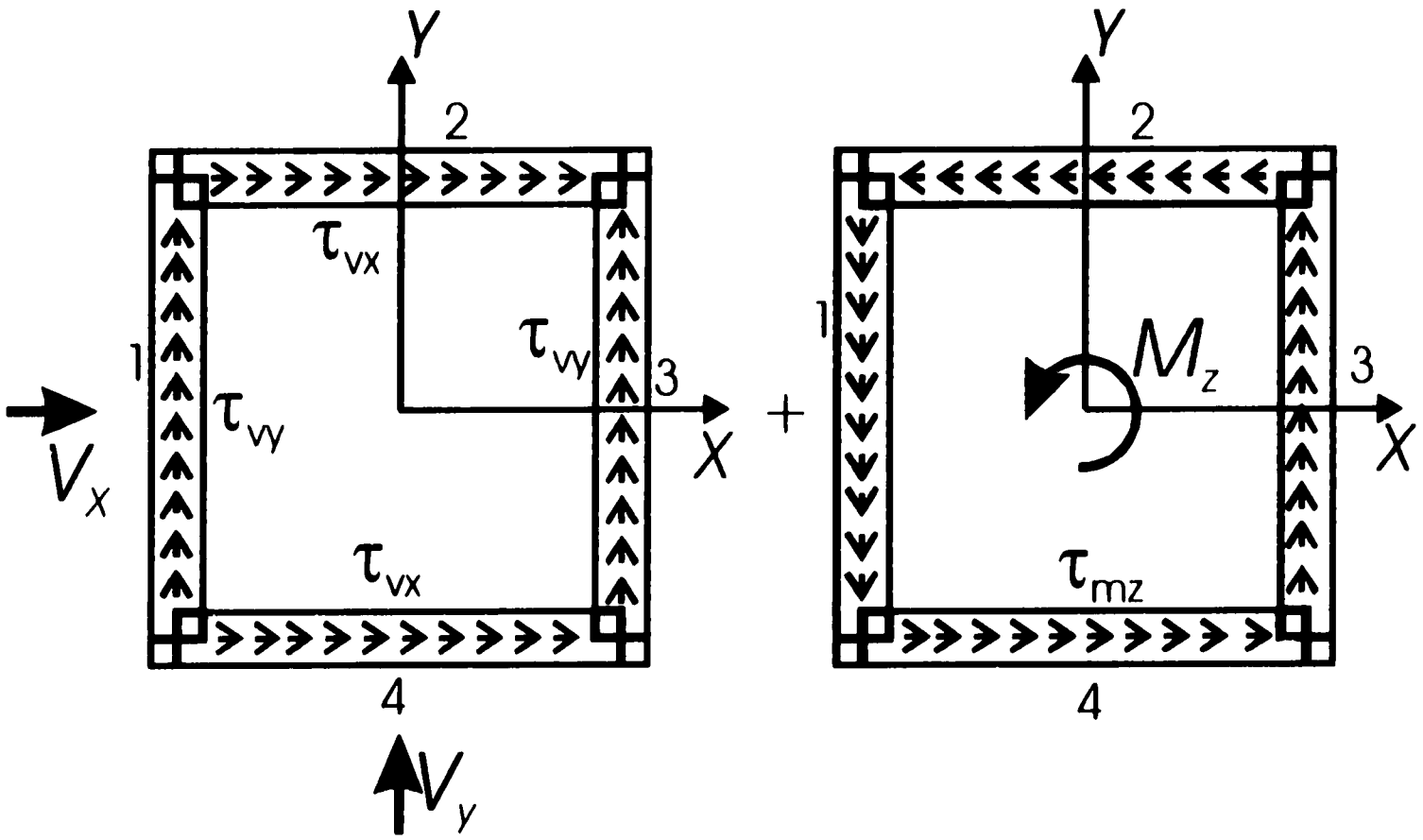

Figure 3.8 Shear Stress Distribution due to Shear Forces and Twist

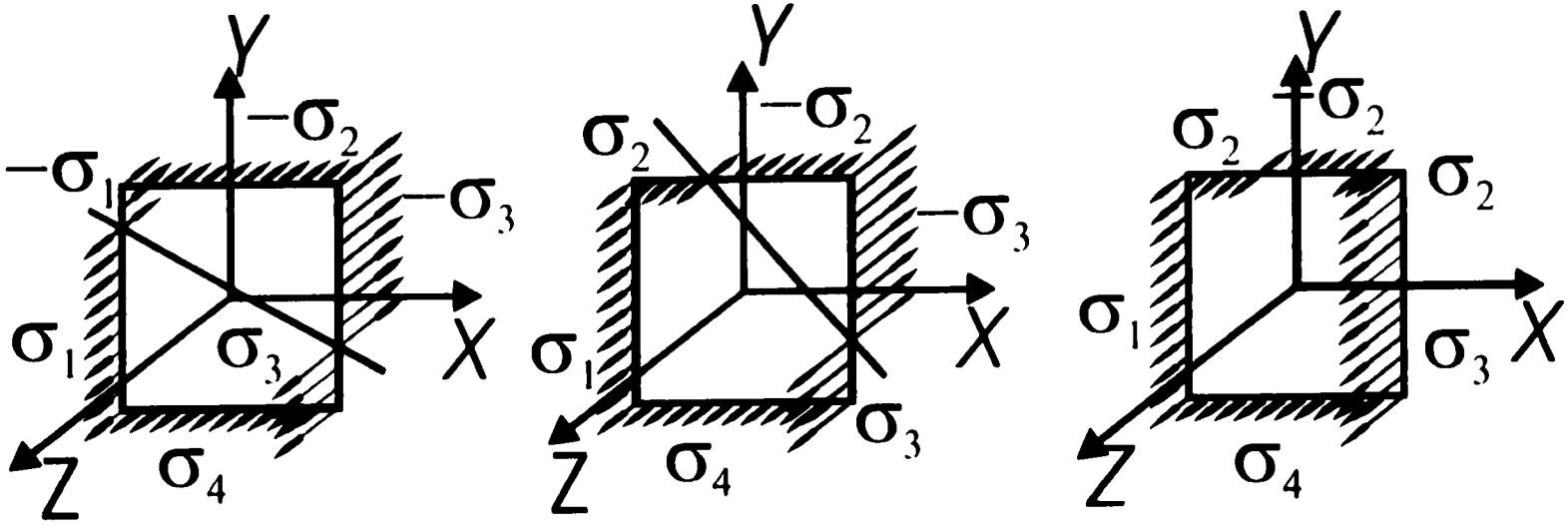

(a) Case I-1 **(b)** Case II-1 **(c)** Case III-1

Figure 3.9 Normal Stress Distribution

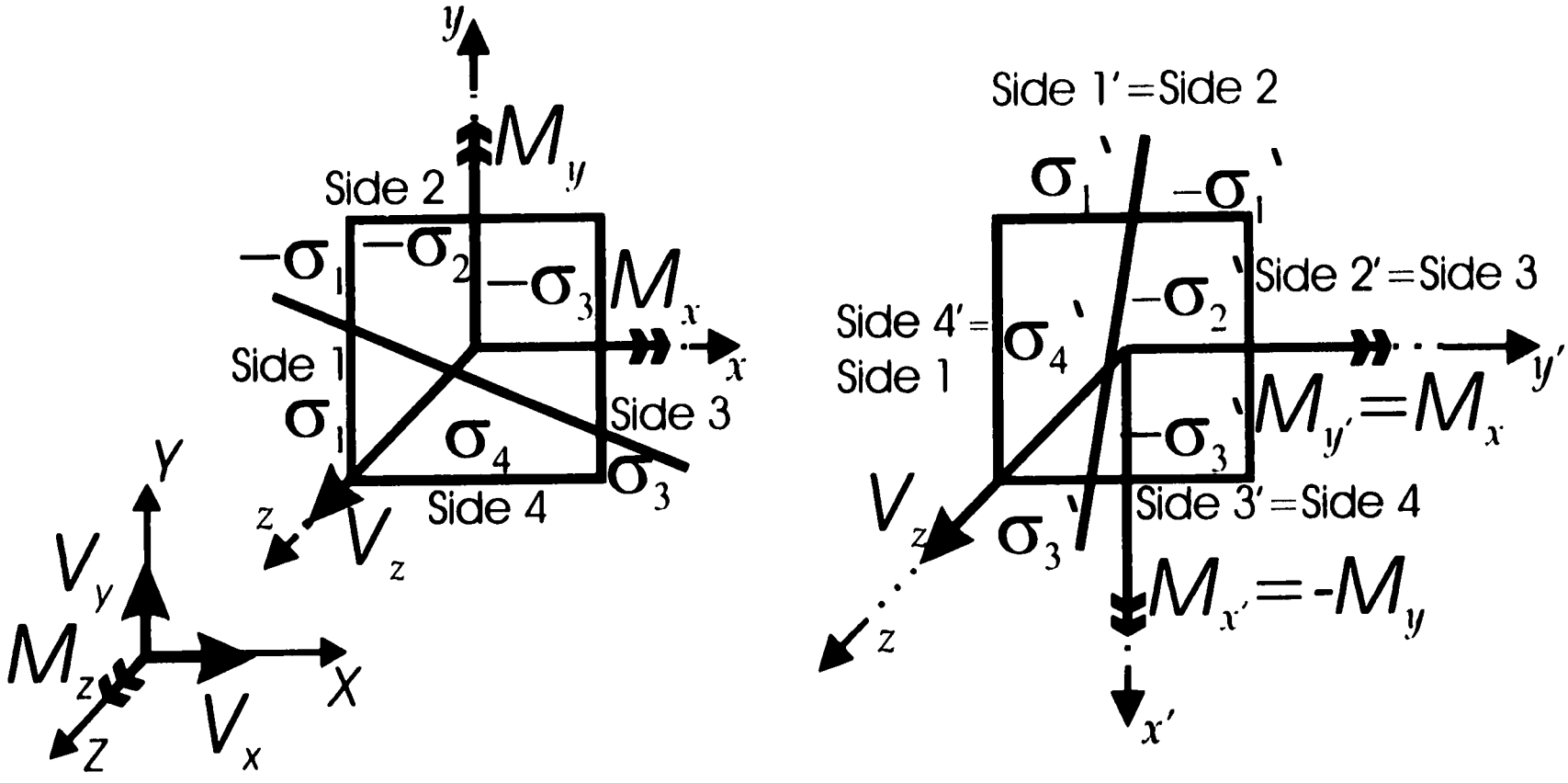

(a) Case I-1

(b) Case I-2

Figure 3.10 Axes Transformation

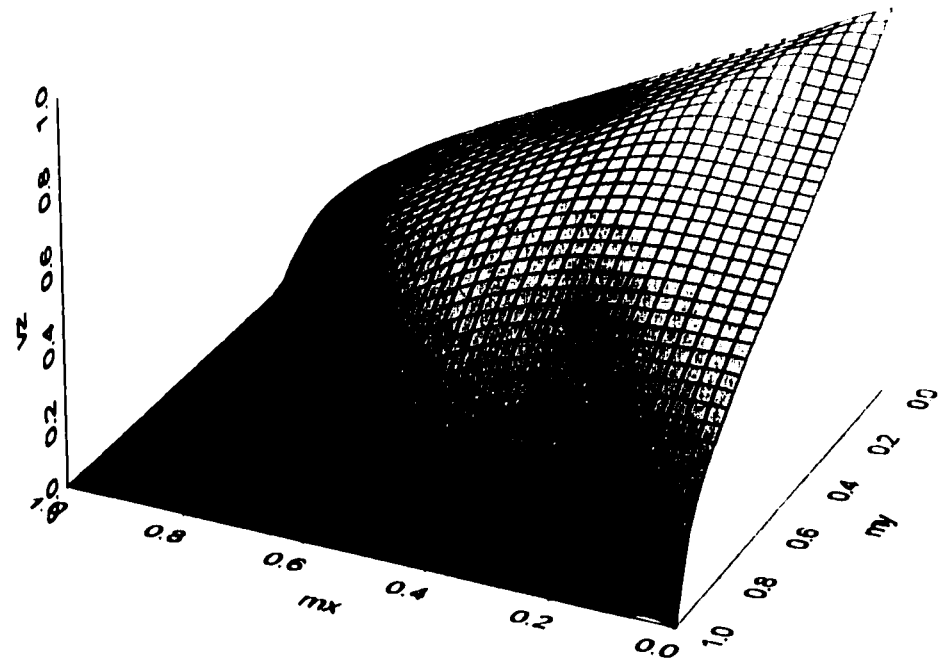

(a) Interaction surface

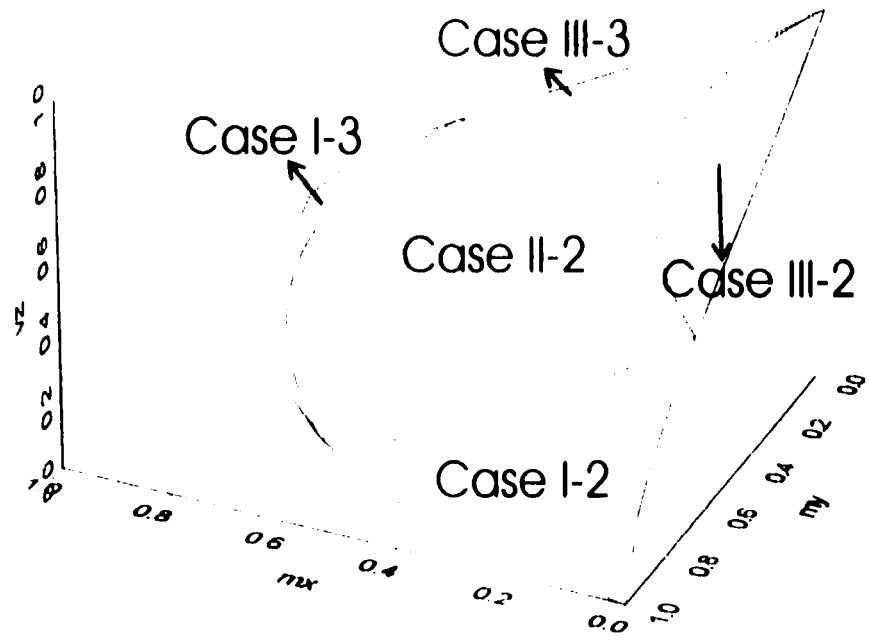

(b) Borders of the different cases on the interaction surface

Figure 3.11 Interaction Surface ($m_x = v_x = v_y = 0$)

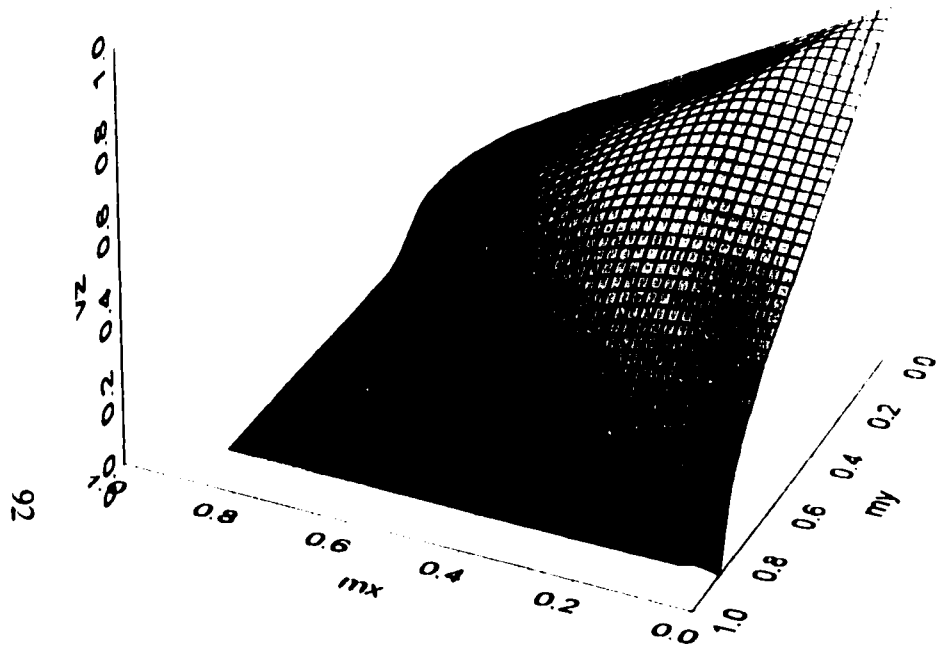

(a) Interaction Surface ($m_z = 0.5, v_x = v_y = 0$)

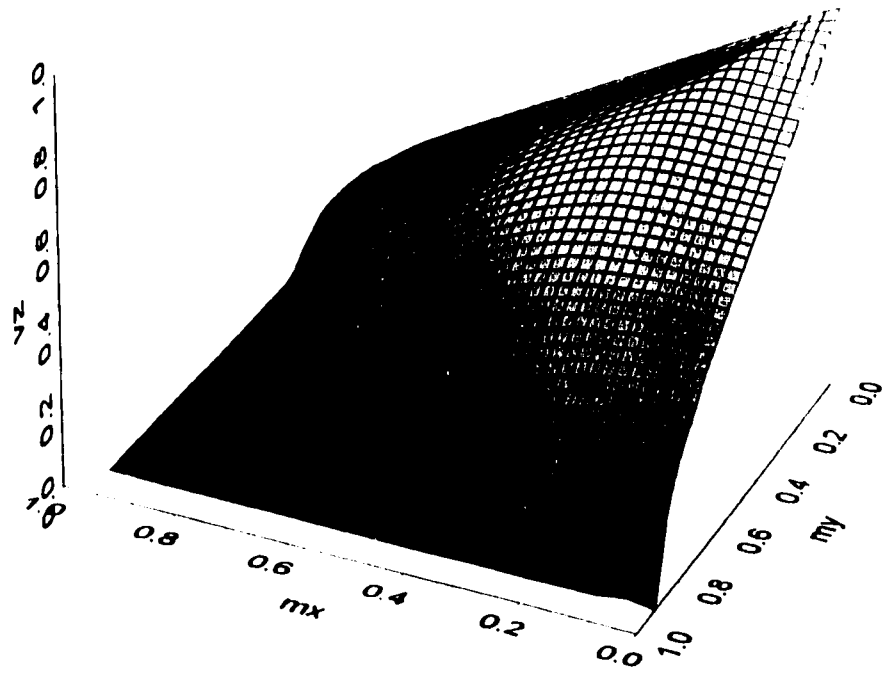

(b) Interaction Surface ($v_x = 0.5, m_z = v_y = 0$)

Figure 3.12 Interaction Surfaces

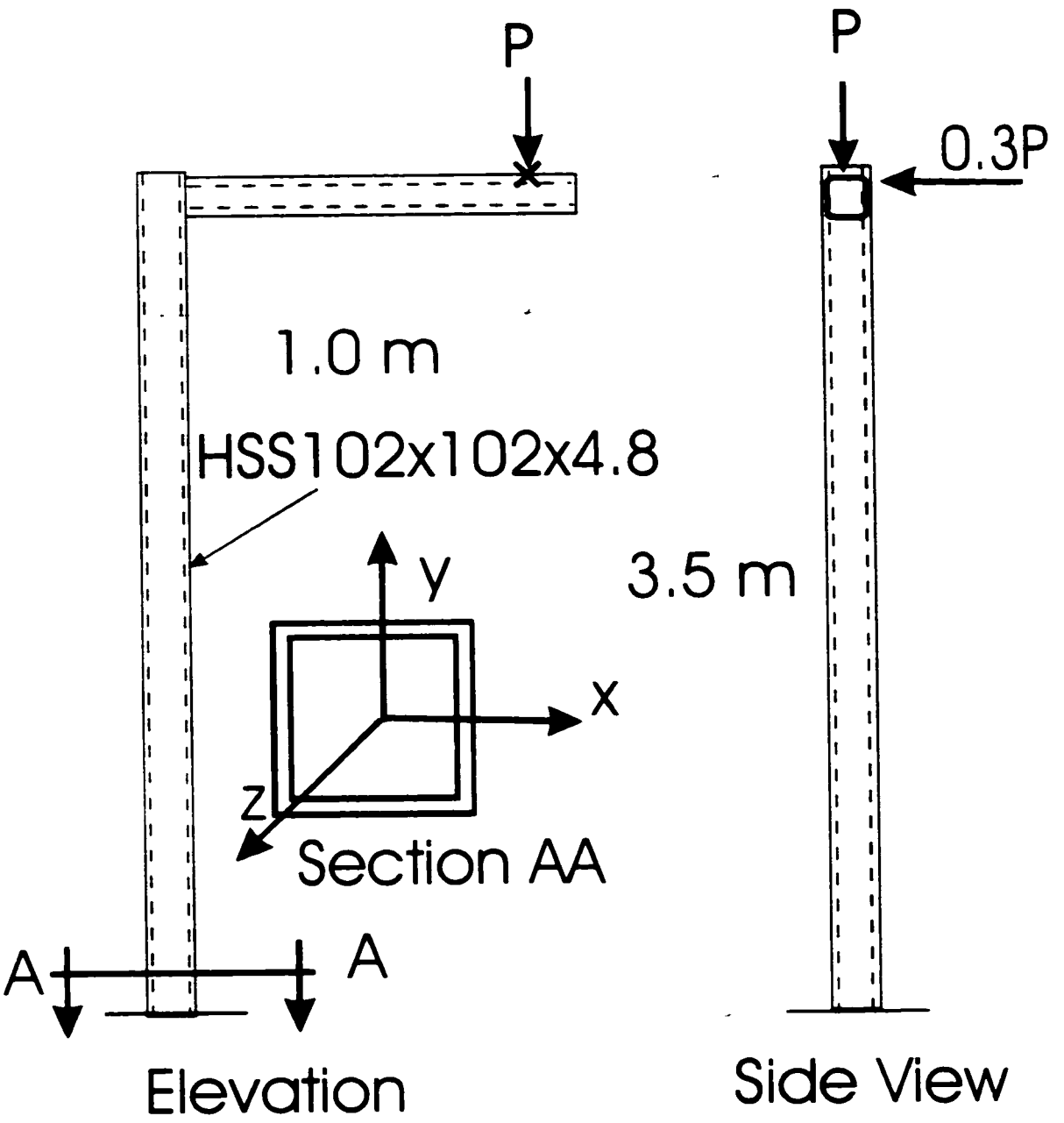

Figure 3.13 Design Example

CHAPTER 4

SUMMARY AND RECOMMENDATIONS FOR FUTURE RESEARCH

4.1 Summary:

1) An experimental program consisting of six full-scale tests on steel pipes under load combinations of bending, shear, and torsion was conducted. The experimental results agreed very well with recently developed interaction relations. All specimens attained failure loads that are slightly higher than the analytically predicted ones. The predicted to experimental failure load averaged 91% with a standard deviation of 2.8%, when the material yield strength is defined using the 0.002 plastic strain offset method. When the 0.005 extension-under-load method is used, the agreement between the two values improves to 94% with a standard deviation of 2.5%.

2) In all tests, local buckling was detected immediately before the specimens attained their peak load.

3) Based on previous experimental validation for bending, shear, and internal pressure and current research, it is believed that the interaction relations yield good results for pipes with D/t=41 and smaller.

4) A lower bound solution was used to derive general plastic interaction relations for square hollow structural sections subject to biaxial bending, biaxial shear, normal force and twist.

5) The relations are potentially applicable to the design of square hollow structural beam columns where local buckling does not occur prior the section attaining its fully plastic resistance. Besides their applicability in design problems, the interaction relations developed can be used to characterize the elasto-plastic force-deformation behavior of generalized plastic hinges in space frames consisting of square hollow structural sections in conjunction with well-established procedures of elasto-plastic frame analysis.

6) The interaction equations obtained for square hollow structural members are cast in a non-dimensional form and are suitable for limit states design.

4.2 Recommendations for Future Research

4.2.1 Pipe Sections

1) Current structural steel design codes provide the rules under which tubular sections subject to pure bending or pure compression will develop their fully plastic resistance prior loosing their strength due to local buckling. The current rules impose a threshold value on pipe diameter-to-thickness ratio as a function of the yield strength. The same concept can be borrowed in the design of pipelines under more general loading including twist, shear, and pressure. Similar rules will generally depend on a large number of geometric and loading parameters. In the current state of knowledge, such rules, although of practical importance, do not exist. It is required to mathematically describe those conditions using extensive non-linear finite element analysis with some experimental corroboration. The presence of these rules together with the experimentally verified interaction relations will form a complete set of design rules to be incorporated in pipeline codes.

2) The interaction relations recently developed were shown to closely match the results in this experimental program for common pipe sections. The validated

interaction relations can be used to characterize the generalized pipe plastic hinge behavior. This characterization can be used in developing elasto-plastic analysis procedures of pipelines that are more accurate than conventional elastic analysis and simpler to use than finite element shell analysis.

3) Full-scale tests on pipes under more general load combinations including bending, twist, axial force, internal pressure, and shear force, are of interest and would provide further assessment of the general interaction relations.

4.2.2 Square Hollow Structural Sections

1) The derived plastic interaction relations need to be checked against full-scale experiments on square hollow structural sections under combined loads.

2) The geometric and loading conditions under which the interaction relations developed need to be mathematically described. Given the large number of parameters involved, non-linear finite element analysis including both geometric and material non-linearity is proposed with some full-scale tests to corroborate the analysis results.

3) Further interaction research including residual stress patterns is practical interest for welded box girder applications

4) It is of interest to develop upper-bound interaction relations in order to assess the exactness of the solution.

5) It is of interest to extend the methodology used in this research to other closed sections such as rectangular hollow structural sections. For rectangular sections, warping effects due to twisting moments will occur and an exact treatment of the problem is expected to be more challenging.

APPENDIX A

LOCATION OF THE SENSORS AND DATA

Contents

- Tables A.1 and A.2 present the data collected to obtain stress vs. engineering strain curves for tension tests 1 and 2 in Fig. 2.5, respectively.

- Figures A.1, A.2, A.3, A.4, A.5, and A6 illustrate the location of the deflection measuring devices for specimens V15T86M31, V12T68M66, V17T00M98, V25T00M97, V13T77M51, and V24T71M51, respectively. The arrows in the figures show the location of sensors. Every sensor reads positive data in the direction of the shown arrow. Data obtained from these sensors can be seen in Tables A.3, A.4, A.5, A.6, A.7, and A.8, for specimens V15T86M31, V12T68M66, V17T00M98, V25T00M97, V13T77M51, and V24T71M51, respectively.

- Longitudinal strain readings for specimens V15T86M31, V12T68M66, V17T00M98, V25T00M97, V13T77M51, and V24T71M51 are shown in Tables A.9, A.10, A.11, A.12, A.13, and A.14, respectively. Tangential strain readings for specimens V15T86M31, V12T68M66, V17T00M98, V25T00M97, V13T77M51, and V24T71M51 are shown in Tables A.15, A.16, A.17, A.18, A.19, and A.20, respectively. Diagonal strain readings for specimens V15T86M31, V12T68M66, V17T00M98, V25T00M97, and V24T71M51 are shown in Tables A.21, A.22, A.23, A.24, and A.25, respectively. Strain readings are positive when the strain gage is in tension and negative when the strain gage is in compression.

Table A.1 Tension Coupon Test 1

Stress (MPa)	Strain (Microstrain)
0.0	0
60.8	328
107.0	573
160.4	854
214.0	1311
267.4	2048
274.1	2120
280.7	2253
287.4	2429
294.1	2633
300.8	2909
307.5	3196
314.2	3743
320.9	4568
327.5	6184
334.2	8618
340.9	11752
347.6	15157
354.3	19650
361.0	23969
367.6	28072
374.3	33470
381.0	41244
394.4	53336
401.1	60462
407.8	69100
414.4	82056
421.1	96092
427.8	116605
434.5	135300
427.8	360000

Table A.2 Tension Coupon Test 2

Stress (MPa)	Strain (Microstrain)
0.0	0
26.7	135
53.5	293
80.2	429
107.0	566
133.7	701
160.4	884
187.2	1089
213.9	1319
240.6	1539
267.4	1907
280.7	2163
294.1	2433
307.5	2714
314.2	3161
320.9	3465
327.5	3861
334.2	4481
340.9	5814
347.6	8871
354.3	14400
361.0	21154
367.6	26923
374.3	35192
381.0	42960
387.7	50000
394.4	57692
401.1	66840
407.8	79200
414.4	94231
421.1	107692
425.7	122304
432.3	135600
425.7	388000

Table A.3 Deflection and Load Readings-Specimen V15T86M31

Sensor ID	LVDT1	LVDT2	LVDT3	LVDT4	PT101A	PT101B	Actuator Stroke	Actuator Load	
Scan ID	mm	mm	mm	mm	mm	mm	mm	kN	Comments
1	0.4	0.2	0.1	-0.1	-0.1	0.1	5.0	40.4	No zero readings are taken
2	0.6	0.3	0.1	-0.1	-0.1	0.0	10.0	64.1	
3	0.9	0.5	0.1	-0.1	-0.2	0.0	15.0	88.5	
4	1.2	0.6	0.0	-0.2	0.0	-0.1	20.0	115.0	
5	1.7	0.7	0.0	-0.3	0.0	0.2	25.0	140.0	
6	2.5	0.7	0.0	-0.3	0.0	0.0	30.0	159.0	
7	3.5	0.8	-0.1	-0.4	-0.1	-0.1	35.0	171.0	
8	4.7	0.8	-0.2	-0.4	-0.1	-0.1	40.0	179.0	
9	6.1	0.8	-0.3	-0.5	0.0	0.0	45.0	183.0	
10	7.2	0.8	-0.5	-0.8	0.1	-0.2	50.0	186.0	
11	8.1	0.8	-0.6	-1.0	0.0	-0.1	55.0	189.0	
12	9.0	0.8	-0.7	-1.2	-0.1	-0.2	60.0	192.0	
13	10.1	0.7	-0.9	-1.4	-0.2	-0.2	65.0	194.0	
14	11.2	0.7	-1.0	-1.6	-0.3	-0.5	70.0	194.0	
15	13.3	0.6	-1.2	-2.2	-0.3	-0.5	79.9	199.0	
16	15.5	0.5	-1.5	-2.6	-0.3	-0.6	89.9	202.0	
17	17.6	0.3	-1.8	-3.0	-0.4	-0.6	99.9	205.0	
18	19.7	0.2	-2.1	-3.4	-0.4	-0.7	109.9	205.0	
19	21.7	0.0	-2.4	-3.6	-0.5	-0.6	120.0	209.0	Load released due to computer break down
20	20.0	-0.6	-2.3	-3.2	-0.4	-0.8	6.6	8.3	The positions of LVDT1 and LVDT2 are changed
21	-5.8	-17.8	-2.3	-3.2	-0.5	-0.7	6.6	8.4	
22	1.5	-17.8	-3.1	-3.9	-0.5	-0.7	39.9	201.0	
23	10.1	-18.7	-4.4	-3.8	-0.5	-0.8	80.0	-210.0	
24	14.6	-19.1	-4.8	-4.0	-0.5	-1.2	99.0	208.0	The position of LVDT3 is changed
25	14.6	-19.1	-6.0	-4.0	-0.6	-1.2	99.0	205.0	
26	19.1	-19.5	-6.4	-4.5	-1.0	-1.2	119.0	205.0	
27	21.4	-19.7	-6.6	-4.9	-1.0	-1.7	130.0	201.0	
28	26.0	-20.1	-7.1	-6.6	-1.1	-2.7	150.0	191.0	
29	28.4	-20.2	-7.4	-7.1	-1.3	-3.4	159.0	190.0	
30	30.7	-20.3	-7.9	-7.8	-1.4	-3.7	169.0	185.0	changed
31	3.6	-20.4	-7.9	-7.8	-1.4	-3.7	169.0	184.0	
32	5.9	-20.5	-8.4	-8.8	-1.7	-4.4	179.0	179.0	
33	8.2	-20.7	-9.0	-9.2	-2.0	-4.9	189.0	174.0	
34	10.5	-20.9	-9.7	-9.9	-2.2	-5.4	199.0	168.0	
35	12.9	-21.2	-10.5	-10.5	-2.3	-6.5	209.0	161.0	

Table A.4 Deflection and Load Readings-Specimen V12T68M66

Sensor ID	LVDT	PT101A	PT101B	Temposonic #1	Temposonic #2	Temposonic #3	Actuator Stroke	Actuator Load
Scan ID	mm	mm	mm	mm	mm	mm	mm	kN
1	0 0	0 2	0 1	0.0	0 0	0.0	0.0	0 0
2	-0 1	0.2	0 1	-1 9	0.0	2.1	5 0	10.8
3	-0 1	0.2	0.1	-3.5	0.0	4.3	10.0	22.3
4	-0.2	0 1	0.1	-4.7	-0.1	6.3	15.0	32.8
5	-0.2	0.2	-0.4	-5.8	-0.1	8.1	20.0	42.9
6	-0.2	0.2	-0.5	-6.8	-0.1	9.9	25.0	53.8
7	-0.2	0 1	-0.7	-7.7	-0.1	11.6	30.0	62 8
8	-0 2	0 0	-0.8	-8.8	-0.1	13.5	35.0	74.7
9	-0 2	0 2	-0.9	-9.7	-0 1	15.3	40.0	86 0
10	-0.2	0 0	-1 1	-10 8	-0 1	17 1	45 0	96.9
11	-0 2	0.0	-1 4	-11 8	-0 1	18 9	50.0	106.9
12	-0.2	0.0	-1.6	-12.7	-0.1	20.7	55.0	116 0
13	-0.2	0.2	-1.8	-13.7	-0 1	22.5	60 0	124 4
14	-0 1	0.2	-2.4	-15.8	-0.1	26.2	70.0	136 7
15	-0 1	0 1	-2 5	-16 8	-0 1	28 1	75 0	142 1
16	-0 1	0 2	-2 8	-17 9	-0 1	29 9	80 0	145.3
17	-0 1	0 2	-3 2	-18 9	-0 1	32 0	85 0	148 2
18	0 0	0 0	-3 2	-20 0	-0 2	33 9	90 0	151 4
19	0 0	0 0	-3 9	-22.2	-0.2	38 0	100 0	154 7
20	0.1	0.2	-4.3	-24.5	-0.5	41.9	110.0	157 7
21	0.1	0.0	-4.8	-26.8	-0.6	46.0	120 0	160.1
22	0 2	0 0	-5.2	-29.2	-0.8	50.1	130 0	161.2
23	0 2	0 0	-5 7	-31 5	-0 9	54.3	140.0	163 3
24	0 3	0 1	-6 1	-33.9	-1 1	58.4	150 0	164 5
25	0 4	0 1	-6 7	-36 4	-1 3	62 6	160 0	166 0
26	0 5	0 1	-7 3	-38.9	-1 6	66 8	170.0	167 0
27	0.6	0.1	-7.8	-41.3	-1.8	71.2	180.0	167 8
28	0.6	0.0	-8.1	-43.8	-2.0	75.4	190.0	168 6
29	0 7	0.1	-8.9	-46.3	-2.2	79 7	200.0	169 6
30	0 8	0 1	-9 4	-48 9	-2 3	84 1	210.0	170 3
31	0 9	0 0	-10 0	-51 6	-2 4	88.5	220.0	170.6
32	0 9	0 0	-10 5	-54 4	-2 5	93 1	230.0	170 7
33	1 0	0.2	-11 3	-57.4	-2.5	97.8	240.0	170 8
34	1 0	0.2	-12.0	-60 5	-2.5	102.6	250.0	169.9
35	1.0	0.1	-12.8	-63.6	-2.5	107.3	260 0	169 9
36	1.1	0.1	-13.5	-67.1	-2.6	112.3	270.0	168 5
37	1 1	-0 1	-15 3	-74.4	-2.6	122.5	290.0	165.5
38	1 3	-0 4	-17 2	-81.9	-2.6	133.2	310.0	160.3
39	2 4	-0 5	-19.2	-93 1	-4.2	146 5	330.0	136 5

Table A.5 Deflection and Load Readings-Specimen V17T00M98

Sensor ID	LVDT1	LVDT2	PT101A	PT101B	Temposonic #1	Temposonic #2	Actuator Stroke	Actuator Load
Scan ID	mm	mm	mm	mm	mm	mm	mm	kN
1	0.0	0.0	0.1	0.0	0.0	0.0	0.0	0.1
2	0.3	0.0	0.1	0.1	1.3	-0.1	3.0	15.4
3	0.6	0.1	0.1	0.0	3.3	-0.1	6.0	30.3
4	0.6	0.0	0.4	-0.4	5.1	-0.1	9.0	47.2
5	0.5	-0.1	0.4	-0.8	6.9	-0.1	12.0	65.7
6	0.4	-0.2	0.4	-1.0	8.8	-0.1	15.0	83.7
7	0.2	-0.2	1.0	-1.4	10.8	-0.1	18.0	102.8
8	0.1	-0.3	1.2	-1.8	12.8	0.0	21.0	120.9
9	-0.1	-0.3	1.6	-1.9	14.8	0.1	24.0	138.7
10	-0.2	-0.4	1.6	-2.5	16.8	0.2	27.0	155.7
11	-0.4	-0.4	2.2	-2.7	18.8	0.4	30.0	171.5
12	-0.5	-0.5	2.4	-3.1	21.0	0.5	33.0	185.0
13	-0.7	-0.5	3.1	-3.5	23.1	0.6	36.0	198.9
14	-0.9	-0.6	3.1	-4.0	25.3	0.7	39.0	209.6
15	-1.0	-0.6	3.8	-4.3	27.7	0.7	42.0	218.8
16	-1.2	-0.6	4.0	-4.9	29.9	0.8	45.0	223.3
17	-1.4	-0.7	4.8	-5.3	32.3	0.9	48.0	230.4
18	-1.6	-0.7	5.0	-5.9	34.8	0.9	51.0	234.7
19	-1.7	-0.7	5.5	-6.0	37.3	0.9	54.0	238.3
20	-1.9	-0.8	6.5	-6.6	39.8	1.0	57.0	240.8
21	-2.1	-0.9	6.5	-7.1	42.4	1.0	60.0	243.4
22	-2.5	-1.0	7.3	-7.9	47.6	1.0	66.0	247.3
23	-2.8	-1.1	7.9	-8.6	51.0	1.0	70.0	247.8
24	-3.1	-1.2	8.5	-9.3	55.3	1.0	75.0	249.9
25	-3.4	-1.4	9.3	-10.1	59.6	1.0	80.0	251.6
26	-3.7	-1.5	10.1	-11.1	64.0	1.0	85.0	251.4
27	-4.1	-1.6	10.5	-11.8	68.3	1.0	90.0	252.6
28	-4.4	-1.8	11.3	-12.7	72.7	0.9	95.0	251.1
29	-4.7	-1.9	12.0	-13.4	77.2	0.9	100.0	251.4
30	-5.0	-2.1	12.8	-14.2	81.6	0.9	105.0	250.1
31	-5.1	-2.2	13.8	-15.1	86.1	0.9	110.0	246.3
32	-5.1	-2.6	14.6	-16.8	95.1	0.8	120.0	244.2
33	-5.1	-2.9	16.0	-18.7	104.1	0.6	130.0	241.7
34	-5.1	-3.3	17.3	-20.6	113.3	0.1	140.0	238.7

Table A.6 Deflection and Load Readings-Specimen V25T00M97

Sensor ID	LVDT1	LVDT2	PT101A	PT101B	Temposonic #1	Temposonic #2	ActuatorStroke	Actuator Load
Scan ID	mm	mm	mm	mm	mm	mm	mm	kN
1	0 0	0 0	0.2	-0.1	0.0	0.0	0.0	-0.2
2	-0 2	0 3	0 2	-0 1	0.0	0.1	2.0	19 5
3	-0 4	0 4	0 5	-0.3	0 0	0.1	4 0	40 3
4	-0 6	0 5	0 4	-0 6	0 7	0.1	6.0	62.6
5	-0 7	0 5	0.5	-0.7	1 6	0.1	8.0	87 4
6	-0.8	0.6	0.9	-1.1	3.3	0.1	12.0	138.6
7	-0.9	0.7	0.8	-1.4	4.2	0.1	14.0	164.4
8	-0 9	0.7	1.4	-1.8	5.1	0.1	16.0	189.3
9	-0 9	0 7	2 0	-2.1	6.0	0.1	18.0	212.8
10	-1 0	0 7	2.2	-2.5	7 1	0 1	20.0	235.8
11	-1 0	0.7	2.3	-3 0	9 7	0.1	25.0	284.6
12	-1 1	0.7	3.1	-4.0	12.6	0.1	30.0	321.5
13	-1.0	0.6	3.9	-5.0	15 7	0.1	35.0	343.9
14	-1.0	0.6	4.3	-5.4	17.1	0.1	37.0	349.8
15	-1.0	0.5	4.9	-6.2	19.4	0.1	40.0	355.6
16	-0 9	0 3	5 9	-7 0	23.1	0.1	45.0	361 9
17	-0 9	0 3	5 8	-7 1	23 1	0.1	50.0	360.7
18	-0 8	0 2	6 8	-8.2	26 8	0.1	55 0	366 1
19	-0 7	0 0	7 8	-9 3	30 7	0.1	60 0	369 1
20	-0 7	-0.2	9 1	-10 5	34 6	0.1	65 0	369 8
21	-0.6	-0.5	10.0	-11 7	38.8	0.1	70 0	367 0
22	-0 5	-1 3	11.7	-12.9	43.5	0.0	80 0	337 9
23	-0 1	-4 2	15 5	-14 3	53 8	-2.6	90 0	260.3

Table A.7 Deflection and Load Readings-Specimen V13T77M51

Sensor ID	LVDT	PT101A	PT101B	Temposonic #1	Temposonic #2	Temposonic #3	Actuator Stroke	Actuator Load
Scan ID	mm	mm	mm	mm	mm	mm	mm	kN
1	0 0	0.1	-0.1	0.0	0.0	0.0	3.8	0.1
2	0 0	0.0	0.0	0.0	-0.1	0.0	5.0	5.6
3	0 1	0.0	-0.2	1.3	-0 6	0.0	10.0	26.2
4	0.3	0.0	0.1	2.8	-1.1	0.0	15.0	42.6
5	0.3	-0.1	0.1	4.1	-1.5	0.0	20.0	58 1
6	0.3	0.0	0.2	4.7	-1 6	0.0	22.0	60.1
7	0 3	0 0	0 1	5.5	-1 8	0.5	25.0	67 0
8	0 3	0 0	0 3	6 1	-1 9	0 5	27 0	76 2
9	0 3	0 1	0 3	7 0	-2.1	0 5	30 0	81 3
10	0 3	0 0	0 4	7 6	-2.3	0.5	32.0	90 6
11	0 3	-0 2	0 6	8.5	-2.6	0.5	35 0	98 7
12	0.3	-0.2	0.6	8.9	-2.7	0.5	37.0	107 0
13	0.3	0.0	0.6	9.8	-3.0	0.5	40.0	113.9
14	0.3	-0.1	0.8	11.2	-3.4	0.6	45.0	129 0
15	0 3	-0 3	0 9	12.6	-3.9	0.6	50.0	140.8
16	0 3	-0 1	0 9	14 0	-4 2	0 5	55 0	151 2
17	0 3	0 1	1 3	15.3	-4 6	0 6	60 0	158 8
18	0 3	-0 1	1 4	16 6	-4 9	0 6	65.0	164 9
19	0 3	-0 1	1.3	18.0	-5 2	0 6	70.0	169 7
20	0.3	-0.2	1 7	19.5	-5.5	0.6	75.0	172.9
21	0.2	-0.2	2.0	21.0	-5.9	0.6	80.0	175 2
22	0.2	-0.2	2.1	22.3	-6.2	0.6	85.0	177 2
23	0 2	-0 1	2.3	23 8	-6 5	0 6	90.0	179 0
24	0 2	-0 2	2 3	25.2	-6 9	0 6	95.0	180 8
25	0 1	-0 1	2 5	26 7	-7 2	0 6	100.0	181.8
26	0 1	-0 4	2 6	28 1	-7 5	0.6	105.0	183 2
27	0 1	-0 4	2 8	29.5	-7 8	0 6	110.0	184.0
28	0.1	-0.2	2.8	31.0	-8.2	0.6	115.0	185 0
29	0.1	-0 3	3.1	32.5	-8 5	0.6	120.0	186 1
30	0.0	-0 4	3.4	34.0	-8.9	0.6	125.0	186 4
31	0 0	-0 3	3 5	35 5	-9.2	0.6	130.0	187 3
32	0 0	-0 4	3 5	36.9	-9 5	0.6	135 0	188 1
33	-0 1	-0 4	3 7	38 3	-9 9	0 6	140.0	189.2
34	-0 1	-0 6	4 0	39 8	-10.2	0.6	145.0	189.8
35	-0 1	-0.6	4.2	41.4	-10.5	0.6	150.0	190.5
36	-0.1	-0.5	4.2	42.9	-10.9	0.6	155.0	191.6
37	-0.1	-0.6	4.7	46.0	-11.7	0.6	165.0	192.7
38	-0.2	-0.6	4.9	47.6	-12.1	0.6	170.0	193.4
39	-0 2	-0 6	5 1	50.5	-12.9	0.6	180 0	193.8
40	-0 3	-0 6	5 9	56 5	-14 3	0.6	200 0	195 5
41	-0 3	-0 8	6 1	59.7	-15.2	0.6	210.0	196 5
42	-0 3	-0 8	6 6	62.7	-16.0	0.6	220.0	197 1
43	-0.3	-0 8	7.2	66 1	-17 0	0.6	230.0	197.7
44	-0.3	-0.9	7.6	69.3	-17.9	0.6	240.0	197.9
45	-0.3	-1.0	8.0	72.7	-18.9	0.6	250.0	197.7
46	-0.3	-0.7	8.6	76.3	-20.0	0.6	260.0	197 4
47	-0 1	-1 1	9.8	83.2	-22.5	0.6	280.0	195.2
48	0 1	-1 5	11 5	90.2	-25.2	1 2	300.0	190.4

Table A.8 Deflection and Load Readings-Specimen V24T71M51

Sensor ID	LVDT1	LVDT2	PT101	Temposonic #1	Temposonic #2	Actuator Stroke	Actuator Load
Scan ID	mm	mm	mm	mm	mm	mm	kN
1	0.0	0.0	-0.2	0.0	0.0	-1.4	0.1
2	0.0	0.0	0.0	0.0	0.0	2.0	11.0
3	0.0	0.0	-0.1	0.0	0.0	4.0	12.0
4	0.0	0.0	-0.1	0.0	0.0	6.0	11.8
5	0.0	0.0	0.0	0.0	0.0	8.0	16.1
6	0.0	0.0	0.0	0.0	0.0	10.0	21.6
7	0.1	0.1	-0.1	0.8	0.0	12.0	30.1
8	0.1	0.1	-0.1	1.2	0.0	14.0	44.0
9	0.1	0.1	-0.2	1.7	-0.1	16.0	65.6
10	0.1	0.2	-0.5	2.3	-0.2	18.0	92.3
11	0.1	0.2	-0.4	3.0	-0.4	20.0	121.0
12	0.2	0.3	-0.6	4.0	-1.0	25.0	194.0
13	0.3	0.4	-0.7	5.6	-1.4	30.0	256.0
14	0.4	0.5	-0.8	7.2	-1.8	35.0	295.0
15	0.4	0.5	-1.4	8.8	-1.8	40.0	311.0
16	0.4	0.4	-1.5	10.7	-1.7	45.0	323.0
17	0.4	0.4	-1.9	12.5	-1.6	50.0	330.0
18	0.4	0.4	-2.1	14.6	-1.9	55.0	338.0
19	0.4	0.4	-2.7	17.3	-2.3	60.0	343.0
20	0.4	0.4	-3.1	19.9	-2.6	65.0	348.0
21	0.4	0.4	-3.0	22.4	-2.8	75.0	352.0
22	0.3	0.3	-2.7	27.3	-3.2	80.0	360.0
23	0.3	0.3	-3.0	29.3	-3.5	85.0	364.0
24	0.3	0.3	-3.5	31.4	-3.7	90.0	367.0
25	0.3	0.3	-4.5	33.5	-3.8	95.0	370.0
26	0.2	0.2	-4.5	35.2	-4.2	100.0	373.0
27	0.2	0.2	-4.7	37.1	-4.6	105.0	375.0
28	0.1	0.2	-5.0	39.4	-5.0	110.0	377.0
29	0.0	0.1	-5.4	41.5	-5.0	115.0	376.0
30	-0.2	0.0	-6.2	43.8	-5.2	120.0	376.0
31	-0.5	0.0	-5.9	46.1	-5.4	125.0	375.0
32	-1.1	-0.2	-6.8	51.3	-6.0	135.0	368.0
33	-2.2	-0.4	-7.8	57.2	-7.0	145.0	357.0
34	-3.5	-0.8	-8.8	62.1	-8.0	155.0	345.0
35	-5.1	-1.3	-9.9	66.3	-8.9	165.0	332.0

Table A.9 Measured Longitudinal Strains-Specimen V15186M31

Location*	A	B	C	D	E	F	G	H	
Scan ID	Microstrain	Microstrain	Microstrain	Microstrain	Microstrain	Microstrain	Microstrain	Microstrain	Comments
1	-32	-88	76	133	139	28	-3	-14	zero reading is not taken
2	68	-150	100	225	213	39	-45	-19	
3	-117	-222	-116	327	294	40	-103	-28	
4	-182	-299	-123	433	394	33	-124	-47	
5	268	-381	-114	545	497	23	-115	-96	
6	-373	-471	-91	676	626	42	-102	-180	
7	-492	-572	-54	848	768	148	-85	-278	
8	-607	-679	-12	1100	892	283	-37	-375	
9	-716	-788	34	1430	1020	411	23	-470	
10	-823	-901	81	1810	1190	533	137	-556	
11	-930	-1020	130	2190	1380	656	227	-628	
12	-1040	-1130	176	2550	1590	779	309	-719	
13	-1150	-1260	224	2900	1820	904	355	-775	
14	-1250	-1380	270	3230	2050	1030	362	-819	
15	-1470	-1620	359	3800	2540	1270	305	-866	
16	-1680	-1860	448	4320	3050	1500	-158	-875	
17	-1900	-2100	539	4820	3600	1740	-132	-843	
18	-2120	-2330	632	5300	4160	1980	-123	-771	
19	-2350	-2550	723	5760	4770	2230	-100	-653	Load released due to computer break down
20	-2060	-2100	808	4990	4090	1910	-178	-712	
21	-2060	-2100	808	4990	4090	1910	-178	-712	The positions of LVDT1 and LVDT2 are changed
22	-2970	-3070	941	6860	6460	2920	-3	-92	
23	-4310	-3790	1250	8380	OFFSCALE +	4080	119	1800	
24	-5190	-4110	1320	8910	OFFSCALE +	4960	150	4270	
25	-5180	-4090	1320	8910	OFFSCALE +	5150	144	7770	The position of LVDT3 is changed
26	-6160	-4430	1280	9370	OFFSCALE +	6520	197	OFFSCALE +	
27	-6630	-4600	1220	9610	OFFSCALE +	12500	234	OFFSCALE +	
28	-7480	-4920	1040	10100	OFFSCALE +	OFFSCALE +	392	OFFSCALE +	
29	-7830	-5090	999	10500	OFFSCALE +	OFFSCALE +	467	OFFSCALE +	
30	-8020	-5260	980	11000	OFFSCALE +	OFFSCALE +	548	OFFSCALE +	
31	-8000	-5260	979	11000	OFFSCALE +	OFFSCALE +	549	OFFSCALE +	The position of LVDT1 is changed
32	-8180	-5430	971	11500	OFFSCALE +	OFFSCALE +	640	OFFSCALE +	
33	-8320	-5580	983	12000	OFFSCALE +	OFFSCALE +	732	OFFSCALE +	
34	-8420	-5720	1010	12500	OFFSCALE +	OFFSCALE +	835	OFFSCALE +	
35	-8470	-5840	1060	13200	OFFSCALE +	OFFSCALE +	948	OFFSCALE +	

*The location of the strain gages are shown in Fig. 2.14b

Table A.10 Measured Longitudinal Strains-Specimen V12168M66

Location*	A	B	C	D	E	F	G	H	K	L
Scan ID	Microstrain	Microstrain	Microstrain	Microstrain	Microstrain	Microstrain	Microstrain	Microstrain	Microstrain	Microstrain
1	-1	0	0	0	0	0	1	0	0	-1
2	-55	55	-25	70	90	46	26	-37	1	-1
3	-124	121	-32	131	165	96	12	-78	0	0
4	-191	177	-37	179	228	147	-58	-115	1	4
5	-255	230	-38	221	286	191	-70	-154	1	6
6	-330	-284	-39	265	348	245	-82	-198	0	8
7	-392	-329	-35	300	392	285	-88	-234	0	10
8	-491	390	-30	346	455	348	-99	-292	0	12
9	-594	-451	-22	392	513	411	-111	-352	1	16
10	-703	-519	-18	438	568	482	-122	-417	1	18
11	-830	-595	-11	486	628	558	-130	-485	1	20
12	-973	-677	-5	533	690	645	-133	-558	3	21
13	-1142	-768	1	586	757	745	132	-637	2	21
14	-1580	-987	17	706	934	973	-113	-815	2	21
15	-1850	-1110	26	782	1048	1106	-94	-924	0	20
16	-2171	-1251	39	866	1206	1248	-68	-1054	-2	19
17	-2531	-1409	55	965	1386	1406	-33	-1212	-5	16
18	-2917	-1577	76	1078	1596	1576	5	-1392	-9	15
19	-3841	-1976	138	1340	2161	1983	95	-1861	-17	12
20	-4795	-2391	214	1672	2809	2446	186	-2386	-27	10
21	-5794	-2826	300	2067	3513	2968	282	-2738	-35	7
22	-6848	-3270	395	2520	4255	3545	376	-3055	-43	5
23	-7902	-3675	487	2991	4981	4130	469	-3363	-52	5
24	-9007	-4068	578	3489	5711	4731	501	-3561	-61	5
25	-10153	-4431	665	4000	6433	5325	601	-3836	-69	6
26	-11357	-4793	749	4526	7150	5914	692	-4030	-77	7
27	-12617	-5144	821	5053	7845	6478	721	-4140	-85	8
28	-13979	-5445	887	5593	8537	7041	806	-4238	-92	8
29	OFFSCALE -	-5756	941	6133	9222	7595	878	-4346	-98	6
30	OFFSCALE -	-6084	981	6679	9908	8143	937	-4236	-105	3
31	OFFSCALE -	-6411	1003	7228	10598	8697	982	-4130	-109	-2
32	OFFSCALE -	-6745	1003	7771	11296	9242	992	-3677	-112	-12
33	OFFSCALE -	-7064	968	8302	11991	9813	962	-3246	-115	-25
34	OFFSCALE -	-7357	889	8827	12730	10415	820	-2128	-115	-43
35	OFFSCALE -	-7607	759	9301	13432	11009	688	-2268	-116	-61
36	OFFSCALE -	-7804	566	9761	14134	11663	521	-2149	-114	-82
37	OFFSCALE -	-8025	-15	10614	15445	13150	82	-2293	-110	-127
38	-14286	-8016	-899	11497	15650	15628	-486	-1403	-107	-172
39	-13085	-8335	-238	7645	13890	6905	-956	-1253	-178	-108

* The location of the strain gages are shown in Fig. 2.14b

Table A.11 Measured Longitudinal Strains-Specimen V17T00M98

Location*	A	B	C	D	E	F	G	H
Scan ID	Microstrain	Microstrain	Microstrain	Microstrain	Microstrain	Microstrain	Microstrain	Microstrain
1	0	-1	-1	0	0	-1	-1	0
2	-84	-102	-39	97	105	46	-16	-58
3	-151	-194	-63	188	201	111	-27	-129
4	-275	-284	-70	278	291	195	-21	-221
5	-423	-375	-67	376	377	285	-4	-331
6	-562	-465	-63	479	453	375	16	-436
7	-720	-566	-62	593	529	465	37	-547
8	-886	-674	-64	707	593	545	60	-668
9	-1051	-793	-68	823	650	618	85	-807
10	-1256	-933	-72	937	711	689	110	-970
11	-1508	-1109	-78	1048	782	757	137	-1171
12	-1801	-1345	-86	1151	870	819	168	-1424
13	-2174	-1653	-93	1262	1004	898	204	-1727
14	-2629	-2045	-102	1369	1164	991	246	-2105
15	-3207	-2523	-112	1494	1375	1112	295	-2566
16	-3982	-3104	-122	1636	1723	1282	355	-3157
17	-4823	-3716	-128	1824	2091	1533	422	-3785
18	-5883	-4374	-131	2031	2775	1941	503	-4549
19	-7024	-4521	-131	2329	3434	2510	588	-5350
20	-8400	-4810	-135	2745	4064	3279	684	-6293
21	-9876	-5266	-141	3225	3910	4080	782	-7277
22	-12865	-5767	-182	2193	1759	5759	995	-9083
23	-12819	-5068	-241	2205	1731	6888	1137	-10470
24	-11226	-4759	-353	2661	1120	8257	1299	-11880
25	-4717	-4497	-529	1823	1170	9626	1417	-13442
26	-4487	-3131	-797	1298	1138	11051	1447	-14597
27	-4475	-2851	-1155	1344	878	12446	1377	-15280
28	-4408	-2730	-1643	1286	847	13913	1178	OFFSCALE -
29	-4390	-2614	-2205	1291	814	15334	881	-12203
30	-4382	-2610	-2866	841	780	OFFSCALE +	451	-13078
31	-4373	-2533	-3603	773	763	OFFSCALE +	-118	-13526
32	-4394	-2188	-5109	740	814	OFFSCALE +	-1469	-14679
33	-4363	-2253	-6677	498	813	OFFSCALE +	-3073	-15010
34	-4466	-2288	-8274	430	731	OFFSCALE +	-4797	-15239

* The location of the strain gages are shown in Fig. 2.14b

Table A.12 Measured Longitudinal Strains-Specimen V25100M97

Location*	A	B	C	D	E	F	G	H
Scan ID	microstrain	microstrain	microstrain	microstrain	microstrain	microstrain	microstrain	microstrain
1	1	0	-1	-1	-1	-1	0	1
2	-75	-60	-5	55	81	62	-9	-64
3	-164	-141	-8	136	169	128	-16	-132
4	-265	-225	-6	221	266	199	-21	-207
5	-386	-309	3	313	370	278	-18	-300
6	-657	-472	31	499	585	448	5	-508
7	-804	-561	47	590	698	533	20	-625
8	-965	-658	64	679	813	617	37	-749
9	-1148	-765	81	760	932	701	55	-884
10	-1357	-889	101	837	1058	788	72	-1031
11	-2074	-1327	172	986	1506	1035	114	-1513
12	-3371	-2108	303	1105	2888	1440	167	-2277
13	-5681	-3474	486	1265	5740	2398	224	-3713
14	-6850	-4177	553	1371	7013	3077	241	-4507
15	-8860	-5376	635	1580	8992	4346	251	-5922
16	-12237	-7563	714	2153	12156	6711	183	-8535
17	OFF	-9454	727	2988	15325	9027	-33	-11097
18	OFF	-11403	689	2479	OFF	11397	-464	-13589
19	OFF	-13293	629	2451	OFF	13844	-1137	OFF
20	OFF	-14579	769	2322	OFF	OFF	-2021	OFF
21	OFF	OFF	2180	1491	OFF	OFF	-2395	OFF
22	OFF	-14936	2880	1372	OFF	OFF	-1732	OFF

*The location of the strain gages are shown in Fig. 2.14b

Table A.13 Measured Longitudinal Strains-Specimen V13T77M51

Location*	A	B	C	D	E	F	G	H
Scan ID	Microstrain	Microstrain	Microstrain	Microstrain	Microstrain	Microstrain	Microstrain	Microstrain
1	-1	-1	-1	0	0	0	0	0
2	-11	-19	-18	17	31	16	-2	-11
3	-74	-108	-85	104	167	76	-21	-70
4	-131	-184	-129	182	266	124	-31	-118
5	-195	-255	-144	252	348	179	-26	-156
6	-207	-266	-145	267	363	185	-27	-165
7	-239	-295	-148	297	399	214	-23	-186
8	-279	-333	-152	331	447	253	-16	-216
9	-308	-360	-151	357	479	275	-13	-236
10	-354	-403	-152	393	529	320	-5	-269
11	-399	-447	-150	432	577	360	2	-300
12	-447	-492	-148	467	627	407	12	-334
13	-492	-542	-144	507	675	447	16	-364
14	-605	-647	-130	593	785	554	41	-439
15	-722	-748	-111	680	890	657	74	-509
16	-880	-854	-84	789	1009	774	132	-595
17	-1051	-958	-54	909	1127	877	206	-681
18	-1262	-1072	-18	1063	1262	984	305	-789
19	-1493	-1190	18	1242	1397	1082	415	-909
20	-1766	-1322	60	1457	1537	1180	535	-1048
21	-2069	-1466	101	1698	1682	1280	665	-1202
22	-2424	-1631	150	1978	1848	1394	812	-1382
23	-2795	-1807	197	2263	2022	1514	965	-1572
24	-3200	-1999	246	2571	2218	1648	1133	-1781
25	-3612	-2200	297	2885	2424	1790	1302	-1996
26	-4039	-2407	348	3205	2645	1944	1479	-2220
27	-4475	-2618	398	3533	2878	2104	1660	-2448
28	-4911	-2829	448	3859	3113	2272	1839	-2676
29	-5337	-3036	497	4180	3351	2441	2015	-2901
30	-5783	-3248	548	4514	3598	2616	2192	-3130
31	-6218	-3451	595	4834	3838	2790	2362	-3348
32	-6648	-3649	642	5150	4079	2963	2526	-3561
33	-7080	-3839	688	5462	4319	3135	2686	-3768
34	-7502	-4022	732	5769	4554	3299	2834	-3964
35	-7942	-4207	777	6083	4797	3469	2984	-4163
36	-8381	-4387	820	6395	5039	3639	3129	-4356
37	-9284	-4730	906	7033	5534	3973	3404	-4729
38	-9730	-4894	945	7341	5773	4136	3527	-4899
39	-10657	-5214	1020	7970	6251	4445	3757	-5227
40	-12648	-5828	1145	9228	7203	5032	4140	-5809
41	-13735	-6128	1186	9850	7667	5299	4286	-6058
42	-14918	-6427	1212	10471	8127	5546	4399	-6274
43	OFFSCALE -	-6724	1212	11075	8579	5771	4473	-6447
44	OFFSCALE -	-7002	1173	11640	9017	5974	4500	-6553
45	OFFSCALE -	-7238	1083	12155	9396	6157	4472	-6556
46	OFFSCALE -	-7406	933	12593	9817	6333	4383	-6398
47	OFFSCALE -	-7471	440	13231	10751	6694	4022	-5298
48	OFFSCALE -	-7227	-252	13667	11246	7508	3430	-2717

*The location of the strain gages are shown in Fig. 2.14b

Table A.14 Measured Longitudinal Strains-Specimen V24T71M51

Location*	A	B	C	D	E	F	G	H	K20	L
Scan ID	Microstrain	Microstrain	Microstrain	Microstrain	Microstrain	Microstrain	Microstrain	Microstrain	Microstrain	Microstrain
1	0	-1	0	0	0	-1	-1	0	0	0
2	-21	-26	-7	27	18	7	-9	-15	-3	-2
3	-24	-30	-9	30	20	8	-10	-18	-3	-2
4	-23	-29	-10	29	21	9	-10	-18	-2	-2
5	-34	-39	-9	41	28	11	-15	-26	-2	-3
6	-48	-54	-11	54	38	16	-20	-39	0	-5
7	-76	-74	-10	74	52	26	-23	-58	2	-5
8	-120	-100	-3	106	69	47	-23	-87	7	-2
9	-182	-127	5	142	106	91	-27	-148	13	-3
10	-265	-164	15	190	154	141	-31	-219	19	-4
11	-368	-207	27	243	205	193	-31	-292	29	-6
12	-711	-334	50	381	352	325	-20	-473	49	-12
13	-1170	-491	66	531	552	477	-10	-680	66	-18
14	-1840	-715	93	724	913	658	-117	-1000	86	-38
15	-2760	-1030	138	999	1440	916	-267	-1480	102	-91
16	-3740	-1440	200	1340	2020	1260	-385	-1990	113	-176
17	-4720	-1930	273	1780	2580	1660	-486	-2490	120	-273
18	-5640	-2490	355	2400	3110	2080	-575	-2960	124	-349
19	-6530	-3080	443	3160	3640	2530	-669	-2960	128	-402
20	-7370	-3680	534	3970	4150	2990	-775	-3110	132	-424
21	-8190	-4310	627	4840	4690	3480	-900	-3000	136	-410
22	-9720	-5540	813	6580	5750	4550	-1210	-3350	141	-252
23	-10400	-6160	902	7450	6270	5140	-1410	-3480	141	-89
24	-11100	-6770	988	8310	6800	5760	-1640	-3580	140	142
25	-11800	-7380	1060	9140	7300	6410	-1900	-3730	136	451
26	-12400	-8010	1130	9950	7800	7120	-2210	-3760	127	861
27	-13000	-8640	1170	10700	8290	7890	-2570	-3730	114	1380
28	-13700	-9320	1190	11500	8750	8730	-2950	-3650	96	1990
29	-14300	-10100	1180	12200	9180	9630	-3380	-3510	68	2670
30	-15000	-10800	1130	12900	9580	10600	-3840	-3340	39	3360
31	OFFSCALE -	-11600	1050	13500	9930	11600	-4320	-3120	7	4010
32	OFFSCALE -	-13100	786	14800	10500	13800	-5330	-2560	-49	5130
33	OFFSCALE -	-14400	410	OFFSCALE +	10900	OFFSCALE +	-6390	-1900	-76	5880
34	OFFSCALE -	-15300	-54	OFFSCALE +	11100	OFFSCALE +	-7400	-1300	-63	6200
35	OFFSCALE -	OFFSCALE -	-555	OFFSCALE +	11200	OFFSCALE +	-8320	-627	-7	6330

*The location of the strain gages are shown in Fig. 2.14b

Table A.15 Measured Tangential Strains-Specimen V15T86M31

Location*	A	B	C	D	E	F	G	H	
Scan ID	Microstrain	Microstrain	Microstrain	Microstrain	Microstrain	Microstrain	Microstrain	Microstrain	Comments
1	0	9	19	-47	-59	-3	-11	-8	No zero readings are taken
2	1	0	26	-74	-132	-2	19	-14	
3	4	28	31	-140	-181	-1	78	-21	
4	14	37	32	-179	-175	14	143	-24	
5	45	53	28	-230	-281	77	240	-16	
6	110	82	20	-311	-383	193	361	20	
7	205	120	7	-402	-481	286	469	87	
8	300	213	-5	-528	-570	340	570	160	
9	390	245	-19	-684	-632	376	670	226	
10	473	284	-34	-861	-706	409	769	284	
11	552	328	-52	-1040	-789	445	816	332	
12	624	382	-69	-1220	-872	487	876	373	
13	690	439	-91	-1390	-964	537	943	407	
14	754	500	-113	-1560	-1060	592	995	437	
15	861	619	-151	-1870	-1250	720	1200	484	
16	964	746	-192	-2160	-1460	873	1100	535	
17	1080	874	-232	-2440	-1650	1050	1030	597	
18	1170	1010	-273	-2710	-1750	1250	899	674	
19	1270	1130	-311	-2980	-1840	1470	915	754	
20	1250	1170	-323	-2660	-1690	1410	727	729	load released due to computer break down
21	1250	1160	-323	-2660	-1680	1410	725	729	LVDT1 and LVDT2 are
22	1420	1520	-407	-3600	-1540	2150	681	1040	
23	1470	1940	-537	-4380	-1330	3570	461	1750	
24	1390	2160	-567	-4570	-1090	4490	338	2320	
25	1400	2170	-566	-4590	-1130	4490	305	2330	The position of LVDT3 is changed
26	1050	2400	-558	-4690	-1430	5470	259	3070	
27	895	2540	-540	-4740	-1380	5960	228	3480	
28	359	2830	-490	-4830	-1360	6890	90	4290	
29	63	2980	-481	-4910	-1290	7370	42	4670	
30	-227	3130	-480	-5010	-1310	7840	10	5030	
31	-223	3130	-479	-5010	-1320	7840	8	5030	The position of LVDT1 is changed
32	-485	3270	-484	-5100	-1330	8300	-29	5380	
33	-726	3410	-494	-5190	-1340	8740	-66	5710	
34	-931	3490	-508	-5290	-1350	9170	-97	6050	
35	-1100	3600	-528	-5390	-1300	9610	-129	6400	

*The location of the strain gages are shown in Fig 2.14b

Table A.16 Measured Tangential Strains-Specimen V12168M66

Location*	A	B	C	D	E	F	G	H
Scan ID	Microstrain	Microstrain	Microstrain	Microstrain	Microstrain	Microstrain	Microstrain	Microstrain
1	0	-1	-1	0	1	-1	0	-2
2	13	-1	2	-1	0	-3	10	-4
3	32	1	3	-3	0	26	21	-5
4	48	1	3	3	2	24	32	-3
5	65	3	3	3	4	35	55	1
6	85	3	3	0	6	72	86	6
7	113	4	1	5	-9	294	80	15
8	145	4	0	12	-12	276	17	33
9	181	11	-3	22	-15	265	33	58
10	224	23	-6	35	-20	225	37	87
11	280	45	-9	47	-24	162	62	124
12	351	74	-12	58	30	168	-8	168
13	441	112	-16	64	-39	196	53	218
14	713	211	-24	44	-75	-143	79	344
15	892	267	-29	19	-101	-195	237	418
16	1110	336	-35	-26	-138	-287	507	511
17	1353	410	-44	-79	-181	-350	722	618
18	1606	483	-57	-135	-227	-418	775	738
19	2206	658	-97	-270	-341	-594	266	1041
20	2816	829	-153	-382	-460	-788	171	1386
21	3446	999	-213	-476	-578	-983	164	1884
22	4106	1168	-274	-569	-703	-1193	134	2395
23	4751	1321	-326	-658	-822	-1399	137	2868
24	5409	1465	-372	-751	-937	-1612	156	3320
25	6059	1598	-413	-843	-1051	-1817	182	3709
26	6711	1726	-448	-944	-1168	-2009	222	3939
27	7352	1847	-481	-1046	-1285	-2200	256	4181
28	7993	1966	-511	-1152	-1399	-2385	310	4697
29	8623	2089	-537	-1259	-1511	-2548	362	5143
30	9259	2219	-556	-1373	-1624	-2705	425	4852
31	9909	2363	-569	-1487	-1741	-2849	494	5295
32	10547	2523	-576	-1605	1860	-2988	577	5280
33	11218	2693	-576	-1721	-1980	-3124	665	5235
34	12815	2879	-560	-1842	-2112	-3658	761	5283
35	14631	3042	-531	-1953	-2244	-3849	857	4988
36	15857	3194	-482	-2068	-2383	-4066	969	5039
37	OFFSCALE +	3418	-333	-2310	-2666	-4582	1264	3887
38	13573	3540	-90	-2633	-2732	-5445	1824	2536
39	12679	3873	135	-1493	-2379	-1640	1912	2389

*The location of the strain gages are shown in Fig 2 14b

Table A.17 Measured Tangential Strains-SpecimenV17100M98

Location*	A	B	C	D	E	F	G	H
Scan ID	Microstrain	Microstrain	Microstrain	Microstrain	Microstrain	Microstrain	Microstrain	Microstrain
1	-1	0	0	-3	-1	-1	-1	0
2	13	19	9	2	-6	2	6	7
3	28	33	14	19	-19	2	10	15
4	46	44	15	17	-32	5	11	28
5	68	52	17	44	-45	16	11	40
6	92	59	18	65	-61	29	9	51
7	118	66	18	79	-83	45	7	62
8	152	72	19	111	-109	65	4	74
9	196	81	20	147	-143	89	0	95
10	257	97	21	180	-191	119	8	136
11	348	128	21	214	-258	155	16	204
12	487	193	21	256	-350	202	29	317
13	666	306	20	315	-464	260	42	463
14	910	475	19	392	-611	338	62	663
15	1216	688	15	490	-790	442	87	908
16	1619	961	10	618	-1034	583	123	1230
17	2044	1228	2	758	-1286	741	163	1550
18	2563	1535	-11	887	-1579	941	214	1939
19	3100	1852	-29	1070	-1856	1158	270	2340
20	3721	2208	-54	1276	-2148	1413	334	2816
21	4351	2550	-81	1488	-2424	1663	397	3299
22	5668	3029	-135	1307	-699	2162	518	4352
23	6527	2778	-163	1251	-594	2489	588	5065
24	7920	1924	-173	1377	-12	2880	660	6023
25	2483	1644	-162	787	73	3264	717	7003
26	2376	1502	-110	843	132	3648	760	7703
27	2386	1292	-10	765	-159	4016	788	8634
28	2393	1230	167	723	-170	4396	801	7249
29	2428	958	406	692	-170	4757	790	5525
30	2472	929	723	470	-184	5128	743	5690
31	2443	856	1099	473	-193	5500	633	4565
32	2368	219	1926	480	-165	6208	207	3649
33	2423	205	2917	538	-164	6889	501	2982
34	2343	200	4076	537	-204	7548	1465	2752

*The location of the strain gages are shown in Fig 2 14b

Table A.18 Measured Tangential Strains-Specimen V25T00M97

Location*	A	B	C	D	E	F	G	H
Scan ID	Microstrain	Microstrain	Microstrain	Microstrain	Microstrain	Microstrain	Microstrain	Microstrain
1	-1	-1	-1	0	0	-1	3	0
2	14	8	-3	-10	-19	-5	7	11
3	33	21	-5	-20	-41	-8	10	23
4	56	34	-8	-34	-68	-13	9	37
5	83	48	-12	-52	-99	-23	6	53
6	149	74	-17	-98	-173	-49	5	89
7	186	89	-20	-126	-221	-67	-2	111
8	232	110	-23	-157	-277	-90	-8	135
9	294	137	-25	-189	-345	-118	-16	164
10	378	174	-29	-219	-422	-152	-19	199
11	806	339	-39	-280	-721	-302	-17	373
12	1718	689	-59	-339	-1304	-573	-19	824
13	3353	1417	-102	-434	-2249	-991	-38	1879
14	4190	1839	-132	-482	-2666	-1215	-52	2516
15	5664	2639	-196	-566	-3314	-1596	-91	3742
16	8511	4348	-344	-756	-4317	-2251	-169	6303
17	8539	4366	-345	-760	-4323	-2257	-171	6332
18	11614	6412	-497	-1010	-5284	-2876	-214	9253
19	14838	8764	-642	-1175	-6195	-3479	-139	12473
20	OFFSCALE +	11341	-783	-1300	-6992	-4075	115	OFFSCALE +
21	OFFSCALE +	14014	-957	-1334	-7969	-4699	544	OFFSCALE +
22	OFFSCALE +	15699	-1147	-1698	-10059	-5583	714	OFFSCALE +
23	OFFSCALE +	OFFSCALE +	-511	-1628	-11037	-5461	527	OFFSCALE +

*The location of the strain gages are shown in Fig 2 14b

Table A.19 Measured Tangential Strains-Specimen V13T77M51

Location*	A	B	C	D	E	F	G	H
Scan ID	Microstrain	Microstrain	Microstrain	Microstrain	Microstrain	Microstrain	Microstrain	Microstrain
1	1	0	0	-1	0	-1	-1	0
2	2	4	2	-4	-3	-6	-5	3
3	11	26	19	-17	-16	-19	-23	15
4	20	45	28	-29	-27	-31	-37	27
5	30	63	30	-52	-40	-44	-51	35
6	32	67	30	-59	-42	-46	-52	37
7	37	76	30	-70	-48	-52	-59	42
8	43	87	29	-86	-57	-61	-68	48
9	49	96	28	-98	-63	-65	-72	52
10	57	111	27	-116	-73	-75	-82	60
11	67	127	24	-137	-83	-84	-91	67
12	80	148	22	-157	-95	-95	-100	76
13	95	171	20	-181	-107	-103	-108	86
14	140	227	13	-236	-139	-129	-132	112
15	199	289	6	-291	-171	-152	-155	145
16	284	360	-2	-357	-215	-180	-190	194
17	384	427	-10	-428	-262	-202	-232	250
18	511	498	-18	-514	-318	-227	-291	322
19	652	569	-29	-607	-373	-249	-358	405
20	813	641	-41	-715	-427	-275	-434	505
21	986	717	-55	-828	-478	-302	-519	621
22	1182	802	-73	-956	-531	-336	-617	760
23	1380	887	-93	-1085	-582	-374	-718	907
24	1587	979	-117	-1221	-635	-418	-831	1071
25	1791	1071	-140	-1360	-689	-467	-946	1243
26	1995	1165	-164	-1500	-745	-520	-1065	1425
27	2200	1258	-190	-1644	-802	-577	-1187	1614
28	2405	1350	-215	-1786	-861	-637	-1308	1805
29	2601	1437	-238	-1926	-918	-697	-1427	1997
30	2795	1527	-261	-2070	-977	-761	-1546	2198
31	2964	1610	-284	-2208	-1035	-825	-1662	2393
32	3141	1688	-302	-2343	-1093	-888	-1774	2589
33	3305	1763	-322	-2476	-1151	-951	-1884	2783
34	3461	1833	-338	-2607	-1209	-1011	-1985	2974
35	3615	1902	-355	-2741	-1269	-1074	-2090	3173
36	3759	1967	-370	-2873	-1328	-1137	-2190	3371
37	4032	2090	-398	-3143	-1448	-1260	-2385	3782
38	4163	2146	-411	-3273	-1508	-1320	-2473	3981
39	4385	2254	-433	-3536	-1631	-1434	-2643	4401
40	4709	2453	-465	-4060	-1865	-1649	-2939	5295
41	4806	2546	-474	-4319	-1979	-1745	-3063	5782
42	4860	2637	-476	-4579	-2090	-1842	-3167	6319
43	4877	2724	-472	-4832	-2161	-1924	-3248	6926
44	4843	2801	-454	-5070	-2226	-1995	-3301	7595
45	4747	2858	-421	-5291	-2292	-2058	-3320	8352
46	4580	2878	-370	-5482	-2363	-2111	-3300	9192
47	4111	2796	-218	-5758	-2570	-2234	-3129	11042
48	3619	2615	-6	-5923	-2843	-2516	-2712	12669

*The location of the strain gages are shown in Fig. 2.14b

Table A.20 Measured Tangential Strains-Specimen V24171M51

Location*	A	B	C	D	E	F	G	H
Scan ID	Microstrain	Microstrain	Microstrain	Microstrain	Microstrain	Microstrain	Microstrain	Microstrain
1	0	0	-1	0	-1	-1	0	0
2	3	4	1	-2	-2	1	6	3
3	5	7	2	-2	-2	1	7	4
4	4	7	3	-1	-2	2	8	5
5	6	8	2	-1	-2	2	11	7
6	9	11	4	-1	-1	4	15	11
7	15	17	5	-1	-1	6	20	15
8	22	24	4	-6	-3	8	27	23
9	32	29	0	-11	-7	5	36	32
10	57	38	-5	-19	-14	0	50	45
11	97	48	-11	-27	-20	-1	62	60
12	290	78	-27	-48	-35	17	91	109
13	627	108	-39	-70	-61	78	102	226
14	1160	143	-46	-126	-123	118	164	450
15	1800	227	-53	-269	-208	115	338	788
16	2420	385	-65	-456	-284	92	563	1150
17	3010	611	-92	-663	-352	61	797	1520
18	3570	868	-127	-885	-418	21	1030	1870
19	4120	1150	-174	-1130	-491	-27	1270	2200
20	4650	1430	-225	-1380	-572	-82	1510	2510
21	5200	1720	-280	-1640	-660	-143	1760	2820
22	6300	2260	-388	-2140	-851	-282	2350	3380
23	6860	2510	-438	-2390	-952	-361	2580	3640
24	7440	2740	-487	-2630	-1050	-448	2810	3870
25	8010	2940	-529	-2870	-1150	-540	3020	4090
26	8600	3130	-569	-3090	-1250	-637	3260	4240
27	9210	3310	-601	-3310	-1350	-739	3490	4340
28	9840	3460	-623	-3520	-1440	-847	3710	4360
29	10500	3610	-635	-3730	-1510	-955	3910	4330
30	11200	3730	-636	-3930	-1570	-1040	4090	4240
31	11900	3840	-625	-4130	-1610	-1110	4260	4110
32	13400	3990	-570	-4530	-1610	-1110	4550	3680
33	14900	4030	-469	-4950	-1500	-948	4790	3070
34	OFFSCALE +	3970	-323	-5390	-1260	-648	5010	2280
35	OFFSCALE +	3830	-151	-5890	-929	-228	5220	1540

*The location of the strain gages are shown in Fig 2.14b

Table A.21 Measured Diagonal Strains-Specimen V15T86M31

Location*	A	C	
Scan ID	Microstrain	Microstrain	Comments
1	189	129	No zero readings ara not taken
2	301	212	
3	420	303	
4	554	405	
5	734	512	
6	999	609	
7	1350	677	
8	1760	738	
9	2210	797	
10	2710	867	
11	3240	941	
12	3800	1020	
13	4380	1100	
14	4970	1180	
15	6130	1350	
16	7290	1520	
17	8450	1710	
18	9610	1890	
19	10700	2080	Load released due to computer break down
20	9750	1350	
21	9750	1350	LVDT1 and LVDT2 are changed
22	13600	2510	
23	OFFSCALE +	3130	
24	OFFSCALE +	3310	
25	OFFSCALE +	3300	The position of LVDT3 is changed
26	OFFSCALE +	3420	
27	OFFSCALE +	3460	
28	OFFSCALE +	3500	
29	OFFSCALE +	3530	
30	OFFSCALE +	3560	
31	OFFSCALE +	3550	The position of LVDT1 is changed
32	OFFSCALE +	3590	
33	OFFSCALE +	3620	
34	OFFSCALE +	3660	
35	OFFSCALE +	3690	

*The location of the strain gages are shown in Fig. 2.14b

Table A.22 Measured Diagonal Strains-Specimen V12T68M66

Location*	A	G	E
Scan ID	Microstrain	Microstrain	Microstrain
1	0	-1	-1
2	40	47	110
3	78	103	219
4	115	158	315
5	130	214	404
6	168	279	500
7	196	336	574
8	237	419	676
9	279	507	775
10	325	608	878
11	380	721	982
12	440	846	1092
13	513	989	1208
14	734	1312	1483
15	889	1483	1632
16	1080	1662	1821
17	1297	1848	2047
18	1523	2042	2313
19	2124	2491	3010
20	2693	2998	3857
21	3287	3583	4805
22	3815	4261	5823
23	4464	4994	6822
24	5126	5788	7824
25	5741	6637	8808
26	6352	7520	9783
27	6959	8390	10725
28	7599	9285	11662
29	8217	10178	12575
30	8851	11073	13480
31	9471	11961	14374
32	10190	12829	15257
33	11244	13653	OFFSCALE +
34	13362	14426	OFFSCALE +
35	14506	15081	OFFSCALE +
36	15827	15676	OFFSCALE +
37	OFFSCALE +	OFFSCALE +	OFFSCALE +
38	12778	OFFSCALE +	OFFSCALE +
39	11427	OFFSCALE +	OFFSCALE +

*The location of the strain gages are shown in Fig. 2.14b

Table A.23 Measured Diagonal Strains-Specimen V17T00M98

Location*	A	E
Scan ID	Microstrain	Microstrain
1	-2	0
2	-29	53
3	-63	86
4	-111	109
5	-170	128
6	-228	137
7	-285	148
8	-343	149
9	-407	147
10	-471	151
11	-539	152
12	-611	148
13	-688	153
14	-793	151
15	-916	155
16	-1095	190
17	-1305	315
18	-1562	519
19	-1875	708
20	-2249	945
21	-2696	1119
22	-3219	1089
23	-2613	1077
24	-263	224
25	-1214	204
26	-776	155
27	-749	133
28	-674	133
29	-648	139
30	-627	167
31	-600	165
32	-569	200
33	-576	190
34	-568	50

*The location of the strain gages are shown in Fig. 2.14b

Table A.24 Measured Diagonal Strains-Specimen V25T00M97

Location*	A	E
Scan ID	Microstrain	Microstrain
1	-1.4316	-0.47697
2	-35.312	25.757
3	-72.531	54.377
4	-114.04	81.569
5	-165.56	110.67
6	-275.75	160.28
7	-334.88	180.32
8	-395.92	197.03
9	-459.33	209.91
10	-524.17	221.84
11	-695.74	244.74
12	-946.8	492.96
13	-1441.8	1203
14	-1697.2	1510.5
15	-2116.9	1973.9
16	-2786.8	2670.9
17	-2793.4	2677.1
18	-3363.3	3421.2
19	-3821.8	4180.4
20	-4255.2	4970.2
21	-4576.7	5795.6
22	-4645.7	6754.9
23	-4361.1	6718.2

*The location of the strain gages are shown in Fig. 2.14b

Table A.25 Measured Diagonal Strains-Specimen V24T71M51

Location*	A	E	G
Scan ID	Microstrain	Microstrain	Microstrain
1	0	-1	-1
2	20	40	35
3	24	45	39
4	23	44	38
5	31	60	51
6	41	81	69
7	53	112	97
8	75	160	152
9	107	231	242
10	159	325	355
11	225	427	481
12	462	712	853
13	843	1050	1320
14	1510	1550	1910
15	2430	2420	2910
16	3420	3590	4370
17	4450	4860	6120
18	5510	6110	7960
19	6610	7380	9850
20	7720	8640	11700
21	8910	9950	13600
22	11400	12600	OFFSCALE +
23	12600	13900	OFFSCALE +
24	13900	15200	OFFSCALE +
25	15100	OFFSCALE +	OFFSCALE +
26	OFFSCALE +	OFFSCALE +	OFFSCALE +
27	OFFSCALE +	OFFSCALE +	OFFSCALE +
28	OFFSCALE +	OFFSCALE +	OFFSCALE +
29	OFFSCALE +	OFFSCALE +	OFFSCALE +
30	OFFSCALE +	OFFSCALE +	OFFSCALE +
31	OFFSCALE +	OFFSCALE +	OFFSCALE +
32	OFFSCALE +	OFFSCALE +	OFFSCALE +
33	OFFSCALE +	OFFSCALE +	OFFSCALE +
34	OFFSCALE +	OFFSCALE +	OFFSCALE +
35	OFFSCALE +	OFFSCALE +	OFFSCALE +

*The location of the strain gages are shown in Fig. 2.14b

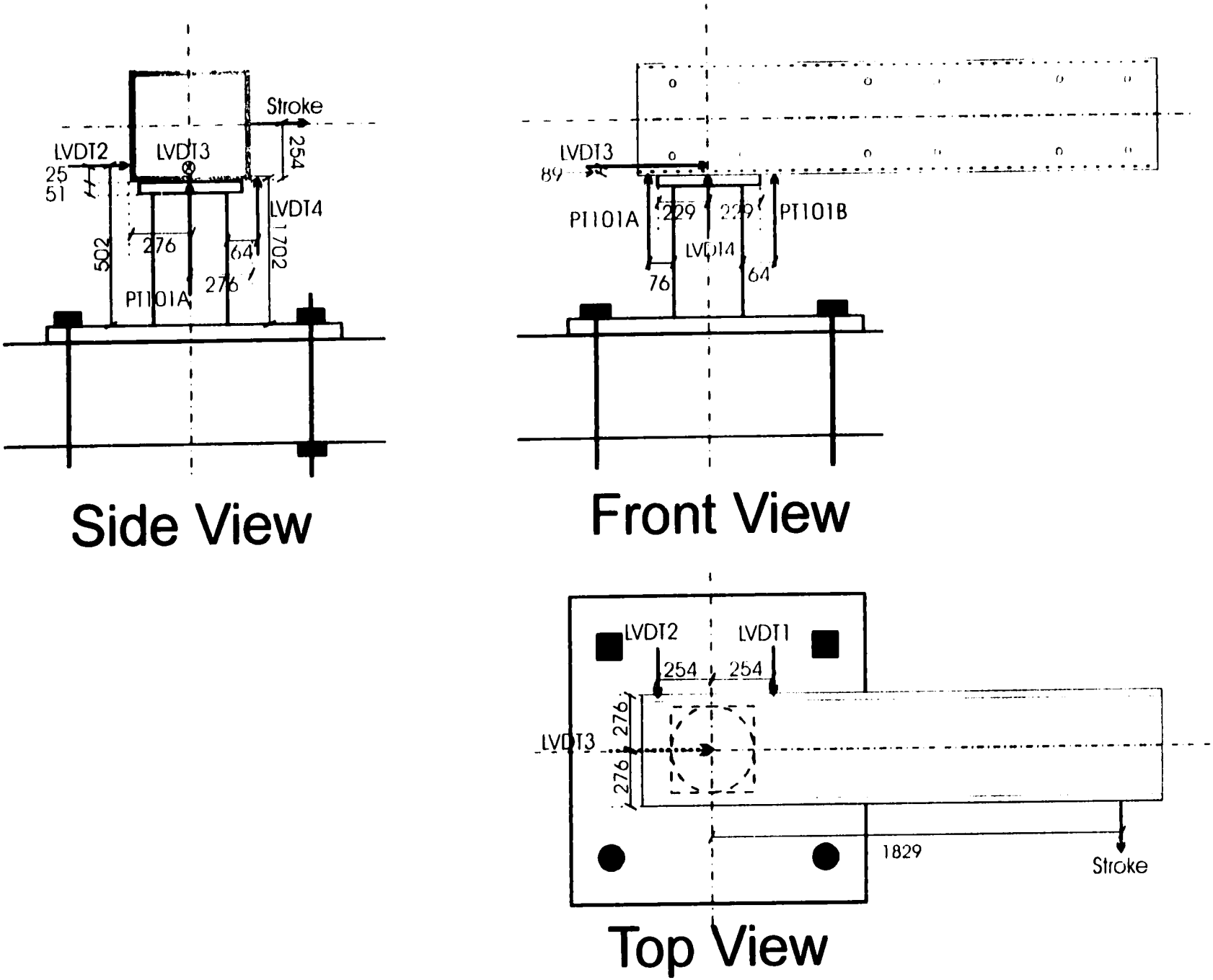

Figure A.1 Location of the Sensors for Specimen V15T86M31 (All shown dimensions are in mm units)

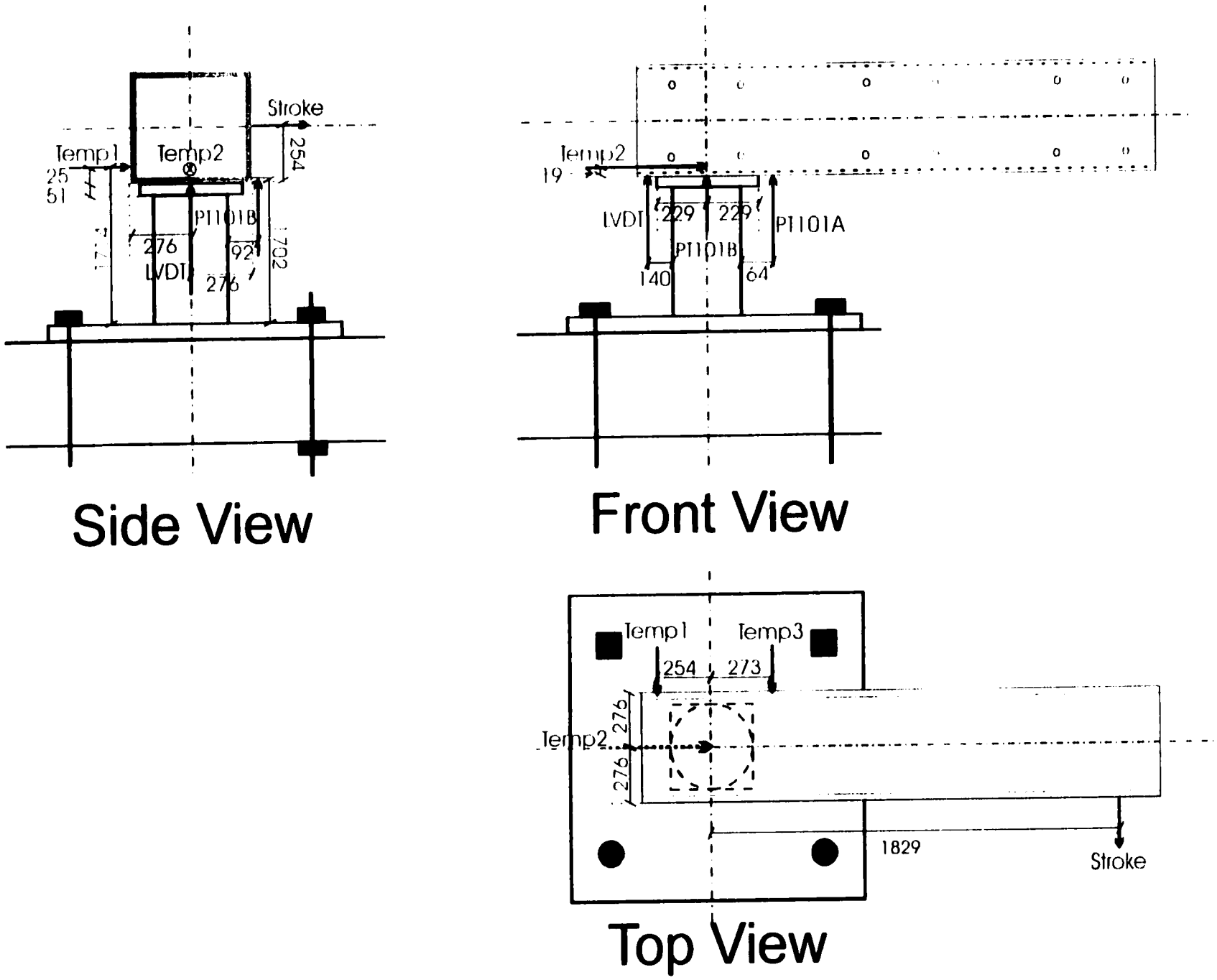

Figure A.2 Location of the Sensors for Specimen V12T68M66 (All shown dimensions are in mm units)

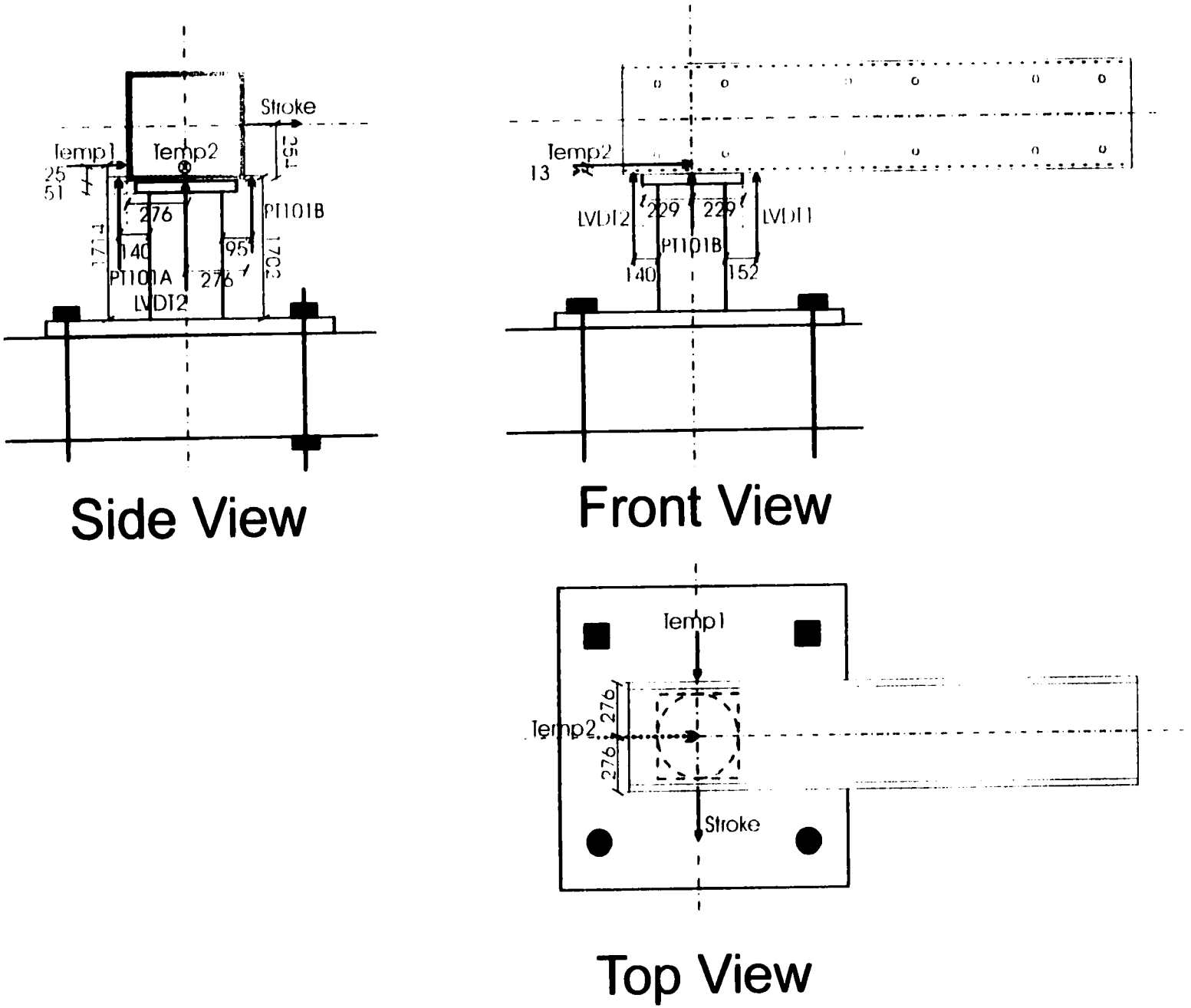

Figure A.3 Location of the Sensors for Specimen V17T00M98 (All shown dimensions are in mm units)

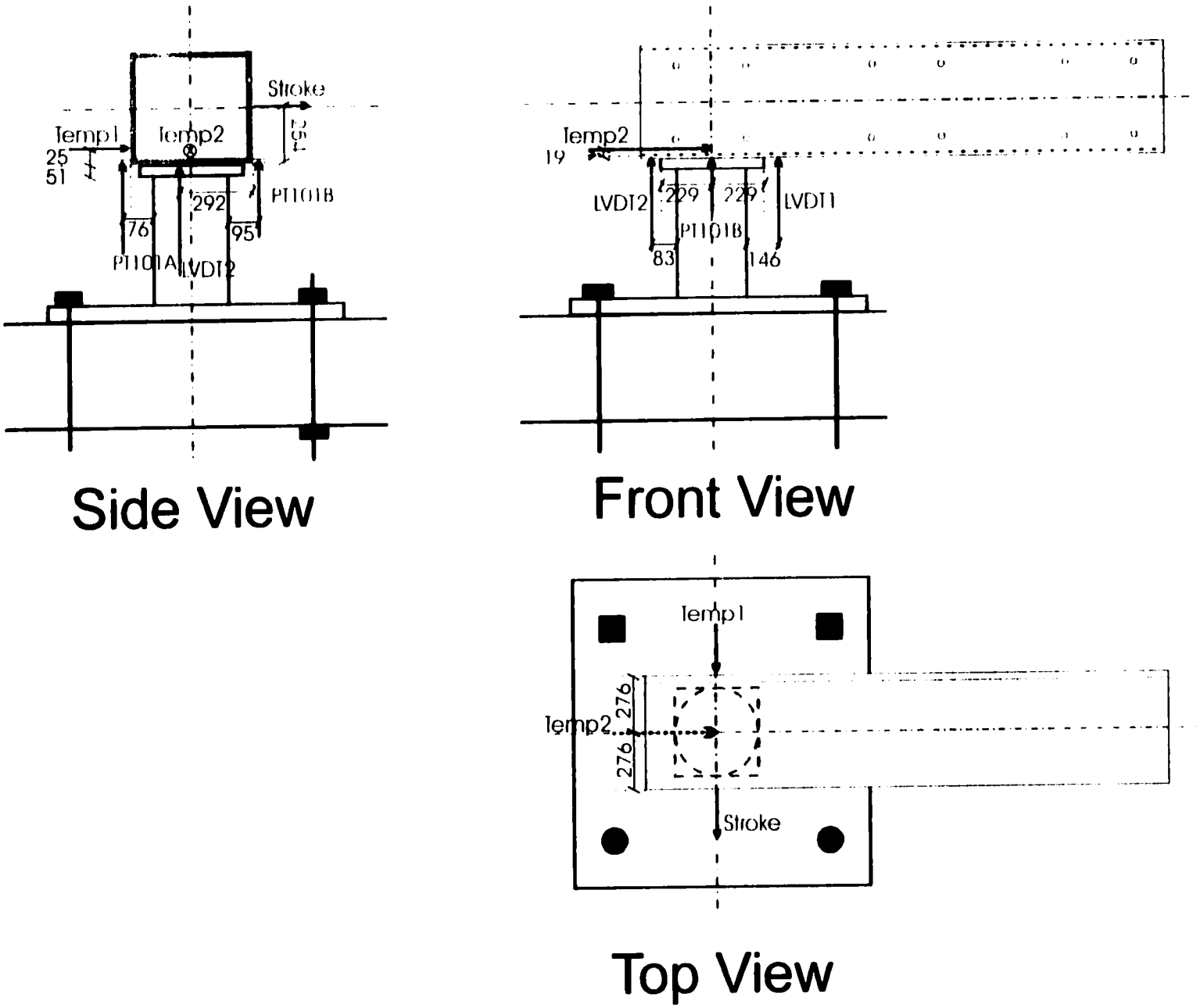

Figure A.4 Location of the Sensors for Specimen V25T00M97 (All shown dimensions are in mm units)

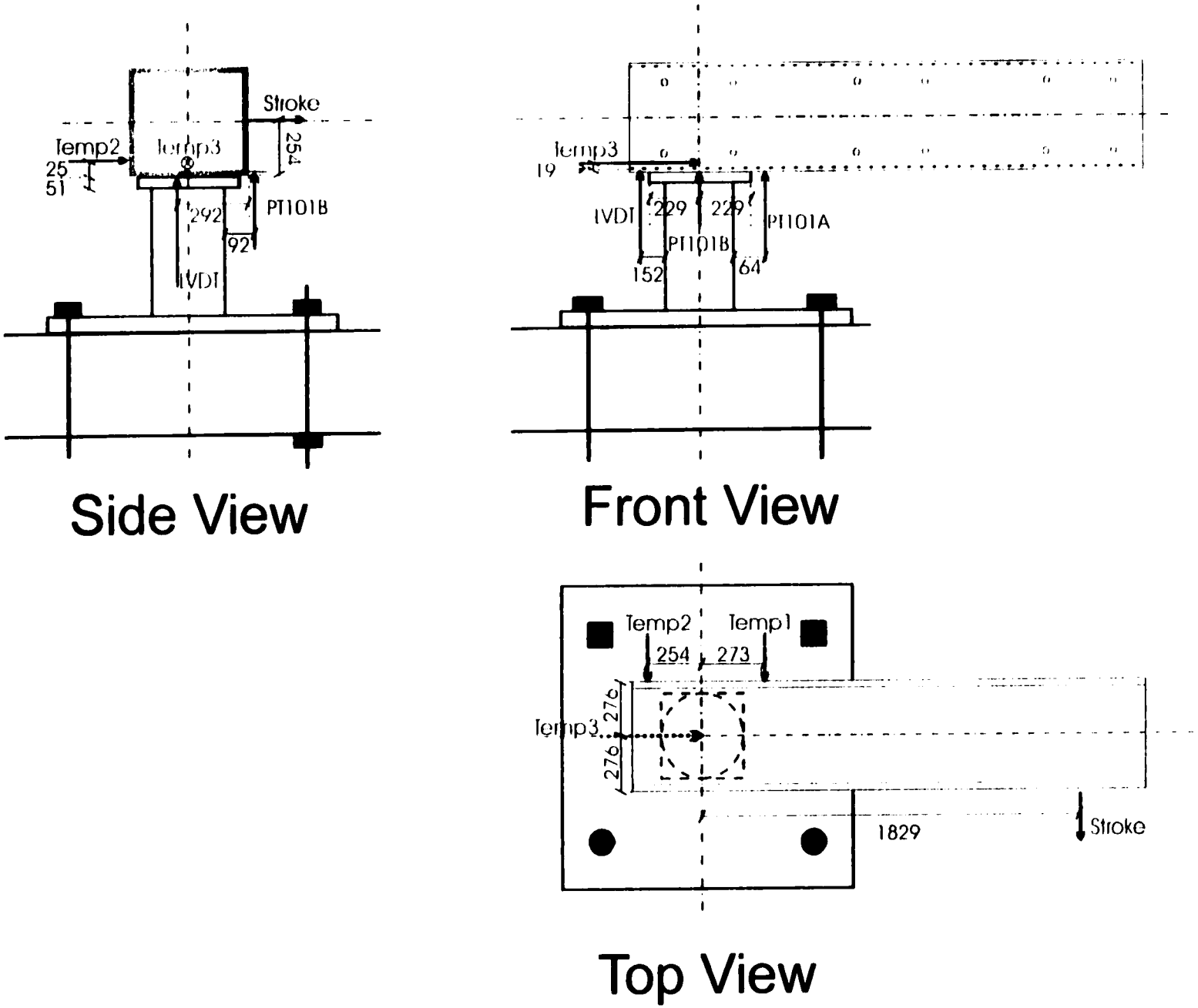

Figure A.5 Location of the Sensors for Specimen V13T77M51 (All shown dimensions are in mm units)

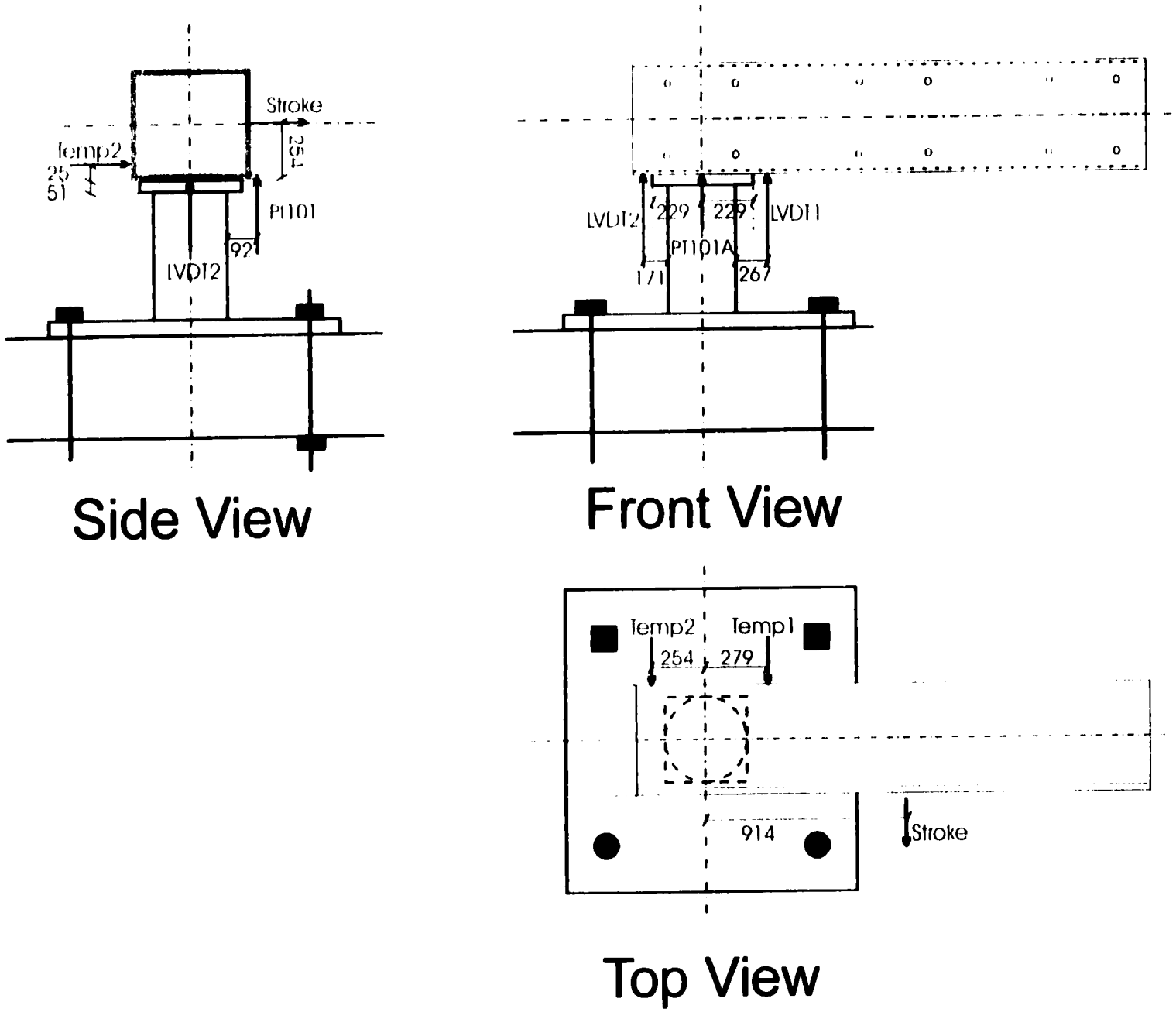

Figure A.6 Location of the Sensors for specimen V24T71M51 (All shown dimensions are in mm units)

APPENDIX B

Contents

APPENDIX B.1

Section Corners as Points of Shear Stress Discontinuity

It is demonstrated in this section that the tangential shear stresses acting on two faces connected to the corner $s = s_i = ia$, ($i = 1,2,3$ and 4), are in general unequal, i.e., $\tau(s)_- \neq \tau(s)_+$.

The 3D equilibrium conditions for an infinitesimal element on the corner of the cross-section of a square hollow section under no body forces (Timoshenko and Goodier 1987) are (Fig. B.1.1):

$$\frac{\partial \sigma_{xx}}{\partial x} + \frac{\partial \tau_{xy}}{\partial y} + \frac{\partial \tau_{xz}}{\partial z} = 0 \tag{B.1.1}$$

$$\frac{\partial \tau_{yx}}{\partial x} + \frac{\partial \sigma_{yy}}{\partial y} + \frac{\partial \tau_{yz}}{\partial z} = 0 \tag{B.1.2}$$

$$\frac{\partial \tau_{zx}}{\partial x} + \frac{\partial \tau_{zy}}{\partial y} + \frac{\partial \sigma_{zz}}{\partial z} = 0 \tag{B.1.3}$$

For the corner of the cross-section, from the Figure. B.1.1, the following can be written.

$$\sigma_{xx} = \sigma_{yy} = 0, \text{ and } \sigma_{zz} = \sigma \tag{B.1.4}$$

$$\tau_{xy} = \tau_{yx} = 0, \frac{\partial \tau_{zx}}{\partial x} = \frac{\tau_2}{t}, \text{ and } \frac{\partial \tau_{zy}}{\partial y} = \frac{\tau_1}{t} \tag{B.1.5}$$

By substituting the Eqs B.1.4 and B.1.5 in equilibrium conditions (Eqs B.1.1 through B.1.3), the following can be obtained.

$$\frac{\tau_2}{t} + \frac{\tau_1}{t} + \frac{\partial \sigma}{\partial z} = 0 \tag{B.1.6}$$

By solving the Eq. B.1.6 for τ_2, it can be shown that

$$\tau_2 = -\tau_1 - t\frac{\partial \sigma}{\partial z} \Rightarrow \tau_2 \neq \tau_1 \tag{B.1.7}$$

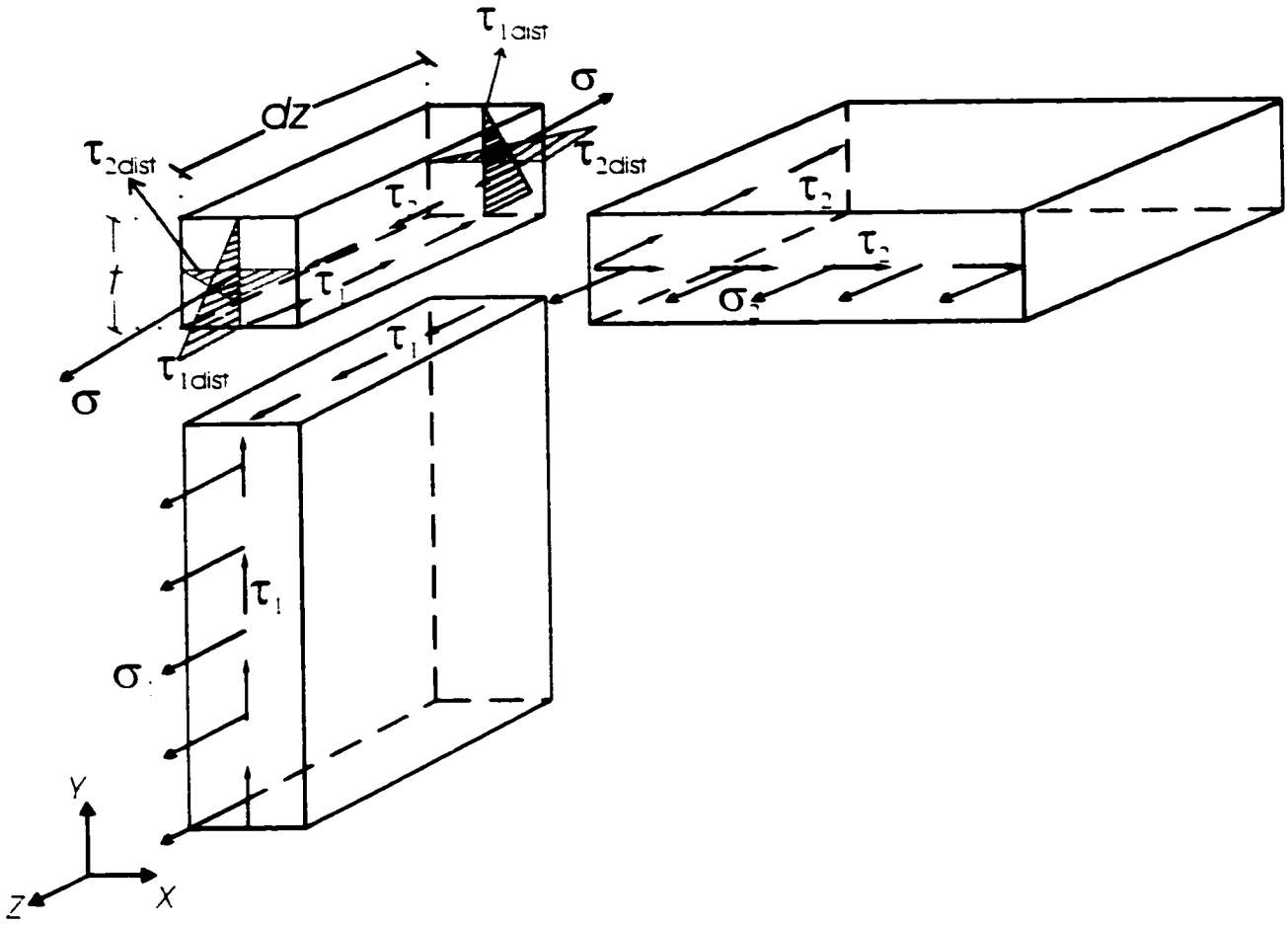

Figure B.1.1 Free-body Diagram of a Section Corner

APPENDIX B.2

Applicability Limits of Case I-1

This section demonstrates the derivation of applicability limits of Case I-1.

The coordinates identifying the location of the neutral axis in Fig. 3.5a have to remain within the bounds $0 \le \alpha \le 1$ and $0 \le \gamma \le 1$. The subscript, i, is either 1 or 2.

For the first pair of the coordinates defining the location of the PNA, the following equations are written.

$$\alpha_1 = \frac{B + \sqrt{A}}{C} \tag{B.2.1}$$

$$\gamma = \frac{E + \sqrt{A}}{F} \tag{B.2.2}$$

The limiting bounds for Eqs. B.2.1 and B.2.2 are as below.

$$0 \le \alpha_1 \le 1 \Rightarrow 0 \le \frac{B + \sqrt{A}}{C} \le 1 \tag{B.2.3}$$

$$0 \le \gamma_1 \le 1 \Rightarrow 0 \le \frac{E + \sqrt{A}}{F} \le 1 \tag{B.2.4}$$

Since C and F are always greater then 0, the above inequalities can be rewritten in the following form.

$$-B \le \sqrt{A} \le C - B \tag{B.2.5}$$

$$-E \le \sqrt{A} \le F - E \tag{B.2.6}$$

If we substitute the equivalents of B, C, E, and F in Eqs. B.2.5 and B.2.6, we can obtain the following bounds for $\sqrt{A}$, respectively.

$$-\sigma_1(\sigma_1 - \sigma_2 - 3m_1) \le \sqrt{A} \le \sigma_1(\sigma_1 + \sigma_2 + 3m_1) \tag{B.2.7}$$

$$-\sigma_2(\sigma_1 + \sigma_2 + 3m_1) \le \sqrt{A} \le \sigma_2(\sigma_1 + \sigma_2 - 3m_1) \tag{B.2.8}$$

After making the necessary arrangements, the following four applicability limits can be obtained.

$$-\sigma_1(\sigma_1 + \sigma_2 - 3m_1) - \sqrt{A} \le 0 \tag{B.2.9}$$

$$\sigma_1(-\sigma_1 - \sigma_2 - 3m_1) - \sqrt{A} \le 0 \tag{B.2.10}$$

$$\sigma_2(-\sigma_1 - \sigma_2 - 3m_1) - \sqrt{A} \le 0 \tag{B.2.11}$$

$$-\sigma_2(\sigma_1 - \sigma_2 - 3m_1) + \sqrt{A} \le 0 \tag{B.2.12}$$

For the second pair of the coordinates defining the location of the PNA, the following equations are found.

$$\alpha_2 = \frac{B - \sqrt{A}}{C} \tag{B.2.13}$$

$$\gamma_2 = \frac{E - \sqrt{A}}{F} \tag{B.2.14}$$

The limiting bounds for Eqs. B.2.13 and B.2.14 are as below.

$$0 \le \alpha_2 \le 1 \Rightarrow 0 \le \frac{B - \sqrt{A}}{C} \le 1 \tag{B.2.15}$$

$$0 \le \gamma_2 \le 1 \Rightarrow 0 \le \frac{E - \sqrt{A}}{F} \le 1 \tag{B.2.16}$$

Since C and F are always greater then 0, the above inequalities can be rewritten in the following form.

$$B - C \le \sqrt{A} \le B \tag{B.2.17}$$

$$E - F \le \sqrt{A} \le E \tag{B.2.18}$$

If we substitute the equivalents of B, C, E, and F in Eqs. B.2.17 and B.2.18, we can obtain the following bounds for $\sqrt{A}$, respectively.

$$\sigma_{1r}(\sigma_{1r} + \sigma_{3r} - 3m_1) - 2\sigma_{1r}(\sigma_{1r} + \sigma_{3r}) \le \sqrt{A} \le \sigma_{1r}(\sigma_{1r} + \sigma_{3r} - 3m_1) \tag{B.2.19}$$

$$\sigma_{3r}(\sigma_{1r} + \sigma_{3r} + 3m_1) - 2\sigma_{3r}(\sigma_{1r} + \sigma_{3r}) \le \sqrt{A} \le \sigma_{3r}(\sigma_{1r} + \sigma_{3r} + 3m_1) \tag{B.2.20}$$

After making the necessary arrangements, the following four applicability limits can be obtained.

$$-\sigma_{1r}(\sigma_{1r} + \sigma_{3r} + 3m_1) - \sqrt{A} \le 0 \tag{B.2.21}$$

$$\sigma_1(-\sigma_1 - \sigma_3 + 3m_1) + \sqrt{A} \le 0 \qquad \text{(B.2.22)}$$

$$\sigma_2(-\sigma_2 - \sigma_3 + 3m_2) - \sqrt{A} \le 0 \qquad \text{(B.2.23)}$$

$$-\sigma_3(\sigma_1 + \sigma_3 + 3m_3) + \sqrt{A} \le 0 \qquad \text{(B.2.24)}$$

It can be concluded that, the interaction relation for Case I-1 (Eq. 3.17) to be applicable, in addition to the applicability limits $g_{1i}(\{\mathbf{x}\}) \le 0, i = 1....3$, the load combinations must satisfy either the conditions from B.2.9 to B.2.12 or from B.2.21 to B.2.24.

APPENDIX B.3

Applicability Limits of Case II-1

This section demonstrates the derivation of applicability limits of Case II-1.

The coordinates (β and γ) in Fig. 3.5b identifying the location of the neutral axis have to remain within the following bounds.

$$0 \le \frac{(\sigma_1 - \sigma_2 - \sigma_3 + \sigma_4 - 4v_2) - \sqrt{G}}{2\sigma_2} \le 1 \qquad \text{(B.3.1)}$$

$$0 \le \frac{\sqrt{G}}{2\sigma_3} \le 1 \qquad \text{(B.3.2)}$$

Noting that σ_2 and σ_3 are both greater than zero, the bounds (B.3.1) and (B.3.2) can be rewritten as following.

$$(\sigma_1 - \sigma_2 - \sigma_3 - \sigma_4 - 4v_2) \ge \sqrt{G} \ge (\sigma_1 - \sigma_2 - \sigma_3 + \sigma_4 - 4v_2) - 2\sigma_2 \qquad \text{(B.3.3)}$$

$$0 \le \sqrt{G} \le 2\sigma_3 \qquad \text{(B.3.4)}$$

By taking the first and second bounds of (B.3.3) into consideration separately, and substituting the equivalent of G, two applicability limits can be recovered as below.

$$\sqrt{2\sigma_2(3m_1 - 4v_2 - \sigma_1 - \sigma_3 - 2\sigma_4)} - (\sigma_1 + \sigma_2 + \sigma_3 + \sigma_4 - 4v_2) \le 0 \qquad \text{(B.3.5)}$$

$$(\sigma_1 - \sigma_2 + \sigma_3 + \sigma_4 - 4v_2) - \sqrt{2\sigma_3(3m_1 - 4v_2 + \sigma_1 + \sigma_3 + 2\sigma_4)} \le 0 \qquad \text{(B.3.6)}$$

The same way, from (B.3.4), following two applicability limits can be obtained.

$$-\sqrt{2\sigma_3(3m_1 - 4v_2 + \sigma_1 + \sigma_3 + 2\sigma_4)} \le 0 \qquad \text{(B.3.7)}$$

$$\sqrt{2\sigma_3(3m_1 - 4v_2 + \sigma_1 + \sigma_3 + 2\sigma_4)} - 2\sigma_3 \le 0 \qquad \text{(B.3.8)}$$

The applicability limit presented by (B.3.7) reduces to the same solution with the Eq. 3.27 in Chapter 3. As a result, it can be concluded that the applicability limits for Case II-1 due to geometric constraints are as below.

$$g_{24}(\{\mathbf{x}\}) = \sqrt{2\sigma_3(3m_1 - 4v_2 + \sigma_1 + \sigma_3 - 2\sigma_4)} - (\sigma_1 + \sigma_2 + \sigma_3 + \sigma_4 - 4v_2) \le 0 \quad \text{(B.3.9)}$$

$$g_{25}(\{\mathbf{x}\}) = (\sigma_1 - \sigma_2 + \sigma_3 + \sigma_4 - 4v_2) - \sqrt{2\sigma_3(3m_1 - 4v_2 + \sigma_1 + \sigma_3 + 2\sigma_4)} \le 0 \quad \text{(B.3.10)}$$

$$g_{26}(\{\mathbf{x}\}) = \sqrt{2\sigma_3(3m_1 - 4v_2 + \sigma_1 + \sigma_3 + 2\sigma_4)} - 2\sigma_{3r} \le 0 \qquad \text{(B.3.11)}$$

APPENDIX B.4

Assessment of Effect of Approximations for Case III-1

In Chapter 3 two approximations have been made. These are: **a)** an idealized thin section has been adopted, and **b)** the straight-line requirement for PNA has been violated in Case III. The effect of these approximations for the case $v_z = v_y = m_z = 0$ and the results are compared to more accurate solutions. It is of interest to note that when $v_y \neq 0, v_z \neq 0, m_z \neq 0$, the agreement between the two solutions is expected to improve. Two scenarios are considered to illustrate the effect of the approximations (Fig. B.4.1). Consider the PNA position for Case a in Fig. B.4.1a, where variables α_a and γ_a are dimensionless coordinates identifying the location of the neutral axis along the edge of the section. Distances $\alpha_a t$ and $\gamma_a t$ give the location where the neutral axis intersects the cross-section. Eqs. B.4.1 through B.4.3 are applicable for the conditions $0 \le \alpha_a \le 1$ and $0 \le \gamma_a \le 1$.

The axial force and normalized bending moments due to the assumed stress distribution are:

$$v_{za} = \frac{\sigma[(4-\gamma_a-\alpha_a)a-(\alpha_a+\gamma_a)t]}{4a} \tag{B.4.1}$$

$$m_{za} = \frac{\sigma[t(t-a)(\gamma_a^2+\alpha_a^2)-(\gamma_a+\alpha_a)(a+t)^2]}{3a^2} \tag{B.4.2}$$

$$m_{ya} = \frac{\sigma(a+t)(\alpha_a-\gamma_a)}{9a} \tag{B.4.3}$$

The above ratios give the coordinates of a point $\bar{\mathbf{P}}(m_{za}, m_{ya}, v_{za})$ on the "exact" yield surface (Fig. B.4.2). One way of assessing the proximity of the approximate yield

surfaces proposed in cases I through III to the "exact" yield surface based on a thick section representation is to scale vector $\bar{\mathbf{P}}$ by a factor c_a, i.e., $\bar{\mathbf{P}}_{apx} = c_a \bar{\mathbf{P}}$ (Fig. B.4.2). A value of c_a close to unity would indicate that the approximate solution is in close agreement with the exact solution. The scaling constant c_a is obtained by performing substitute on $v_z = c_a v_{za}, m_x = c_a m_{xa}, m_y = c_a m_{ya}$ in the interaction equations (Eq. 3.16, 3.24, and 3.31). Besides, in the absence of shear and twist, the normal stress terms will be equal to unity ($\sigma_1 = \sigma_2 = \sigma_3 = \sigma_4 = 1$). A plot of the scaling factor c_a against the moment ratios m_{xa} and m_{ya} is presented in Fig. B.4.3a. It is of interest to mention that the scaling factor varies from 0.991 at ($m_{xa} = -0.332$ and $m_{ya} = -0.013$) to 1.000 at ($m_{xa} = 0$ and $m_{ya} = 0$). The difference between the two solutions is always less than 1%. The approximate solution is always erring on conservative side.

A similar treatment for Case b (Fig. B.4.1b) yields the relations

$$v_{zb} = \frac{\sigma[4a - \beta_b \gamma_b (a+t)]}{4a} \tag{B.4.4}$$

$$m_{xb} = \frac{\beta_b \gamma_b \sigma[2\gamma_b t(a+t) - 3(a+t)^2]}{9a^2} \tag{B.4.5}$$

$$m_{yb} = \frac{\beta_b \gamma_b \sigma(3 - 2\beta_b)(a+t)^2}{9a^2} \tag{B.4.6}$$

The scaling factor for Case b is denoted as c_b. The plot of scaling factor c_b against m_{xb} and m_{yb} is presented in Fig. B.4.3b. Factor c_b ranges from 0.993 at ($m_{xb} = -0.293$ and $m_{yb} = 0.101$) to 1 at ($m_{xb} = 0$ and $m_{yb} = 0$). The scaling factors, c_a and c_b, being close to unity is an indication of the accuracy of the approximate solution. The quality of the agreement is expected to improve in the presence of twisting moment and shear forces.

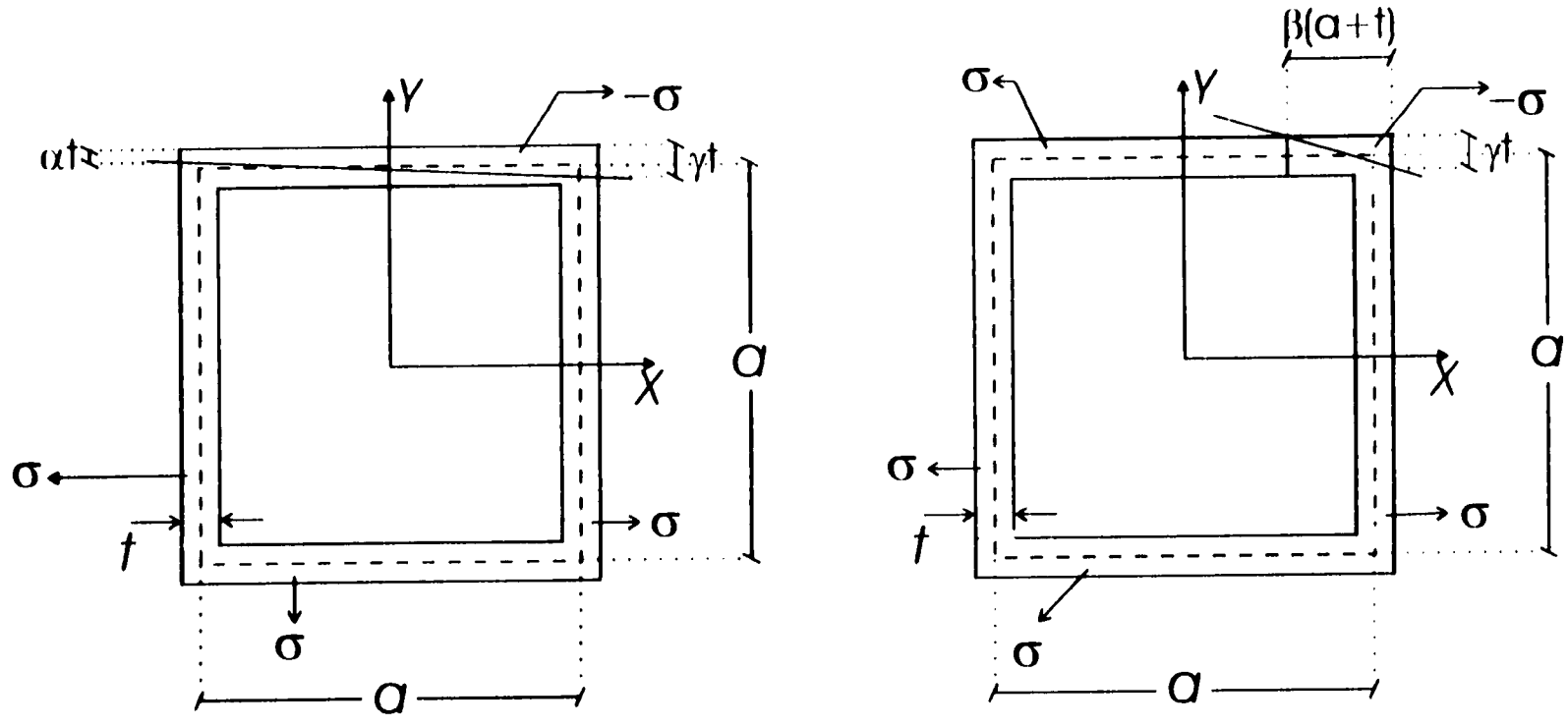

(a) Case a

(b) Case b

Figure B.4.1 PNA Locations for a Thick Walled Hollow Section

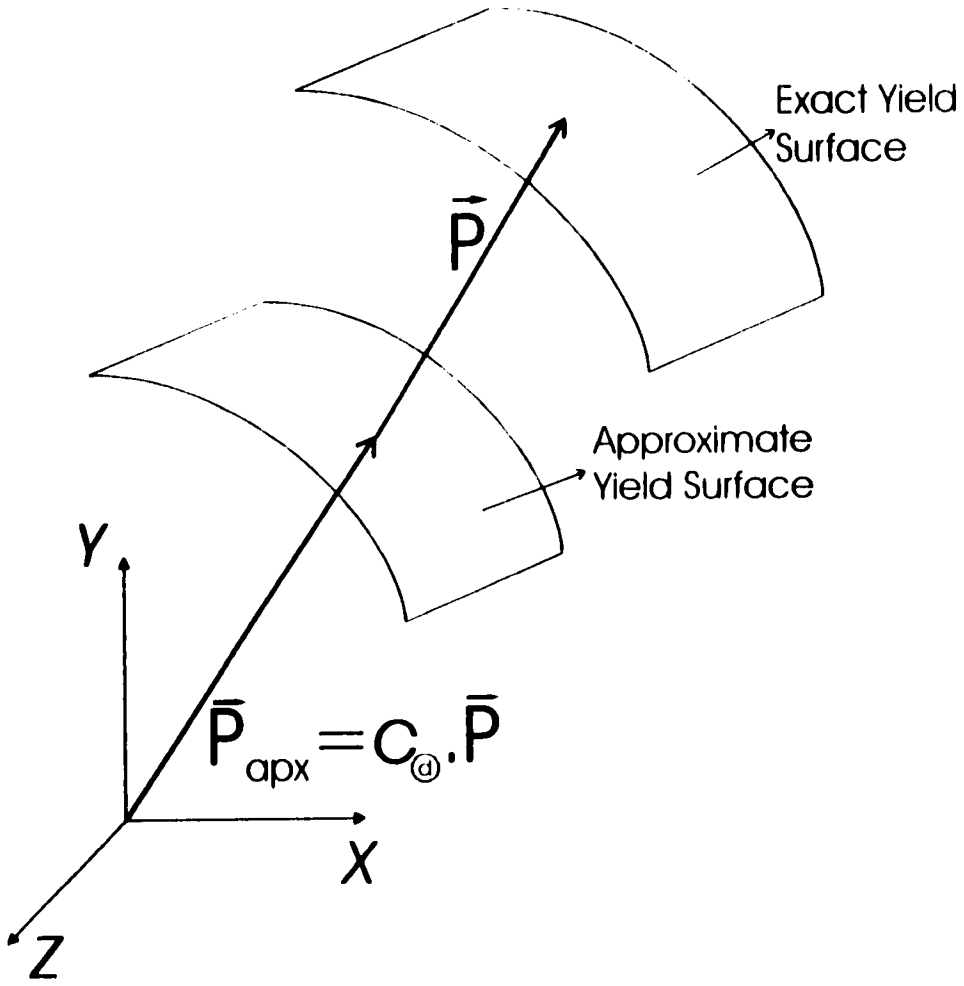

Figure B.4.2 Scaling Factor

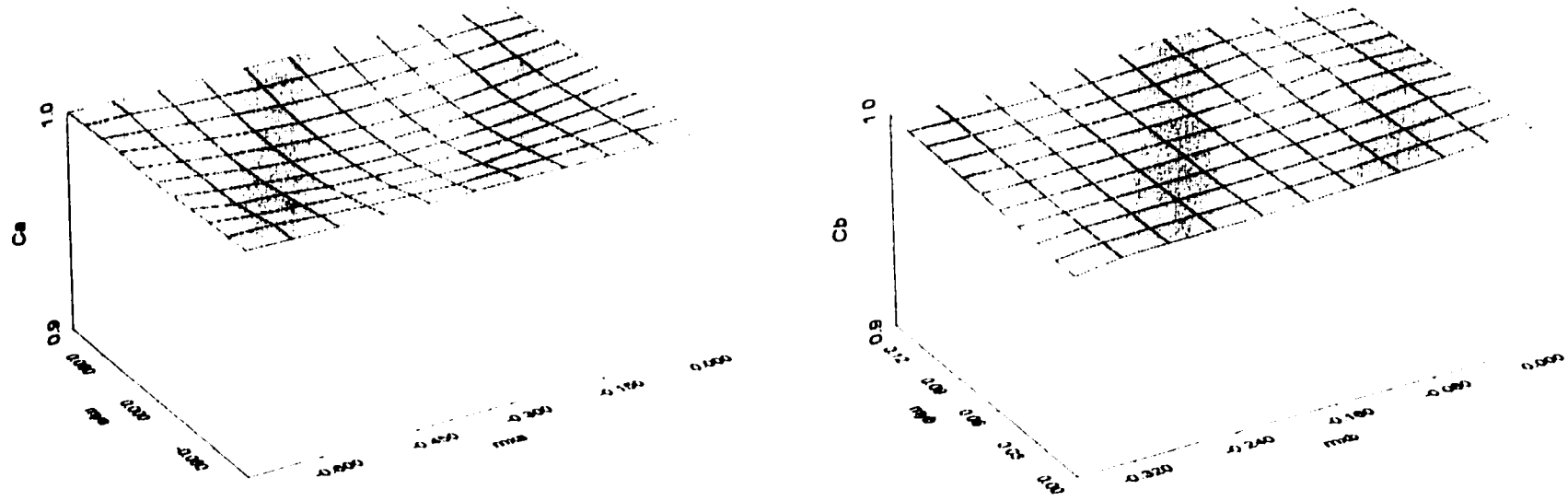

(a) Case a (c_a)

(b) Case b (c_b)

Figure B.4.3 Scaling Factors

APPENDIX B.5

Applicability Limits of Case III-1

This section demonstrates the derivation of applicability limits of Case III-1.

The equivalents of the coordinates β_1 and β_2 (Fig. 3.5c) are found as below.

$$\beta_1 = \frac{(6m_1 - \sigma_2 - 2\sigma_1 + 2\sigma_3)\sigma_2 + (6m_3 + \sigma_4)\sigma_4 + 9m_3^2}{4\sigma_2(\sigma_4 - \sigma_2 + 3m_3)} \tag{B.5.1}$$

$$\beta_2 = \frac{3m_1(4\sigma_2 - 2\sigma_4 - 3m_3) + 3\sigma_2(2m_1 - \sigma_2) - 2\sigma_2(\sigma_1 - \sigma_3 - 2\sigma_4) - \sigma_4^2}{4\sigma_2(\sigma_4 - \sigma_2 + 3m_3)} \tag{B.5.2}$$

For the interaction equation of the Case III-1 (Eq. 3.31) to be applicable, the coordinates have to meet the following geometric constraints.

$$0 \le \beta_2 \le 1 \tag{B.5.3}$$

$$0 \le \beta_1 \le \beta_2 \tag{B.5.4}$$

Noting that $\sigma_2 > 0$, the bound $\beta_1 \le \beta_2$ leads to the following applicability limit.

$$\sigma_4 - \sigma_2 + 3m_3 < 0 \tag{B.5.5}$$

By taking (B.5.5) into consideration, the following applicability limit can be recovered from the bound $0 \le \beta_1$ of (B.5.4).

$$(6m_1 - \sigma_2 - 2\sigma_1 + 2\sigma_3)\sigma_2 + (6m_3 + \sigma_4)\sigma_4 + 9m_3^2 \le 0 \tag{B.5.6}$$

Any given load combination that satisfies the applicability limits (B.5.5) and (B.5.6), at the same time, satisfies the bound $0 \le \beta_2$. As a last step, the bound $\beta_2 \le 1$ ($\beta_2 - 1 \le 0$) must be satisfied which leads to the following applicability limit.

$$\begin{aligned}&(\sigma_4 - 3\sigma_2)(\sigma_2 - \sigma_4) + 2\sigma_2(\sigma_1 - \sigma_3) \\ &- 3m_3(2\sigma_4 + 3m_3) + 6\sigma_2(2m_3 - m_1) \le 0\end{aligned} \tag{B.5.7}$$

As a result, it can be concluded that some of the applicability limits for Case III-1 are as below.

$$g_{31}(\{\mathbf{x}\}) = \sigma_4 - \sigma_2 + 3m_3 \le 0 \tag{B.5.8}$$

$$g_{32}(\{\mathbf{x}\}) = (6m_1 - \sigma_2 - 2\sigma_3 - 2\sigma_2)\sigma_2 + (6m_3 - \sigma_4)\sigma_4 + 9m_3^2 \le 0 \tag{B.5.9}$$

$$\begin{aligned}&g_{33}(\{\mathbf{x}\}) = (\sigma_4 - 3\sigma_2)(\sigma_2 - \sigma_4) + 2\sigma_2(\sigma_1 - \sigma_3) \\ &- 3m_3(2\sigma_4 + 3m_3) - 6\sigma_2(2m_3 - m_1) \le 0\end{aligned} \tag{B.5.10}$$

APPENDIX B.6

Summary of Interaction Equations for Cases I-1 through III-8

Tables B.6.1, B.6.2, and B.6.3 give the interaction equations for the sub-cases of cases I, II, and III, respectively.

Table B.6.1 Interaction Equations of Sub-cases of Case I

Cases	Formulas	Interaction equation
Case I-1	$f(\sigma_1,\sigma_2,\sigma_3,\sigma_4,m_1,m_2,v_2)$	$[(\sigma_2-\sigma_3)(\sigma_1+\sigma_3)+4v_2(\sigma_1+\sigma_3)\ \ 3m_1(\sigma_1-\sigma_3)]^2-$ $4\sigma_1\sigma_3[(\sigma_1+\sigma_3)^2+2(\sigma_1+\sigma_3)(\sigma_2+\sigma_4)+6m_1(\sigma_1+\sigma_3)-9m_1^2]=0$
Case I-2	$f(\sigma_2,\sigma_3,\sigma_1,\sigma_4,-m_1,m_2,v_2)$	$[(\sigma_3-\sigma_1)(\sigma_2+\sigma_4)+4v_2(\sigma_2+\sigma_4)-3m_1(\sigma_2-\sigma_4)]^2-$ $4\sigma_2\sigma_4[(\sigma_2+\sigma_4)^2+2(\sigma_2+\sigma_4)(\sigma_3+\sigma_1)-6m_1(\sigma_2+\sigma_4)-9m_1^2]=0$
Case I-3	$f(\sigma_3,\sigma_4,\sigma_1,\sigma_2,-m_1,-m_2,v_2)$	$[(\sigma_4-\sigma_2)(\sigma_1+\sigma_3)+4v_2(\sigma_1+\sigma_3)+3m_1(\sigma_3-\sigma_1)]^2-$ $4\sigma_1\sigma_3[(\sigma_1+\sigma_3)^2+2(\sigma_1+\sigma_3)(\sigma_2+\sigma_4)-6m_1(\sigma_1+\sigma_3)-9m_1^2]=0$
Case I-4	$f(\sigma_4,\sigma_1,\sigma_2,\sigma_3,m_1,-m_2,v_2)$	$[(\sigma_1-\sigma_3)(\sigma_4+\sigma_2)+4v_2(\sigma_4+\sigma_2)+3m_1(\sigma_4-\sigma_2)]^2-$ $4\sigma_4\sigma_2[(\sigma_4+\sigma_2)^2+2(\sigma_4+\sigma_2)(\sigma_1+\sigma_3)+6m_1(\sigma_4+\sigma_2)-9m_1^2]=0$

Table B.6.2 Interaction Equations of Sub-cases of Case II

Cases	Formula	Interaction Equation
Case II-1	$f(\sigma_1,\sigma_2,\sigma_3,\sigma_4,m_1,m_2,v_2)$	$2\sigma_2(4v_2+3m_1-2\sigma_1-\sigma_2-\sigma_4)+(4v_2-\sigma_1-\sigma_2-\sigma_3-\sigma_4+\sqrt{G})^2=0$ $G=2\sigma_3(3m_1-4v_2+\sigma_1+\sigma_3+2\sigma_4)$
Case II-2	$f(\sigma_2,\sigma_3,\sigma_4,\sigma_1,-m_1,m_2,v_2)$	$2\sigma_3(4v_2+3m_1-2\sigma_2-\sigma_3-\sigma_1)+(4v_2-\sigma_2-\sigma_3-\sigma_4-\sigma_1+\sqrt{G})^2=0$ $G=2\sigma_4(-3m_1-4v_2+\sigma_2+\sigma_4+2\sigma_1)$
Case II-3	$f(\sigma_3,\sigma_4,\sigma_1,\sigma_2,-m_1,-m_2,v_2)$	$2\sigma_4(4v_2-3m_1-2\sigma_3-\sigma_4-\sigma_2)+(4v_2-\sigma_3-\sigma_4-\sigma_1-\sigma_2+\sqrt{G})^2=0$ $G=2\sigma_1(-3m_1-4v_2+\sigma_3+\sigma_1+2\sigma_2)$
Case II-4	$f(\sigma_4,\sigma_1,\sigma_2,\sigma_3,m_1,-m_2,v_2)$	$2\sigma_1(4v_2-3m_1-2\sigma_4-\sigma_1-\sigma_3)+(4v_2-\sigma_4-\sigma_1-\sigma_2-\sigma_3+\sqrt{G})^2=0$ $G=2\sigma_2(3m_1-4v_2+\sigma_4+\sigma_2+2\sigma_3)$
Case II-5	$f(\sigma_1,\sigma_2,\sigma_3,\sigma_4,-m_1,-m_2,-v_2)$	$2\sigma_2(-4v_2-3m_1-2\sigma_1-\sigma_2-\sigma_4)+(-4v_2-\sigma_1-\sigma_2-\sigma_3-\sigma_4+\sqrt{G})^2=0$ $G=2\sigma_3(-3m_1+4v_2+\sigma_1+\sigma_3+2\sigma_4)$
Case II-6	$f(\sigma_2,\sigma_3,\sigma_4,\sigma_1,m_1,-m_2,-v_2)$	$2\sigma_3(-4v_2-3m_1-2\sigma_2-\sigma_3-\sigma_1)+(-4v_2-\sigma_2-\sigma_3-\sigma_4-\sigma_1+\sqrt{G})^2=0$ $G=2\sigma_4(3m_1+4v_2+\sigma_2+\sigma_4+2\sigma_1)$
Case II-7	$f(\sigma_3,\sigma_4,\sigma_1,\sigma_2,m_1,m_2,-v_2)$	$2\sigma_4(-4v_2+3m_1-2\sigma_3-\sigma_4-\sigma_2)+(-4v_2-\sigma_3-\sigma_4-\sigma_1-\sigma_2+\sqrt{G})^2=0$ $G=2\sigma_1(3m_1+4v_2+\sigma_3+\sigma_1+2\sigma_2)$
Case II-8	$f(\sigma_4,\sigma_1,\sigma_2,\sigma_3,-m_1,m_2,-v_2)$	$2\sigma_1(-4v_2+3m_1-2\sigma_4-\sigma_1-\sigma_3)+(-4v_2-\sigma_4-\sigma_1-\sigma_2-\sigma_3+\sqrt{G})^2=0$ $G=2\sigma_2(-3m_1+4v_2+\sigma_4+\sigma_2+2\sigma_3)$

Table B.6.3 Interaction Equations of Sub-cases of Case III

Cases	Formula	Interaction Equation
Case III-1	$f(\sigma_1, \sigma_2, \sigma_3, \sigma_4, m_1, m_2, v_2)$	$v_1 \quad 0.25(3m_1 + 2\sigma_4 + \sigma_1 + \sigma_3) = 0$
Case III-2	$f(\sigma_2, \sigma_1, \sigma_4, \sigma_3, -m_1, m_2, v_2)$	$v_1 - 0.25(-3m_1 + 2\sigma_1 + \sigma_2 + \sigma_4) = 0$
Case III-3	$f(\sigma_3, \sigma_4, \sigma_1, \sigma_2, -m_1, -m_2, v_2)$	$v_1 - 0.25(-3m_1 + 2\sigma_2 + \sigma_3 + \sigma_1) = 0$
Case III-4	$f(\sigma_4, \sigma_1, \sigma_2, \sigma_3, m_1, -m_2, v_2)$	$v_1 - 0.25(3m_1 + 2\sigma_3 + \sigma_4 + \sigma_2) = 0$
Case III-5	$f(\sigma_1, \sigma_2, \sigma_3, \sigma_4, -m_1, -m_2, -v_2)$	$-v_1 - 0.25(-3m_1 + 2\sigma_4 + \sigma_1 + \sigma_3) = 0$
Case III-6	$f(\sigma_2, \sigma_3, \sigma_4, \sigma_1, m_1, -m_2, -v_2)$	$-v_1 - 0.25(3m_1 + 2\sigma_1 + \sigma_2 + \sigma_4) = 0$
Case III-7	$f(\sigma_3, \sigma_4, \sigma_1, \sigma_2, m_1, m_2, -v_2)$	$-v_1 - 0.25(3m_1 + 2\sigma_2 + \sigma_3 + \sigma_1) = 0$
Case III-8	$f(\sigma_4, \sigma_1, \sigma_2, \sigma_3, -m_1, m_2, -v_2)$	$-v_1 - 0.25(-3m_1 + 2\sigma_3 + \sigma_4 + \sigma_2) = 0$